BLACK CARBON AND BLUE CARBON: THE EFFECTS OF PYROLYSIS AND VEGETATION REPLACEMENT ON THE SOLUBILIZATION, DEGRADATION, AND SEQUESTRATION OF TERRESTRIAL ORGANIC CARBON

A Dissertation

by

MATTHEW J. NORWOOD

Submitted to the Office of Graduate and Professional Studies of
Texas A&M University
in partial fulfillment of the requirements for the degree of

DOCTOR OF PHILOSOPHY

Chair of Committee,	Patrick Louchouarn
Committee Members,	Peter Santschi
	Anna Armitage
	Wesley Highfield
Head of Department,	Shari Yvon-Lewis

May 2017

Major Subject: Oceanography

ABSTRACT

Understanding the transformation and transportation of organic carbon is important to elucidate carbon cycling within changing ecosystems. Biomass burning produces a continuum of pyrogenic organic matter (Py-OM) with unique chemical functionality dependent on temperature and the parent plant material. Spectroscopic analysis of lab produced Py-OM and pyrogenic water soluble organic matter (Py-WSOM) indicates that the Py-WSOM extracted from low temperature chars (200-650°) is dominated by carbon associated with polar functionality (-OH and C-O), most likely derived from the depolymerization and defragmentation of lignocellulose. Incubation experiments under aerobic conditions with unsterilized river water suggests that Py-WSOM and associated pyrogenic biomarkers have turnover rates on the order of weeks to months, consistent with mixing and transport timescales for riverine systems. Therefore, the export of Py-WSOM from the aquatic system and its impacts on regional and global level carbon cycling may be heavily influenced by low-mid combustion temperature PyC. This study will aid in understanding the solubilization, degradation, and sequestration of terrestrial organic carbon in light of thermal alteration and vegetation replacement.

Texas coastal wetlands are dynamic tidal zones that have historically been dominated by salt marshes. Due to changes in regional weather patterns, this region has experienced warmer winters with a decrease in freeze intensity, allowing the black mangrove (*Avicennia germinans*) to expand local populations. For the past 2-3 decades, some of these ecosystems have experienced community shifts with A. *germinans*

competing with native salt marsh plants for resources. This study quantifies plant biomass, organic carbon (OC) accumulation, and lignin accumulation for two salt marsh dominated wetlands, two A. *germinans* dominated wetlands, and one mixed salt marsh-A. *germinans* ecotone located along the Texas Gulf Coast, in order to understand the effect of vegetation replacement on OC accumulation. Annual and long term regional carbon accumulation for both A. *germinans* and salt marsh wetlands are significantly similar. Although carbon quantity is significantly similar the quality of carbon storage is different for A. *germinans* and salt marsh wetlands.

ACKNOWLEDGMENTS

Thank you God for walking beside me and giving me the strength to persevere.

I would like to thank Dr. Allison Myers-Pigg. Thank you for being my companion and confidant during our PhD. We have built a life and family together, I am so grateful for your love and support. We truly make a great team as scientists and most importantly partners.

I would like to thank my parents Rick and Barb Norwood. Thank you for raising me to be compassionate, empathetic and a loving individual. Both of you always put your family first and have allowed your three sons to reach for the stars. Dad, you truly are the greatest man I know. Your compassion and work to serve others is a gift and you have shared that gift with countless people. Mom, you are an amazing mother. Your ability to nurture, comfort and support your family is the glue that bonds us all together. Mom and dad, I learned first-hand how to be a great parent to my beautiful daughter Sofia, through watching the two of you.

I would like to thank my two older brothers, Marcus and Richard Norwood. Thank you for watching over me and supporting me through my life. The two of you are my best friends. I am extremely grateful for the memories you have given me and the bond the three of us share.

I would like to thank my sisters Brandi and Marisol. You two are amazing moms and wives. Your support for your children and husbands is inspirational. I love you both.

I would like to thank my extended Norwood, Neumeister, Tanner and Dodd family. Thank you for your love and support throughout my life. Although we are spread around the world, we are united in spirit.

I would like to thank my advisor, Dr. Patrick Louchouarn. Thank you for believing in me and supporting me through my PhD.

A special thank you to Dr. Carrie Masiello for your support over the course of my PhD.

I would like to thank undergraduate students at Texas A&M University Galveston Campus Noah White and Kasey Pierce for their assistance with field work and sample processing.

I would also like to thank my friends; Anne Tamalavage, Andrew McGuffin, Amanda and Travis Stern, Dan and Sam Trundle, Steven Sompels and many more for your friendship and memories that I will enjoy for a lifetime.

CONTRIBUTORS AND FUNDING SOURCES

Contributors

Part 1, faculty committee recognition

This work was supported by a dissertation committee consisting of Professors Dr. Patrick Louchouarn [advisor] Vice President for Academic Affairs and Chief Academic Officer of Texas A&M University Galveston Campus and Professors, Dr. Anna Armitage [committee member] Department of Marine Biology, Dr. Wesley Highfield [committee member] Department of Marine Sciences, and Dr. Peter Santschi [committee member] Department of Marine Sciences.

Part 2, collaborator contributions

All work for this dissertation was completed by Matthew Norwood. Chapter 3, "Characterization and biodegradation of water-soluble biomarkers and organic carbon extracted from low temperature chars" was revised and published in collaboration with Dr. Patrick Louchouarn [Texas A&M University Galveston Campus], Dr. Li-Jung Kuo [Pacific Northwest National Laboratory], and Dr. Omar Harvey [Texas Christian University].

Funding Sources

Graduate study was supported by the Texas Institute of Oceanography and NASA grant NNX11AR08G. Graduate conference travel was assisted by the Welch Foundation and the Emma and Luke Mooney foundation.

NOMENCLATURE

TOM	Terrestrial Organic Matter
TOC	Terrestrial Organic Carbon
HTT	Heat Temperature Treatment
BC	Black Carbon
Py-OM	Pyrogenic Organic Matter
PyC	Pyrogenic Carbon
Py-WSOM	Pyrogenic Water Soluble Organic Matter
Py-WSOC	Pyrogenic Water Soluble Organic Carbon
VOC	Volatile Organic Carbon
POM	Particulate Organic Matter
DOM	Dissolved Organic Matter
LOP	Lignin Oxidation Product
LP	Lignin Phenols
Blu-C	Blue Carbon
SOC	Soil Organic Carbon

TABLE OF CONTENTS

Page

LIST OF FIGURES

Page

LIST OF TABLES

Page

I. INTRODUCTION AND LITERATURE REVIEW

During photosynthesis atmospheric CO_2 is assimilated into organic carbon. Organic matter attributed to plant biomass can be transformed through biodegradation, photochemical oxidation and thermal oxidation. This transformation ultimately depolymerizes larger polymers of lignin, cellulose and hemicellulos into smaller molecular units which can ultimately be recycled as CO_2 back into the atmosphere.

During biodegradation, organic carbon associated with plant biomass is recycled back into CO_2, incorporated into microbial biomass and/or transformed within the environment. Although biodegradation is a major pathway for the recycling of carbon back into CO_2 (Singh and Gupta, 1977); photochemical oxidation plays a major role in reducing the size of aromatic lignin within aquatic systems (Opsahl and Benner, 1998) and destabilizing soil organic matter (Feng et al., 2008, Feng et al., 2011). Therefore, photochemical oxidation of aromatic carbon can increase the reactivity of carbon within the environment (Lindell et al., 1995) and lead to increased biodegradation and respiration of CO_2 (Rosenstock et al., 2005).

The thermal oxidation and transformation of organic matter into increasingly condensed aromatic compounds can increase the recalcitrance of organic carbon in the environment. At a molecular level, the pyrolysis of plant biomass, depolymerizes and defragments larger polymeric compounds associated with lignocellulose into smaller molecular subunits. Initially more labile organic carbon, associated with carbohydrates (hemicellulose and cellulose) are cleaved at aryl-alkyl ether bonds (Kuo et al., 2008b). Polymeric lignin undergoes further depolymerization and defragmentation releasing

individual free lignin phenols ((Hedges and Mann, 1979, Kuo et al., 2011a). Increasing pyrolysis temperatures of organic matter eventually leads to aromatization and condensation of molecular compounds (Harvey et al., 2012a).

In order to understand carbon cycling on a global scale, special attention must be paid to the redistribution of terrestrial carbon and its fate in inland and coastal systems (Battin et al., 2009). While there are large fluxes of carbon from the terrestrial system, enough to account for all the carbon in marine sinks (Hedges et al., 1997), only a small portion of terrestrial organic carbon is stored in marine systems (Hedges et al., 1997). This paradox suggests that the fate of this carbon along its journey from terrestrial to aquatic systems is important for understanding overall carbon cycling, and changes to this cycle with climate (Battin et al., 2009). In particular, the study of tidally influenced systems and the potential fate of thermally altered carbon are missing from global carbon cycling models (Santín et al., 2016, Ward et al., 2017). This dissertation, therefore, aims to understand the solubilization, degradation, and sequestration of terrestrial organic carbon in light of thermal alteration and vegetation replacement.

1.1 Terrestrial biomass and the thermal alteration of terrestrial carbon

Terrestrial carbon is comprised of a variety of complex molecular structures, whose residence time and functionality in the environment varies widely, therefore different residences times and degradability have an impact on overall carbon cycling in the environment. Understanding the fate of terrestrial carbon is important for understanding overall carbon cycling. Terrestrial biomass is made up of approximately 40-50% cellulose, 20-40% hemicellulose and 15-30% lignin, including a small amount

of pectin, protein, lipids and minerals (Horn et al., 2012). Cellulose is a polymer of glucose, while hemicellulose is made up of a heterogeneous polymer of pentose, hexose, and other sugar acids (Pauly and Keegstra, 2008), dependent on plant type. The lignin polymer composition is dependent on plant material type. Lignin contains larger proportions of guaiacyl sub units in softwoods, a combination of guaiacyl and syringyl sub units in hardwoods, while grasses and leaf tissue contain in addition but not exclusively cinnamyl sub units (Hedges and Mann, 1979).

The thermal alteration of terrestrial biomass transforms organic carbon into a continuum of increasingly recalcitrant molecules with the increase in temperature (Goldberg, 1985, Schmidt and Noack, 2000). The pyrolysis of biomass constituents; hemicellulose, cellulose and lignin starts at 220°C, 315°C and 400°C, respectively (Yang et al., 2006). The pyrolysis and combustion of terrestrial plant matter is controlled by both intrinsic factors (i.e., feedstock composition) along with extrinsic factors (i.e., combustion temperature). The difference in the initial intrinsic and extrinsic factors affecting the formation and transformation of thermally altered pyrogenic carbon (PyC) can potentially influence the path and ultimate fate of this low-mid temperature fraction of PyC within environmental carbon cycling pathways.

A continuum model is used to encompass the vastly different physicochemical structures of PyC (also referred to as black carbon (BC) continuum; Figure 1), which is comprised of three major sub-categories- slightly charred, char/charcoal and soot/graphite (Goldberg, 1985, Hedges et al., 2000, Masiello, 2004).

Slightly charred organic matter and char/charcoals are solid residues derived from low-mid temperature combustion that retain most of the original structural information from the original plant feedstock. Low-mid temperature pyrogenic organic matter (Py-OM) is characterized by the abundance of depolymerized oligomers enriched in oxygen and hydrogen-containing functional groups, such as carbohydrates and carboxylated lignin phenols (Kuo et al., 2008b, Kuo et al., 2011a, Harvey et al., 2012a). During the low temperature combustion of plant biomass, free lignin phenols and cellulose derivatives, such as anhydrosugars (levoglucosan), are formed (Figure 1) (Elias et al., 2001, Kuo et al., 2008b, Louchouarn et al., 2009). Results from previous studies indicate that along with photochemical degradation and biodegradation in soils, thermal alteration is an important degradation process for lignin (Hedges and Oades, 1997, Kuo et al., 2008a, Zimmerman et al., 2011, Myers-Pigg et al., 2015). In contrast, high temperature Py-OM and soot are comprised of highly condensed aromatic and turboclastic structures, which retain little information from the unburned plant feedstock (Keluweit et al., 2010, Nguyen et al., 2004, Wiedemeier et al., 2015).

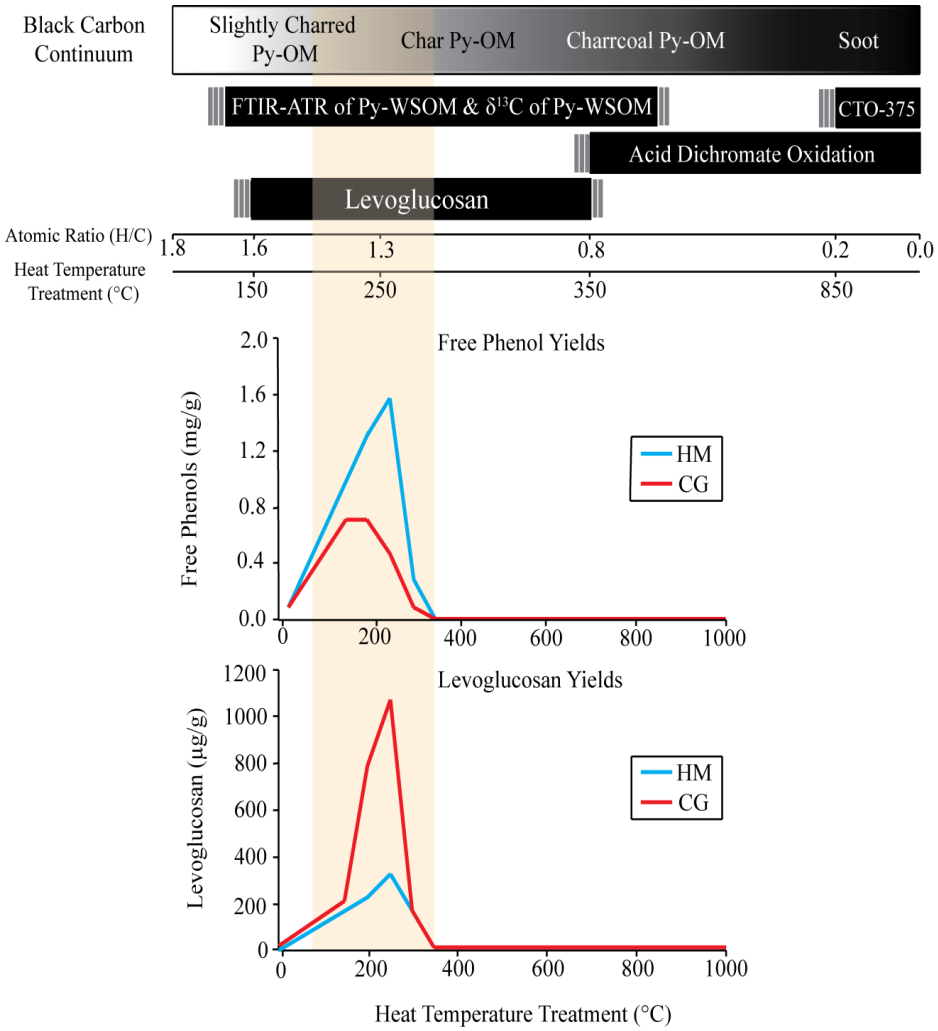

Figure 1. Distribution of solvent extractable lignin phenols and levoglucosan in chars (150-1000°C) *vs*. the black carbon continuum (figure reprinted from (Kuo et al., 2011a, Kuo et al., 2008b, Kuo et al., 2008a). The two bottom graphs illustrate the maximum yields of freely dissolved monomers produced in low-temperature chars (150-300ºC). The free phenol graph also shows the proportion of polymeric-derived lignin phenols remaining in solid-phase chars along the combustion continuum used.

1.1.1 Low temperature pyrogenic carbon in the environment- our current understanding

Long term storage of PyC within coastal margins is dominated by highly condensed aromatic carbon (Masiello and Druffel, 1998, Sánchez-García et al., 2013, Mitra et al., 2013), which is linked to anthropogenic emissions and high temperature terrestrial fires (Schneider et al., 2013). This high temperature fraction of highly condensed carbon has long residence times within coastal sediments and is therefore looked upon as a net sink for terrestrial carbon (Masiello and Druffel, 1998, Kuo et al., 2011b). While traditionally thought of as extremely resistant to degradation processes during transport, higher temperature PyC may be mineralized through abiotic photochemical degradation (Stubbins et al., 2012), while low temperature PyC is comprised of labile fractions of PyC that are readily oxidized within the environment through bacterial mineralization (Myers-Pigg et al., 2015). The process of CO_2 emission into the atmosphere through the thermal combustion of terrestrial organic carbon and the bacterial mineralization of PyC illustrates carbon loss terms that may help explain the decoupling of the mass balance between PyC annually produced and that, which is sequestered within marine sediments on millennial time scales (Jaffé et al., 2013), and has implications on our understanding of the role PyC plays on overall carbon cycling (Santín et al., 2016).

Biomass combustion, from either wildfires and/or prescribed agricultural and forest burning, leads to fluxes of thermally altered organic matter into surrounding soils (Alexis et al., 2007, Preston and Schmidt, 2006). Evidence suggests that charcoal and other forms of PyC are susceptible to environmental processes of degradation that

release water-soluble derivatives into soil pore waters and eventually natural water systems (Hockaday et al., 2007). During the thermal degradation of biomass, the depolymerization of biopolymers produce increased –OH and C-O combustion residues which make them inherently more polar and soluble in water (Norwood et al., 2013).

The water-soluble derivatives are made up of pyrogenic water-soluble organic matter (Py-WSOM), which contributes approximately 3.4% at low temperatures and approximately 10% at high temperatures to the dissolved organic matter (DOM) in river systems (Myers-Pigg et al., 2015, Myers-Pigg et al., 2017). Therefore DOM in a fire-impacted watershed will contain fire and non-fire derived DOM.

Pyrogenic organic carbon is transported by rivers and streams, fueling bacterial production, and is mineralized through biogeochemical/photochemical processes (Masiello and Louchouarn, 2013, Myers-Pigg et al., 2015, Amon and Benner, 1996). Although, the flux of soil PyC into streams has important implications for the global carbon cycle the majority of studies focusing on the solubilization, export and fate of carbon-rich combustion residues have looked at high temperature PyC (Dittmar, 2008, Jaffé et al., 2013), while few studies have looked at low temperature PyC (Myers-Pigg et al., 2015, Myers-Pigg et al., 2017, Norwood et al., 2013).

As terrestrial derived pyrogenic carbon (PyC) accounts for 0.2-0.6% of the annual global net primary production (116-385 Tg-C·yr^{-1}) (Santín et al., 2016), understanding the role of PyC and the flux of PyC into coastal margins important in the context of understanding overall carbon transport and carbon sequestration in these systems.

1.2 Importance of tidally influenced systems in carbon cycling

The preservation of terrestrial organic carbon (TOC) within intermediate coastal margins accounts for approximately 50% of the anthropogenic-induced lateral carbon flux (Regnier et al., 2013). Carbon sequestration within coastal margins can be enhanced depending on the recalcitrant nature of organic carbon being stored within the reservoir. Blue Carbon (Blu-C) (Teal, 1962) is linked to wetland systems where high rates of wetland accretion lead to large quantities of carbon storage. Despite their relatively small area (203 x 103 km^2, which represents only 0.1% of the Earth's surface), tidal wetlands play an important role in the global carbon budget due to both exceptional burial fluxes and negligible CH_4 and N_2O emissions (DeLaune et al., 1990). The large-scale carbon sequestration potential of estuarine coastal wetlands (≈41 $Tg\text{-}C \cdot yr^{-1}$; (Chmura et al., 2003)), suggests that these systems could act as measurable net sinks for atmospheric CO_2, since they are not characterized by substantial emissions of CH_4 (and N_2O) as inshore wetlands (bogs and peatlands), which would limit their potential to moderate global warming (Kuder and Kruge, 2001).

1.3 *Avicennia germinans* expansion along the Texas Gulf Coast

The Texas Gulf Coast has experienced no severe freeze events (≤ -4 ºC for several hours) since 1989, allowing stands of the black mangrove, *Avicennia germinans*, to locally expand in stand size (Armitage et al., 2015), displacing some areas of salt marsh comprised of herbaceous species such as *Spartina alterniflora* and *Batis maritima*. This replacement can be accelerated in conjunction with sea level rise and subsequent fresh water forest dieback which open up potential wetland habitats along

coastal margins (Doyle et al., 2010). Furthermore, carbon sequestration within coastal margins can be enhanced depending on the recalcitrant nature of carbon being stored within the reservoir.

1.3.1 Wetland organic carbon and lignin

In-situ storage of OC, as plant biomass, in wetlands is enhanced within saturated marine soils along the coastal environment. These coastal wetlands contain highly reducing anoxic mineral soils with a relatively thin, oxidized sediment layer (0-15 cm) (Patrick Jr and DeLaune, 1977, Reddy and DeLaune, 2008). Plant tissue from salt marsh plants and mangroves contain lignin, cellulose and hemicellulose. Lignin is the second most abundant naturally occurring polymer after cellulose, and is a complex and important structural component of vascular plants (Sarkanen and Ludwig, 1971). The lignin molecule, which is aromatic in structure, is considered recalcitrant in anoxic soils (Hedges and Mann, 1979, Hedges and Prahl, 1993), and can act as a sink for organic carbon (OC) in wetlands.

1.4 Research outline-labile and recalcitrant organic matter

The production of PyC occurs under a number of different conditions, which is directly influenced by temperature, feedstock and oxygen availability. The resulting PyC is therefore heterogeneous in nature and contains low, mid and high temperature molecular constituents. The solubilization of lignocellulose is potentially coupled to the heat temperature treatment (HTT) which potentially facilitates the release of labile PyC into fire affected watersheds.

Although the majority of studies have focused on high temperature PyC, the first two parts of my work looks at the solubilization and degradation of low temperature pyrogenic molecular markers and low-mid temperature water soluble pyrogenic organic matter. Such information is critical to (a), evaluate the potential for such molecular markers to act as viable tracers for the movement of Py-WSOC in aquatic environments at relevant time scales of transport (days to weeks), and (b) evaluate the characteristics that drive the solubilization of low-mid temperature pyrogenic water soluble organic matter.

The third part of my research looks at the effects of vegetation replacement on carbon accumulation within transitional A. *germinans* wetlands located along the Texas Gulf Coast. The focus of this study is to measure the effects of A. *germinans* regional expansion on the quantity and quality of organic carbon accumulation along the Texas Gulf Coast. Furthermore, I will look at the current monetary value of wetland soil carbon stocks and potential threats to regional carbon stocks along the Texas Gulf Coast.

II. THE SOLUBILIZATION OF LOW-MID TEMPERATURE PYROGENIC WATER SOLUBLE ORGANIC MATTER FROM PARTICULATE CHAR

2.1 Introduction

Pyrogenic carbon (PyC) originates through the incomplete combustion of biomass or fossil fuels, and includes a spectrum of heterogeneous materials ranging from slightly charred organics (i.e. brown carbon) to highly condensed aromatic components (i.e. black carbon; BC). The conceptual illustration of the PyC continuum (Figure 1) illustrates the vastly different physicochemical structures of this material produced along a temperature gradient. This continuum, which is comprised of two major sub-categories- char/charcoal and soot/graphite (Hedges et al., 2000, Kuo et al., 2011a, Harvey et al., 2012a, Masiello, 2004, Goldberg, 1985, Harvey et al., 2012b, Kuo et al., 2008b, Kuo et al., 2008a). Char/charcoals are solid residues, derived from low-temperature combustion, that retain most of the original chemical functionality and structural information from the unburned feedstock (Lammers et al., 2009, Harvey et al., 2012b, Kuo et al., 2011a). In contrast, soot/graphite is comprised of highly condensed aromatic and turbo-clastic structures, which retain little information from the parent feedstock (Nguyen et al., 2004, Louchouarn et al., 2007, Yang et al., 2007, Baldock and Smernik, 2002, Keluweit et al., 2010).

Wildfires and lab produced biochar's create PyC at much lower temperatures than industrial processes (200-750°C vs. > 750°C., respectively) (Kuo et al., 2011a, Alexis et al., 2007, Alexis et al., 2010, Rumpel et al., 2006). Combustion processes, whether natural or anthropogenic in origin, are major sources of PyC and volatile

organic carbon (VOC) to atmospheric, sedimentary and aquatic environments (Hedges et al., 2000, Masiello and Druffel, 1998, Goldberg, 1985, Lammers et al., 2009, Nguyen et al., 2004, Jaffé et al., 2013, Hunsinger et al., 2008, Accardi-Dey, 2003, Dennis et al., 2002); while low temperature PyC can release fractions of labile OC into the environment (Kuo et al., 2011a, Ascough et al., 2011). In lab-produced biochars, these components are characterized by the abundance of oxygen and hydrogen-containing surface functionality, such as freely bounded -OH, COOH and C=O surface functionality (Harvey et al., 2012b). Recent work has shown that pyrogenic water-soluble organic matter, based on molecular markers, are easily degraded within riverine systems on transport time scales, potentially adding to the efflux of carbon to the atmosphere from within riverine systems (Norwood et al., 2013, Myers-Pigg et al., 2015).

In this study, pyrogenic water soluble organic matter (Py-WSOM) was extracted from solid-phase pyrogenic organic matter (Py-OM) (i.e. plant-derived char-feedstocks). Each char-feedstock was produced at a range of temperatures known to be present in wildfires and lab produced biochar (200-650°C). The extracts were characterized using spectral analysis (ATR-FTIR), elemental organic carbon (%OC), stable carbon isotopic ($\delta^{13}C$) and recalcitrance index (R_{50}). Previous results from spectra of lab-produced charcoal and charcoal extracts, illustrate potential for selective solubilization of pyrogenic water-soluble organic carbon from its particulate charcoal feedstock (Norwood et al., 2013). The heat induced dehydration, depolymerization, and fragmentation of lignocellulose creates oxygen rich constituents that are released as pyrogenic water-soluble organic carbon at low heat temperature treatments (200-650°C).

The release of Py-WSOC is potentially facilitated through the interaction of polar-molecular-surface functionality (-OH and C-O) created through the thermal breakdown of lignocellulose. This lignocellulos is likely associated with components within the plant cell wall, identifying carbohydrate rich carbon constituents are selectively released from pyrogenic particulate charcoal feedstocks at low-mid temperature heat treatments (HTT).

2.2 Materials and methods

2.2.1 Charcoal production and Py-WSOM extraction

Three plant species, cordgrass (*Spartina spartinae*), honey mesquite (Prosopis *glandulosa*), and loblolly pine (Pinus *taeda*), were combusted at 200-650°C (detailed in (Kuo et al., 2008a, Kuo et al., 2008b)). Briefly, the plant material was cut into small pieces, dried (60ºC), and combusted (1 h) under O_2 limited conditions. Homogenized char (<60 mesh; ca. 1 g) from each plant was mixed with precombusted sand and extracted using accelerated solvent extraction (ASE), with MilliQ water as solvent (100°C) at 1500 psi. Each extract was filtered through a pre-combusted glass-fiber filter (≈ 0.45 μm). Each extract, totaling approximately 30 ml in volume, was freeze-dried and placed into a desiccator for two weeks before chemical and spectral analysis.

2.2.2 Elemental and isotopic analysis

Carbon weight percentages associated to the gram-dry weight of original charcoal and ash-free gram-dry weight of freeze dried char extract were determined using an Elemental Analyzer (CHN4010; Costech Analytical Technologies Inc., Valencia, CA). Ash- free carbon content was used using a modified method from ASTM

1102-84 (ASTM, 2013). Isotopic analysis, $\delta^{13}C$, was determined at the University of California-Davis Stable Isotope Facility, using an elemental analyzer equipped with a continuous flow isotopic ratio mass spectrometer (EA-IRMS). The enrichment of Py-WSOM from the particulate char-feedstock was calculated by the difference of $\delta^{13}C_{Py\text{-}OM}$ and $\delta^{13}C_{Py\text{-}WSOM}$.

2.2.3 Surface chemistry (ATR-FTIR) and thermogravimetric analysis

Surface spectral signatures were determined with attenuated total reflectance Fourier transform infrared spectrometer, (Varian 3100 IR spectrometer fitted with an ATR from PIKE Technologies Inc., Madison WI). Spectra were collected across 4000-500 cm^{-1} at a resolution of 16 cm^{-1} with 500 co-added scans applied (Norwood et al., 2013, Harvey et al., 2012b). All spectra were background corrected against a crystal reference, baseline corrected, and subjected to a 5-point S-G quad-cubic function as the smoothing filter (Savitzky and Golay, 1964). Peak deconvolution was applied through a second derivative function within the Varian FTIR software. Associated references for stretching and bending modes are reported in Table 1.

Thermogravimetric analysis was performed on Py-WSOM extracts using a TA Instruments Discovery TGA, Q_{50}. Weight loss and heat flow associated with the thermal oxidation of charcoal extracts was analyzed in air with a flow rate of 10 mL min^{-1}. Initial sample mass ranged between 15-20 mg, and the initial oven temperature started at 30°C with cut off temperatures of 750°C. A recalcitrance index (R_{50}), developed by Harvey et al., 2012a was applied, which quantifies the relative thermal degradability of carbon related BC materials (Harvey et al., 2012a). Briefly, the R_{50} index is calculated by

dividing the temperature at which 50% of sample mass is lost due to the oxidation/volatilization of BC material and 50% of graphite mass is lost (Harvey et al., 2012a).

Table 1. Selected ATR-FTIR absorbance for corresponding functionality.

Wavenumber (cm^{-1})	Bond Association	Reference
3650-3100	Dimeric & Polymeric -OH	Coats J., 2000
3100-2700	Alkyl & Aliphatic C-H	Yang et al., 2007
1700	C=O	Yang et al., 2007
1600	Aromatic Ring C=C-C	Yang et al., 2007
1400	OCH_3	Coats J., 2000
1140	C-O	Coats J., 2000
1183	Levoglucosan	Liu et al., 2011
1000	C-O-C	Coats J., 2000

2.3 Results

2.3.1 The solubilization of PyC and stable carbon isotopic enrichment

The percent Py-WSOC to gram-dry weight of parent char (gdw) peaks at 200°C for all of the studied charcoals (CG, PI and HM from 200-650°C; Figure 2 and Table 2). The proportion of Py-WSOC to Py-OC also peaks at 200°C for all three plant types. The release of %Py-WSOC (gdw) at 200°C is highest in the CG, followed by PI and HM, accounting for approximately 8%, 6% and 2% of the Py-OC combusted at 200°C for CG, HM and PI, respectively (Figure 2).

Carbon-13 enrichment of the Py-WSOM fraction ($\delta^{13}C_{Py\text{-}OM}$ - $\delta^{13}C_{Py\text{-}WSOM}$) increases with increasing temperature from 0.1-4.5‰, with the lowest enrichment in the PI 200° and the largest enrichment in the PI 400°C (Table 2 and Figure 3). It should be

noted that the HM 650°C enrichment of $\delta^{13}C$ from Py-OM to Py-WSOM is 11.4‰, but this was removed from the linear correlation because the low sample quantity could have affected the $\delta^{13}C$ measurement.

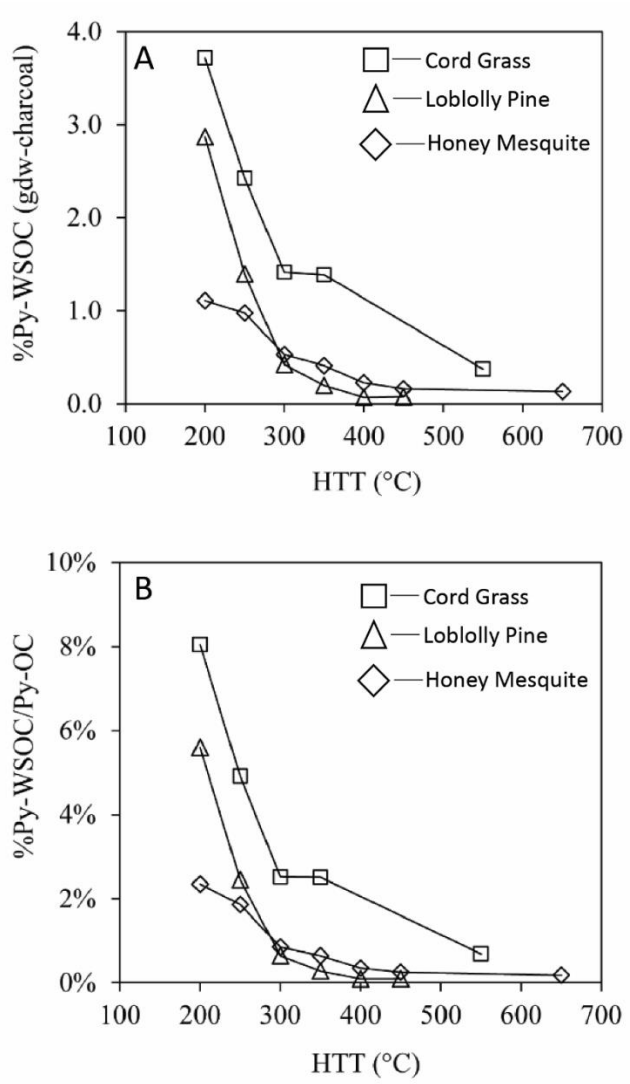

Figure 2. A) Percentage of pyrogenic dissolved organic carbon to gram dry weight of parent char (Py-WSOC) released during charcoal extraction. B) Fraction of %Py-WSOC vs. pyrogenic particulate organic carbon (Py-OC); produced as a function of heat temperature treatment (HTT). Honey mesquite, cord grass and loblolly pine represented by diamonds, squares and triangles, respectively.

Table 2. Py-OM and Py-WSOM; $\delta^{13}C$ and Ash-free %OC (Py-OM %OC = gram dry weight of particulate char and Py-WSOM %OC = gram dry weight of freeze dried char extract) for three different plant types loblolly pine (PI), honey mesquite (HM) and cord grass (CG) produced with increasing heat temperature treatments (200-650°C). The particulate charcoal feedstock is represented by Py-OM while the extracted water soluble fraction is represented by Py-WSOM.

Sample ID (°C)	Py-OM		Py-WSOM	
	$\delta^{13}C$[b] (‰)	Ash-free %OC (gdw)[a]	$\delta^{13}C$[b] (‰)	Ash-free %OC (gdw)[b]
PI (200)	-26.1	52	-26.0	46
PI (400)	-28.5	71	-24.3	21
PI (450)	-28.5	73	-27.0	20
HM (200)	-25.8	47	-24.1	46
HM (450)	-25.7	68	-22.7	34
HM (650)	-25.9	73	-14.6	34
CG (200)	-13.3	46	-13.1	41
CG (350)	-13.3	55	-12.2	37
CG (550)	-13.1	54	-10.0	--

[a]Charcoals (Py-OM) from Kuo et al[26]. [b]Py-WSOM produced for this study.

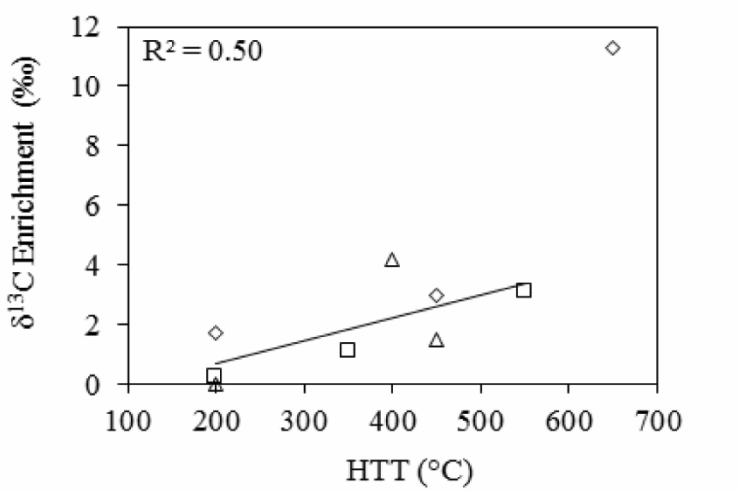

Figure 3. Stable carbon isotope ($\delta^{13}C‰$) enrichment of charcoal extracts (Py-WSOM) in respect to their particulate charcoal feedstock (Py-OM) across the heat temperature treatment (0-650°C). Honey mesquite, cord grass and loblolly pine represented by diamonds, squares and triangles, respectively.

2.3.2 FTIR spectral interpretation and thermogravimetric analysis

The -OH stretch peak broadness (3650-3100 cm^{-1}) is larger for Py-WSOM from all three plant types relative to the Py-OM char-feedstock. The -OH stretch peak broadness for Py-WSOM decreases with increased charcoal feedstock HTT. The relative CH stretch (3100-2700 cm^{-1}) peak intensity is larger for all three Py-OM plant types relative to the Py-WSOM extracts. All three PI, HM and CG Py-OM spectra illustrate increased shouldering at 2700 cm^{-1}, which are most likely associated with aldehyde functional groups (Figures 4-6). Peaks associated with asymmetrical methylene (CH_2) and asymmetric methyl groups (CH_3), 2930 and 2860 cm^{-1}, are sharpest at 200°C for all three Py-OM plant types and their respective Py-WSOM char-extracts. In all three Py-OM plant types the aromatic CH peak intensity (900-650 cm^{-1}) increases with increased HTT (Figures 4-6).

The peak intensity within the C-O/C-O-C bending region (1300-1000 cm^{-1}) is shifted to higher wavenumbers (associated with C-O functional groups) for Py-OM plant types created above 200°C, (Figures 4A, 5A and 6A). Similarly, Py-WSOM created above 200°C has a shift in peak intensity within the C-O/C-O-C bending region to higher wavenumbers, illustrating that the Py-WSOM is enriched in C-O functional groups that are derived from the parent charcoal feedstock (Figures 4B, 5B and 6B).

The Py-OM char-feedstock contains increasing C=O, C=C-C and OCH_3 surface functionality with increasing HTT (Figures 4A, 5A and 6A). In comparison, the increase in HTT, above 200°C, reduces the surface functionality related to C=O, C=C-C and OCH_3 bond associations within the three Py-WSOM plant types (Figures 4B, 5B and 6B). Furthermore, we see that the low temperature, 200°C Py-WSOM char-extracts, contain the largest proportion of C=O, C=C-C and OCH_3 surface functional groups relative to the higher Py-WSOM char-extracts (>200°C).

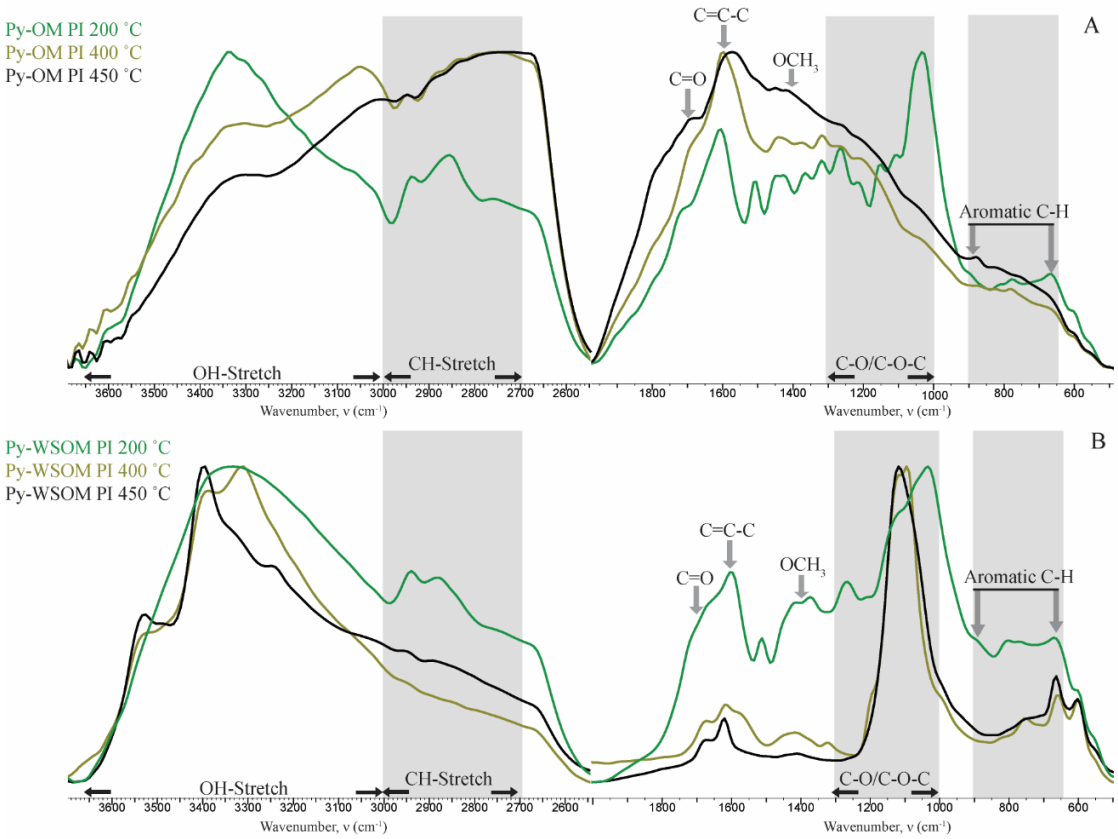

Figure 4. ATR-FTIR spectra of the OH-CH stretching region (3650-2600 cm^{-1}) and fingerprint-bending region (1900-600 cm^{-1}) for loblolly pine (PI), charcoal feedstock (Py-OM), combusted from 200-450°C (A) and water soluble extract (Py-WSOM) (B).

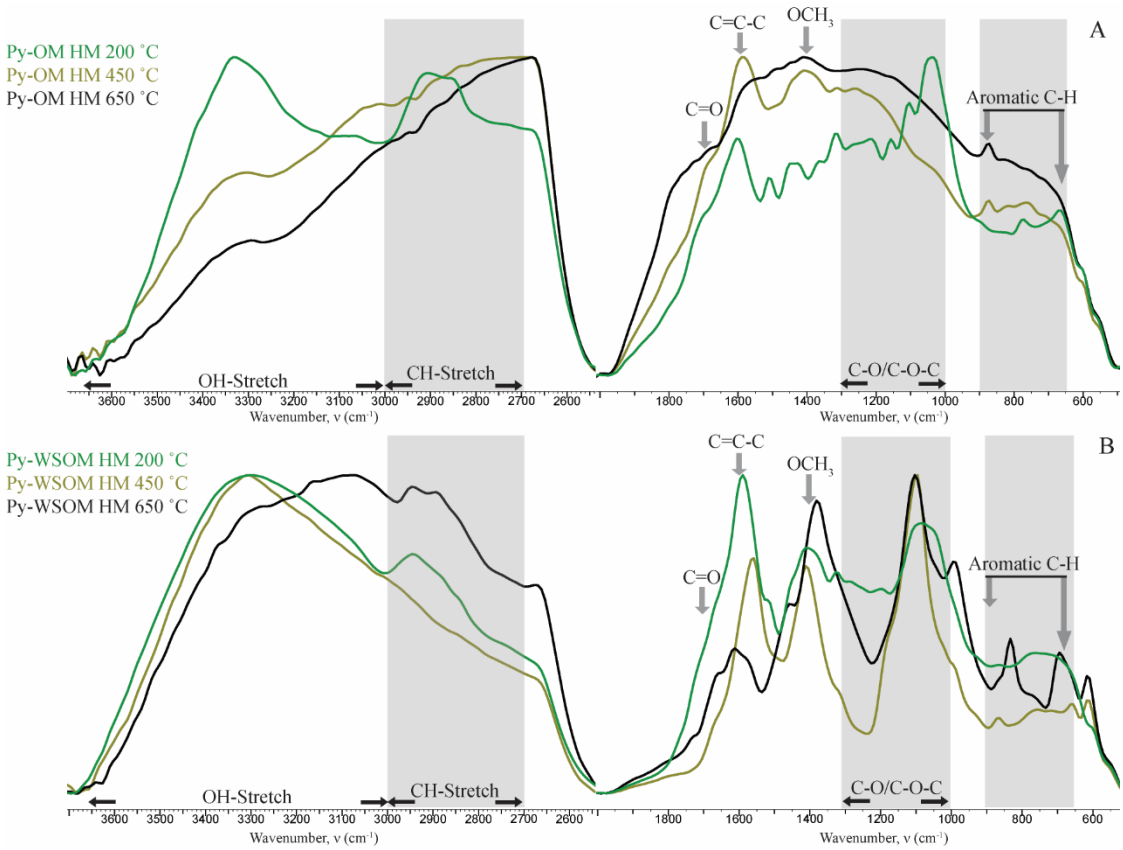

Figure 5. ATR-FTIR spectra of the OH-CH stretching region (3650-2600 cm^{-1}) and fingerprint-bending region (1900-600 cm^{-1}) for honey mesquite (HM), charcoal feedstock (Py-OM), combusted from 200-450°C (A) and water soluble extract (Py-WSOM) (B).

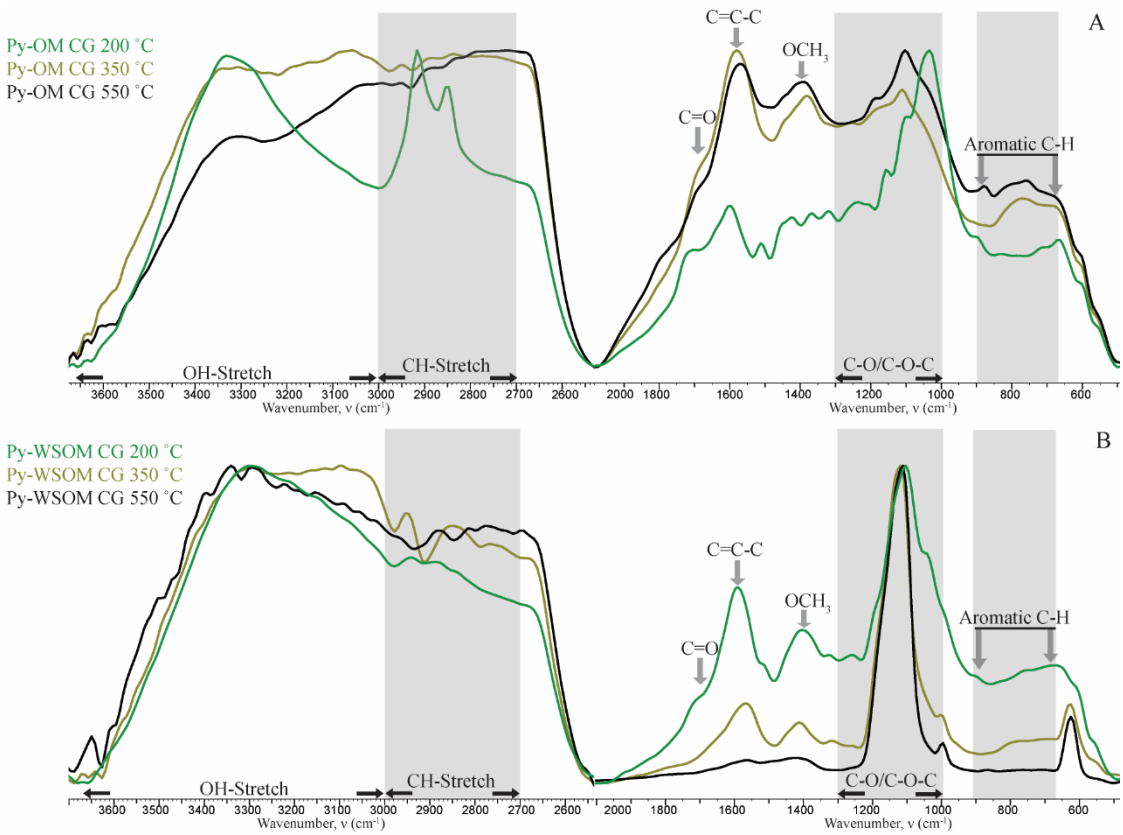

Figure 6. ATR-FTIR spectra of the OH-CH stretching region (3650-2600 cm^{-1}) and fingerprint-bending region (1900-600 cm^{-1}) for cord grass (CG), charcoal feedstock (Py-OM), combusted from 200-450°C (A) and water soluble extract (Py-WSOM) (B).

The Py-WSOM spectral absorption ratio of C-O to C=C-C peaks at relatively low HTT (200-400°C), compared to Py-OM char-feedstocks (Figure7). Similarly, the ratio of C-O to C-O-C is higher in the Py-WSOM compared to the Py-OM feedstock. The spectral absorption ratio of C-O to OCH_3 is higher in the CG Py-WSOM compared to all other char-extracts and Py-OM char-feedstocks. The Py-WSOM spectral absorption ratio of the fire derived molecular marker levoglucosan to C-O-C peaks at relatively low temperatures (200-400°C), compared to the Py-OM char-feedstocks (Figure 7). While the Py-WSOM absorption ratio of levoglucosan to C-O peaks from

200-350°C for only PI 200°C and CG 350°C, likely due to the decomposition of levoglucosan at temperatures above 400°C. Finally, the spectral absorption ratio of levoglucosan to OCH_3 is highest in the CG Py-WSOM char-extracts, peaking at CG 350°C (Figure 7).

The significant linear correlations for the spectral absorption ratios C-O:OCH_3, C-O:C=C-C and levoglucosan:C-O for both Py-OM and the Py-WSOM char-extracts are illustrated in Figure $8_{A\text{-}C}$. The highest significant linear correlation for the spectral absorption ratios is R^2=0.80, for levoglucosan to C-O (p=0.031) (C). The lowest significant linear correlation for the spectral absorption ratios is C-O to C=C-C (R^2=0.50, p=0.003) (B). The significant linear correlation C-O to OCH_3 has an R^2=0.64, (p=0.011) (A). The comparison of Py-WSOM vs. Py-OM spectral absorption ratios (Figure 9) illustrates an enrichment of C-O functionalized carbon which is likely associated with levoglucosan and methoxy-phenol formation at relatively low-mid HTT.

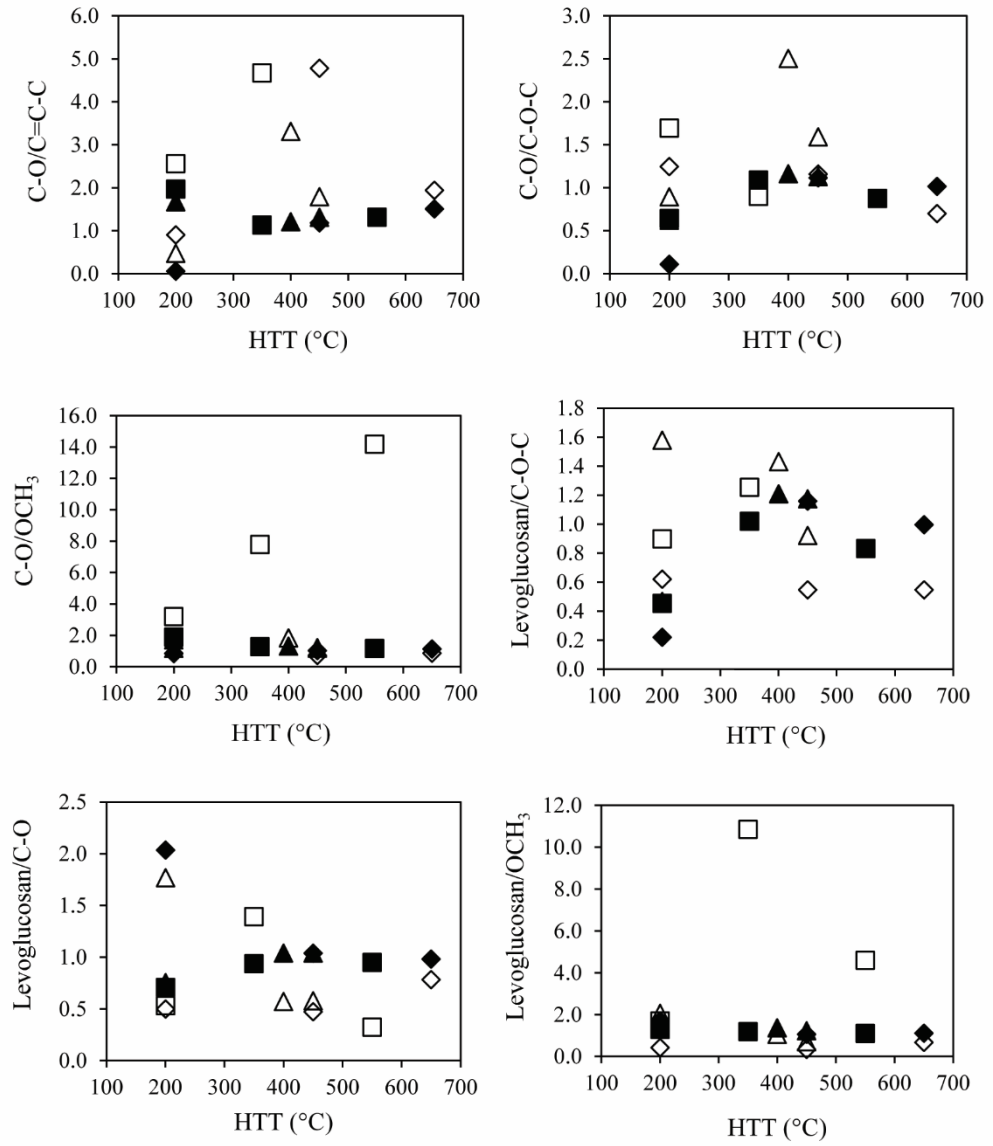

Figure 7. Spectral absorbance ratios of pyrogenic water soluble organic matter (Py-WSOM) and pyrogenic particulate organic matter (Py-OM); created along a low heat temperature treatment (0-650°C). Py-OM, for HM, CG and PI, are represented with solid diamonds, squares and triangles, respectively. Py-WSOM, for HM, CG and PI, are represented with open diamonds, squares and triangles, respectively.

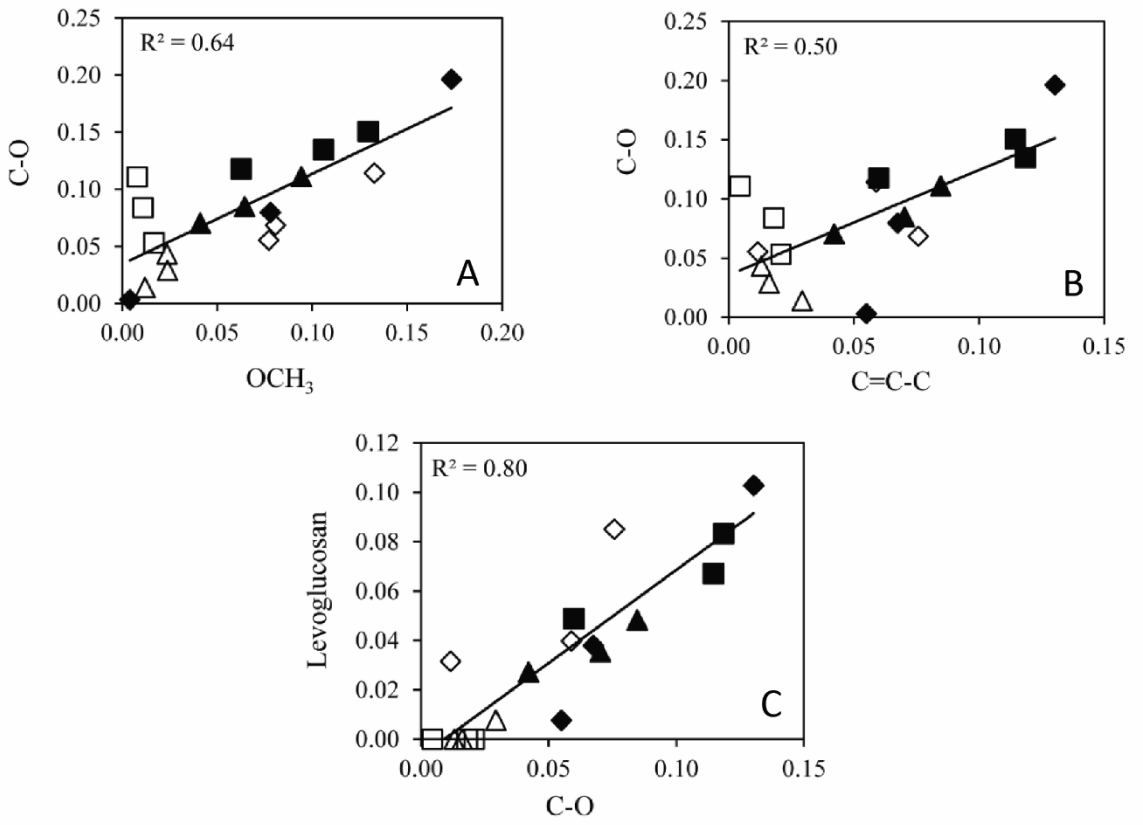

Figure 8. Significant relationships for functional absorbance peak height for pyrogenic water soluble organic matter (Py-WSOM) and pyrogenic particulate organic matter (Py-OM). A, B and C represent the ratios of C-O:OCH_3, C-O:C=C-C and levoglucosan:C-O, respectively. Py-OM, for HM, CG and PI, are represented with solid diamonds, squares and triangles, respectively. Py-WSOM, for HM, CG and PI, are represented with open diamonds, squares and triangles, respectively.

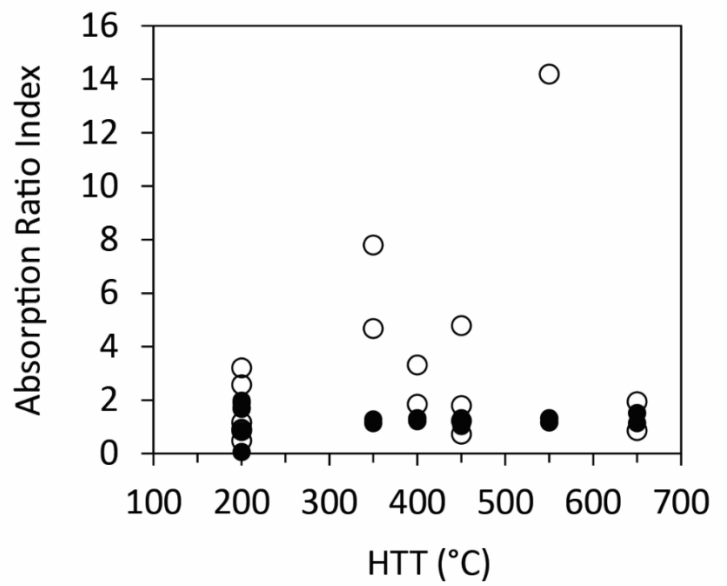

Figure 9. Spectral absorbance ratios for selected functional groups: C-O/C=C-C, C-O/OCH_3 and levoglucosan/C-O. Pyrogenic particulate organic matter (Py-OM) is represented with solid circles and pyrogenic water soluble organic matter (Py-WSOM) is represented with open circles.

Thermograms of Py-WSOM char-extracts are illustrated in Figure 10A-C. Weight loss associated with heat temperature treatment (HTT) is represented by solid lines. The derivative weight percent loss associated with temperature, for all three Py-WSOM char-extract plant types, are illustrated by dashed lines. The multiple peaks of thermal biomass decomposition highlights that Py-WSOM contains a mixture of cellulose, hemicellulos and lignin. For example, both PI and CG 200°C have derivative weight loss peaks around 200-325°C and 500°C. In comparison, 400°C and 450°C Py-WSOM PI have derivative weight loss peaks around 475°C and 625°C. The HM Py-WSOM 200°C extract has a derivative weight loss peak around 200-325°C and 525°C, indicating a mixture of cellulose, hemicellulose and lignin.

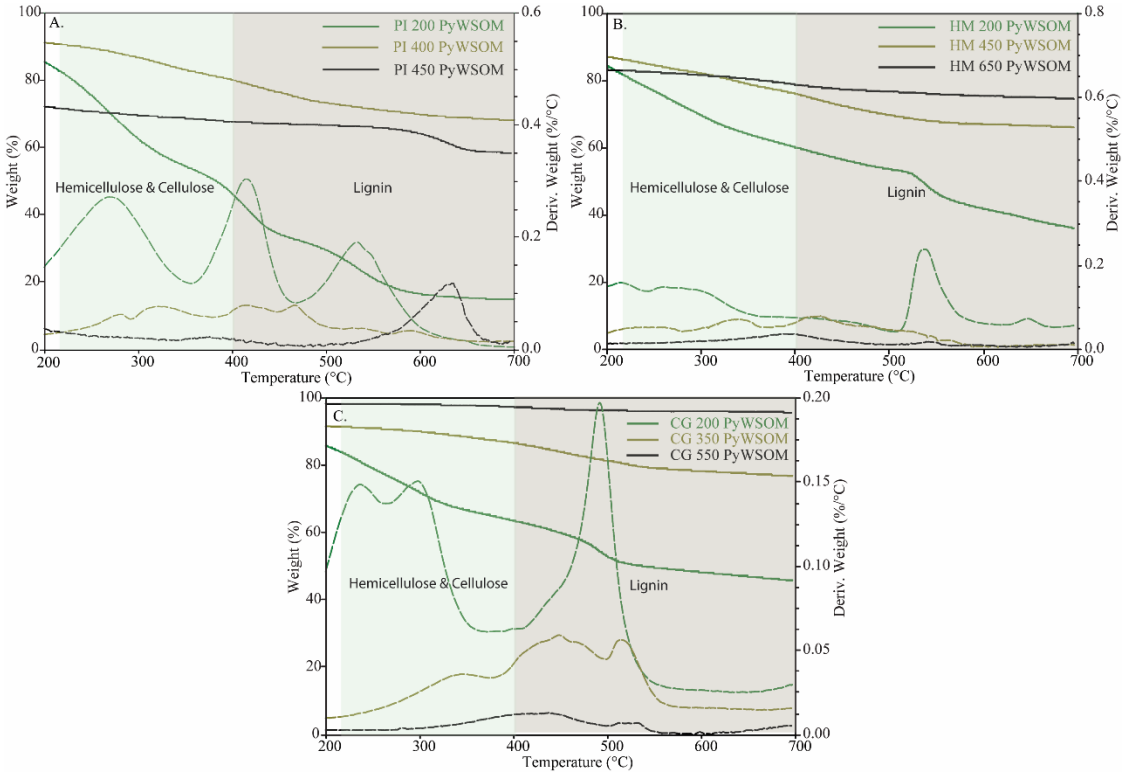

Figure 10. Thermograms of pyrogenic water soluble organic matter (Py-WSOM) representing (A) loblolly pine (PI), (B) honey mesquite (HM) and (C) cord grass (CG). Weight loss associated with heat temperature treatment (HTT) is represented with the solid lines. The second derivative of weight loss associated with HTT is represented with the dashed line.

2.4 Discussion

The spreading of the Py-WSOM spectra toward lower wave numbers in the -OH stretch region (3700-3100 cm^{-1}) suggests a higher amount of -OH bonding with water, which likely indicates increased surface polar functionality (Figures 4-6). There is a shift in intensity towards C-O vibrations in the C-O/C-O-C region (1300-1000 cm^{-1}). The shift in intensity from C-O-C vibrations ≈ 1000 cm^{-1} (attributable to the ring structure of carbohydrates) in the chars towards C-O vibrations (≈ 1108 cm^{-1}) can be attributed to the fact that the Py-WSOM is enriched in C-O functional groups derived from heat-induced

depolymerization and defragmentation of hemicellulose and cellulose during char formation (Pastorova et al., 1994, Bilba and Ouensanga, 1996, Harvey et al., 2012b).

Harvey et al 2012b, identifies three dominant peaks 3285 cm^{-1}, 3350 cm^{-1}, and 3435-3450 cm^{-1} which are indicative of inter-chain -OH bonds in hemicellulose-cellulose that have been weakened and shifted to higher wavenumbers during the charring process (Harvey et al., 2012b). Our spectra for the three Py-OM feedstocks also agree with Harvey et al., 2012b, with observable peaks at 3650-3630 cm^{-1} and 3240-3220 cm^{-1}, which are attributed to free -OH and hydroxyls from carboxylic groups, respectively (Figures 4A, 5A, and 6A). These peaks are most likely associated with molecular transformations in biochars during hemicellulose- cellulose oxidation and are responsible for an increase in the concentration of free -OH and carboxylic groups on the surface of Py-OM formed between 300°C and 400°C (Harvey et al., 2012b).

The thermal degradation of lignocellulose among the charcoal feedstock's not only releases a functional rich Py-WSOM at low HTT (200-650°C), but the type of functional constituents released into the water-soluble fraction is directly related to the HTT of the charcoal feedstock. The PyC associated to Py-WSOM is a dynamic pool of carbon, with highly soluble functional groups being created during the fragmentation of lignocellulose. This creates Py-WSOM rich in –OH and C-O functional groups, potentially facilitating the solubilization of low to mid temperature PyC. Due to this PyC fractions high solubility in water, these organics may bypass soil sorption and act as important contributors to exported DOM in fire-impacted watersheds (Myers-Pigg et al., 2017). In addition, the microbial degradation and alteration of this Py-WSOM could

potentially prime the breakdown of more recalcitrant dissolved pyrogenic carbon (Masiello and Louchouarn, 2013).

The three main components of biomass- hemicellulose, cellulose and lignin undergo thermal decomposition at different temperatures, with little to no significant pyrolytic interaction between the three groups (Yang et al., 2006). In controlled laboratory studies, the initial step in biomass pyrolysis is moisture evolution occurring at temperatures below 220 °C, followed by the thermal decomposition of hemicellulose, cellulose and lignin backbone (at 220-315 °C, 315-400 °C and >400 °C, respectively (Yang et al., 2006, Liu et al., 2011). Therefore, the second derivative weight loss (%/°C) for HM, CG and PI Py-WSOM illustrate three distinct regions attributed to the presence of hemicellulose, cellulose and lignin (Figure 10). Figure 10 illustrates that the largest peaks in %/°C, corresponding to hemicellulose and cellulose, belong to low temperature Py-WSOM (CG, PI and HM 200 °C). In comparison, Py-WSOM extracted from higher temperature Py-OM contain lower proportions of hemicellulose and cellulose and higher proportions of lignin by-products.

Harvey et al., created a recalcitrance index (R_{50}) that uses the temperature in which half of the Py-OM material thermally decomposes (T_{50}) and normalized this to the temperature in which graphite thermally decomposes. Furthermore, Harvey et al., normalized the R_{50} by the ash-free carbon content (%), in order to develop an index for the lability of terrestrial organic matter and Py-OM. We compared the R_{50} and ash-free carbon content of the Py-OM charcoals used in Harvey et al., (2012a) to the Py-WSOM char-extracts associated with these parent char-feedstocks (Harvey et al., 2012a). The

comparison of the char-extracts and char-feedstocks illustrate that across the HTT, Py-OM has a higher R_{50} and ash-free carbon content when compared to Py-WSOM (Figure 11).

The increase in Py-WSOM recalcitrance and decrease in ash-free carbon content is opposite of what we see in the particulate char (Figure 11). We see that at low HTT (200-350°C), the Py-WSOM plots closer to the unburned and low temperature parent charcoal feedstock. In comparison, as the HTT increases for the parent char Py-OM there is a further decrease in ash-free carbon content and increase in recalcitrance, causing a further decoupling from the parent char Py-OM from the Py-WSOM char-extract. This data indicates that Py-WSOM is potentially more labile compared to the parent char-feedstock and that higher temperature Py-WSOM potentially increases in recalcitrance with increasing feedstock HTT (Figure 11).

Ziolkowski and Druffel (2010), used radio carbon and benzene polycarboxylic acids (BPCAs) to quantify riverine and marine BC associated with ultra-filtered dissolved organic matter (UDOM-BC) (Ziolkowski and Druffel, 2010). The authors point out that UDOM-BC measured within rivers have a more modern ^{14}C age and a higher degree of aromatization while oceanic samples contain an older ^{14}C age and lower degree of aromatization (Ziolkowski and Druffel, 2010). The ageing of riverine dissolved BC and dissolved organic carbon (DOC) decreases the degree of aromatization and molecular weight due to photo-chemical and biochemical oxidation (Amon and Benner, 1996, Ziolkowski and Druffel, 2010).

The decrease in carbon density and increase in recalcitrance of high temperature Py-WSOM (Figure 11) illustrates that high temperature Py-WSOM is similar with marine UDOM-BC. Therefore, we would expect that as Py-OM HTT increases the recalcitrance of Py-WSOC released into the water soluble fraction will also increases (Figure 11).

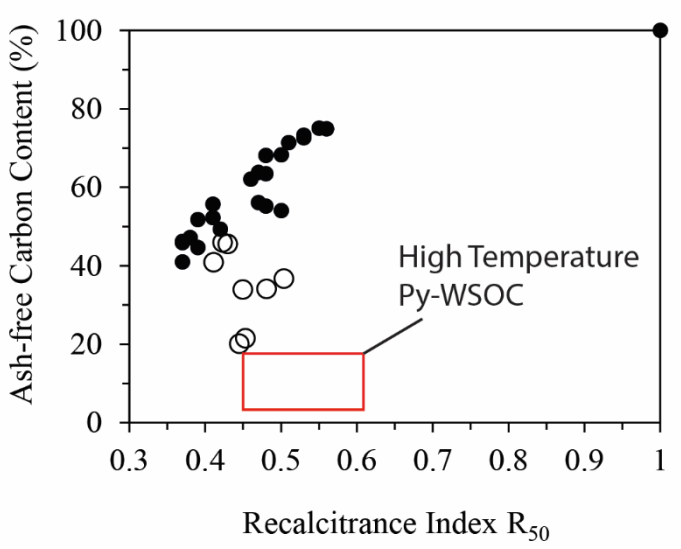

Figure 11. Recalcitrance index (R_{50}) with respect to carbon content. Pyrogenic particulate organic matter (Py-OM) for HM, CG and PI are represented with solid circles (Harvey et al., 2012a). Pyrogenic water soluble organic matter (Py-WSOM) for HM, CG and PI are represented with non-solid circles.

Zmmerman et al., (2011) incubated low-mid temperature char in soils (biochar) for 485 days. They found that the soil evolved $\delta^{13}CO_2$ signature is -27 – -24 ‰, indicating that the labile soil organic matter is associated with C3 biomass. Furthermore, the biochemical fractionation of biochar by microbes is highlighted by the soil $\delta^{13}CO_2$-BC signature being enriched by 0.6 – 7.6 ‰ (Zimmerman et al., 2011). This enrichment

factor illustrates that the labile fraction of carbon that is degraded during the early stages of biochar decomposition is related to isotopically enriched carbohydrates, while, isotopically depleted polymeric lignin is likely preserved within the particulate char (Opsahl and Benner, 1995, Benner et al., 1987).

In comparison, our study illustrates that Py-WSOM becomes more enriched in $\delta^{13}C$ (0.1 – 4.5 ‰) with increasing HTT (Figure 3). This enrichment matches the microbial evolved $\delta^{13}CO_2$-BC signature presented in Zimmerman et al. (2011). This illustrates that microbes are likely degrading labile Py-C in soils that are isotopically similar to low-mid temperature Py-WSOC.

The pyrogenic depolymerization and decomposition of lignocellulose creates a range of molecular components directly related to the HTT and vegetation feedstock. This pyrolysis creates varying size fractions of PyC that potentially have different residence times in the environment due to their recalcitrance nature. The results from this study illustrate that low-mid temperature Py-WSOC is rich in –OH and C-O functional groups and likely associated with labile PyC. The high temperature Py-WSOC is likely associated with smaller molecules, with decreased carbon density, and are more recalcitrant in the environment (Masiello and Druffel, 1998).

The release of Py-WSOC is facilitated through the interaction of polar-molecular-surface functionality (-OH and C-O) created through the thermal breakdown of lignocellulose. The lower R_{50} normalized to ash-free carbon content, in Py-WSOM, suggests solubilization of a more labile fraction of Py-WSOC in comparison to the particulate charcoal feedstock at low temperatures. Stable carbon isotope signatures for

the particulate and water soluble fraction highlights the release of an enriched-labile fraction of Py-WSOC. This indicates that there is a selective solubilization of carbohydrates and free lignin phenols into the water soluble phase. While, the more recalcitrant polymeric lignin is preserved in the particulate parent char-feedstock. Furthermore, emphasizing that during the pyrolysis of plant biomass, there is a fraction of water soluble organic carbon created, which is more labile than its particulate charcoal feedstock. This water soluble fraction is likely associated with components in the plant cell wall (lignocellulose), indicating that carbohydrate rich carbon constituents and free lignin phenols are selectively released from Py-OM into Py-WSOM at low-mid HTT.

III. CHARACTERIZATION AND BIODEGRADATION OF WATER-SOLUBLE BIOMARKERS AND ORGANIC CARBON EXTRACTED FROM LOW TEMPERATURE CHARS*

3.1 Introduction

Biomass burning, whether from wildfires, prescribed burning or heating/cooking activities, is recognized as a significant source of pyrogenic carbon (PyC) in atmospheric, terrestrial, and aquatic systems (Preston and Schmidt, 2006, Running, 2006, Running, 2008, Bowman et al., 2009, Gustafsson et al., 2009, Ding et al., 2012, Singh et al., 2012). However, because current methodologies do not allow detection of the full Py-C continuum, accurate fluxes of PyC to environmental reservoirs cannot be fully constrained. Most studies measure a fraction of the biomass combustion continuum in the mid- to high temperature range and assume a certain "analytical homogeneity" for PyC (Singh et al., 2012), when in fact there exists a large amount of "compositional heterogeneity" in biomass combustion byproducts (Knicker et al., 2008, Alexis et al., 2010, Keluweit et al., 2010, Harvey et al., 2012b). This compositional heterogeneity is often related to combustion conditions, with temperature acting as a predominant control for structural changes in PyC and ultimately its turnover in the environment (Alexis et al., 2010, Keluweit et al., 2010, Zimmerman, 2010, Harvey et al., 2012b, Singh et al., 2012). Despite recent findings that low temperature PyC is characterized by higher

*Reprinted from *Organic Geochemistry* **2013** "Characterization and biodegradation of water-soluble biomarkers and organic carbon extracted from low temperature chars". 59, 111-119. Norwood, M. J., Louchouarn, P., Kuo, L.-J. & Harvey, O. R Copyright (2016), with permission from Elsevier.

reactivity and thus shorter half-life (Zimmerman, 2010, Luo et al., 2011, Singh et al., 2012), tracers of low temperature biomass combustion are only regularly monitored in atmospheric particles, with a handful of studies tracing these markers in sediments (Elias et al., 2001, Hunsinger et al., 2008, Kuo et al., 2011b), ice cores (McConnell et al., 2007, Kawamura et al., 2012) and dissolved organic matter (DOM; (Hockaday et al., 2007, Dittmar, 2008, Dittmar et al., 2012, Ziolkowski and Druffel, 2010)). In fact, little is known about the role that wildfires and other biomass combustion activities may play in the transfer of labile terrigenous OM to the environment, including aquatic systems.

Carbon emissions from fires result in both direct and indirect effects, whereby direct effects include the transformation of vegetation and dead OM into aerosols and greenhouse gases and indirect effects include the transfer of biomass to dead and "slow" decomposing pools where carbon is predicted to be released slowly to the atmosphere (Ghimire et al., 2012). How slowly or rapidly this latter carbon pool turns over is uncertain and will probably depend on the structure of material remaining on stumps or deposited as litter fall. During a prescribed burning experiment in a scrub oak ecosystem, Alexis et al. (2007) showed that, after loss to the atmosphere, the vast majority of post-fire carbon fluxes from the standing vegetation occurred as "unburned" litter fall (75% of the flux) as opposed to char (25% of the flux). In addition, Alexis et al. (2010) indicated that a substantial fraction of the initially labeled unburned fraction actually occurred as thermally altered "brown carbon" with structural characteristics (large proportion of O-alkyl components, limited aromatic structures) very similar to those of low temperature chars (Keluweit et al., 2010, Harvey et al., 2012b). Because soluble

molecular markers of combustion are released in substantial quantity from the solid remains of charred vascular plant materials (Evans et al., 1986, Kuo et al., 2008a, Kuo et al., 2011a), major wildfire events in watersheds may thus promote the rapid transfer of terrigenous DOM to aquatic systems. A recent study by Dittmar et al. (2012) estimated that the land-ocean flux of dissolved PyC, from a relict burnt forest biome in Brazil, is such that it can impact global ocean biogeochemical cycles on centennial to millennial scales. However, these latter fluxes are yet again focused on highly recalcitrant forms of PyC, namely the condensed carbonaceous residues enriched in polycyclic aromatic carbons. Although using such an analytical window can help understand how biomass combustion could increase the size of the refractory pool of dissolved organic carbon in the deep ocean (Dittmar et al., 2012), the fluxes of labile low temperature PyC and their impact on stream and ocean respiration are missing. The addition of hydrophilic markers of biomass combustion to the currently monitored hydrophobic and condensed combustion by-products (e.g. anyhydrosugars and lignin phenols vs. benzenepolycarboxylic acids, respectively; (Kuo et al., 2008a, Kuo et al., 2011a, Ziolkowski et al., 2011, Dittmar et al., 2012) in DOM can extend our understanding of potential impacts of fire on carbon cycling at the watershed scale, and warrant further study.

In this study, the fate of pyrogenic water-soluble organic matter (Py-WSOM) was evaluated by incubating extracts from low temperature chars with natural river water collected from a coastal environment in Eastern Texas. Levoglucosan, lignin biomarkers (free and polymeric), and dissolved organic carbon (DOC) were monitored

over the incubation. The resulting information is critical for evaluating (i) the rate(s) of reaction of different water-soluble constituents of PyC and their potential to act as an energy source for aquatic microorganisms, and (ii) the potential for such molecular markers to act as viable tracers for the movement of Py-WSOM in aquatic environments at relevant time scales of transport in rivers and coastal systems (days to weeks). Finally, the high yield of fragmented and soluble molecular components from vascular plant polymers also provides an ideal mixture for investigating the fate of model compounds of vascular plant OM under ideal incubation conditions.

3.2 Material and methods

3.2.1 Preparation and characterization of chars and Py-WSOM

Two different angiosperms, honey mesquite (HM: P. *glandulosa*) and cordgrass (CG: S. *spartinae*), were selected. The samples were collected from Laguna Atascosa Natural Wildlife Refuge (Rio Hondo, TX) in July 2005. A detailed description of char preparation is given by Kuo et al (2008a). Briefly, the plant material was cut into small pieces, dried (60ºC), and combusted (1 h) at 250°C under O_2 limited conditions. Although this temperature falls in the lower values of the range of measured in forest fires (260-816°C; (Alexis et al., 2007)), combustion temperatures in soils drop rapidly even below 100°C (Alexis et al., 2007). In addition, we chose this particular temperature because it represents a fraction of the black carbon continuum that has been little studied and shows large yields of soluble constituents (see discussion below). Homogenized char (<60 mesh; ca. 2 g) from each plant was mixed with precombusted sand and extracted using accelerated solvent extraction (ASE), with MilliQ water as solvent

(100°C) at 1500 psi. Each extract was filtered through a precombusted GF filter (≈ 0.45 µm) and the solution brought up to a volume of 250 mL using Milli-Q water.

Both the unextracted chars and their respective Py-WSOM were analyzed using Fourier transform infrared spectroscopy (FTIR; Varian 3100 IR spectrometer with ATR from PIKE Technologies Inc., Madison WI). Spectra were collected across the range 4000-500 cm^{-1} at a resolution of 16 cm^{-1}, and a total of 500 co-added scans were applied (Harvey et al., 2012b). All spectra were background corrected against a diamond reference, baseline corrected and subjected to a 5 point S-G quad-cubic function as the smoothing filter (Savitzky and Golay, 1964).

3.2.2 Incubation experiment

The extracts for incubation were inoculated with 2 mL (10%, v/v) filtered water, sampled from the Trinity River, TX (29° 48'45.03" N 94° 43'54.11" W; January 12, 2011). Controls were treated with 1.5 mL (15M) NaN_3 to kill any native bacteria. The low concentration of dissolved organic carbon (DOC: ca. 5 $mg \cdot L^{-1}$), lignin oxidation products (LOPs: ca. 6 $ug \cdot L^{-1}$), and levoglucosan (not detected) in the river water had a negligible effect on the Py-WSOM concentration (< 0.01-0.3% of total). Duplicate vials were prepared for five incubation and control time periods (T_0-T_{12}). Incubations were conducted under aerobic conditions, in the dark, and continuously shaken.

3.2.3 Molecular and elemental analyses

The free monomers (levoglucosan and free lignin phenols) were sequentially extracted from char extracts on the basis of modifications to the methods of (Kuo et al., 2008a, Kuo et al., 2011a) and (Louchouarn et al., 2009). Deuterated trans-cinnamic acid

(d7-trans-cinnamic acid) was used as surrogate standard for lignin phenols, while d7-levoglucosan was used as the surrogate for levoglucosan analysis. The aqueous solutions were acidified to pH < 2 using 6M HCl and lignin phenols were extracted using EtOA. After treatment with Na_2SO_4 to remove excess water, the extracts were evaporated using a LabConco™ solvent concentrator. The post-EtOA extraction water was freeze-dried to a paste. Both dried samples were dissolved in pyridine.

Lignin oxidation products (LOPs) in the char extracts were analyzed using the CuO oxidation method (Hedges and Ertel, 1982, Louchouarn et al., 2010, Louchouarn et al., 2000) with slight modifications. Freeze-dried char extracts were reconstituted with 2N NaOH (pre-sparged with Ar). The NaOH aliquots were transferred to a reaction mini-vessel pre-loaded with CuO $Fe(NH_4)_2(SO_4)_2 \cdot 6H_2O$. The vessels (n = 12) were heated at 155ºC for 3 h in a customized Hewlett-Packard 5890 gas chromatograph fitted with a revolving carousel. Upon oxidation, the surrogate standard d7-trans-cinnamic acid was added directly (ca. 3-12 µg) to each mini-vessel and solutions were extracted with EtOA and reconstituted in pyridine as described above.

Aliquots of pyridine solutions were derivatized (30 min) using N,O-bis (trimethylsilyl)trifluoroacetamide (BSTFA) containing 1% trimethylchlorosilane (TMCS; Supelco, PA, USA) at 75°C. Separation and quantification of trimethylsilyl (TMS) derivatives of levoglucosan and lignin phenols (both free and polymeric) was performed using a Varian triple quadrupole 480-300 gas chromatographer-mass spectrometer (GC-MS) system fitted with a fused silica column (J&W DB-5MS, 30 m x 0.25 mm i.d., 0.25 µm film thickness; Agilent Technologies). Each sample was injected,

in split-less mode using He as carrier gas (1.0 $mL \cdot min^{-1}$). The GC oven was programmed from 65°C (2 min) to 300°C (held 10 min) at $4°C \cdot min^{-1}$. The GC injector and GC-MS interface were maintained at 280°C and 270°C, respectively. The mass spectrometer was operated in the electron ionization mode (EI, 70 eV) using full scan mode (FS). Compound identification was performed using GC retention times and by comparing mass spectra with those of commercially available standards. The recovery of free monomers (levoglucosan and lignin phenols) was tested using the identical sequential extraction described above on a MilliQ solutions spiked with the full suite of monomer and surrogate standards. No trace of levoglucosan was found in the EtOA extract and no trace of phenols was found in the reconstituted freeze-dried water. The average recovery of levoglucosan and lignin phenols was 98 ± 4% and 100 ± 9%, respectively.

Additional tests were performed to quantify the recovery of the free lignin phenols following CuO oxidation. The high recovery observed for free lignin phenols (97 ± 1%) suggested that these monomers are preserved upon CuO oxidation. Thus the LOP values in the char extracts represent the sum of polymeric and monomeric phenols in that particular sample. The total dissolved organic carbon (DOC) concentration in 2 ml subsamples was determined at each sample period using a Shimadzu TOC analyzer.

Analytical and statistical analysis

Duplicate incubations were performed for five time periods (T_0-T_{12}) to evaluate the variability for both biomarker series. The average coefficient of variability (CV) for lignin concentration across replicate periods was 2.6 ± 3.2% and 2.8 ± 3.3% for the

control and incubation time series, respectively. The average CV for levoglucosan concentration was 2.8 ± 3.1% and 3.9 ± 4.2% for the control and incubation series, respectively. To estimate significant departures in biomarker concentrations in incubations from the natural experimental variability of analysis, the expanded uncertainty (U) around the average of all controls (n = 14), was calculated as U = ks, where s is one standard deviation of the analyte mean, and k is the coverage factor determined from the Student's t-distribution corresponding to the associated degrees of freedom at the 95% confidence level (NIST, 2007).

3.3 Results and discussion

3.3.1 Characterization of Py-WSOM

Significant difference between the functional group chemistry of the unextracted chars and Py-WSOM were apparent in all major regions of the FTIR spectrum (Figure 12) and highlighted the strong polar character of the Py-WSOM. For example, the spreading of the Py-WSOM spectra (compared to that of the char) towards lower wavenumbers in the OH-stretch (3700-3100 cm^{-1}) region suggested a higher amount of H bonding with water -OH which is consistent with the expectation for highly polar material. The higher polarity of the Py-WSOM vs. the chars is also supported by the relatively lower intensity/sharpness of vibrations in the CH-stretch (3100-2700 cm^{-1}) region, as well as the shift in intensity towards C-O vibrations in the C-O/C-O-C region (1300-1000 cm-^{1}). The shift in intensity from C-O-C vibrations around 1000 cm^{-1} (attributable to the ring structure of carbohydrates) in the chars towards C-O vibrations (around 1140 cm^{-1}) was consistent with the Py-WSOM being enriched in C-O functional

groups derived from heat-induced depolymerization and defragmentation of lignin and cellulose during char formation (Pastorova et al., 1994, Bilba and Ouensanga, 1996, Harvey et al., 2012b).

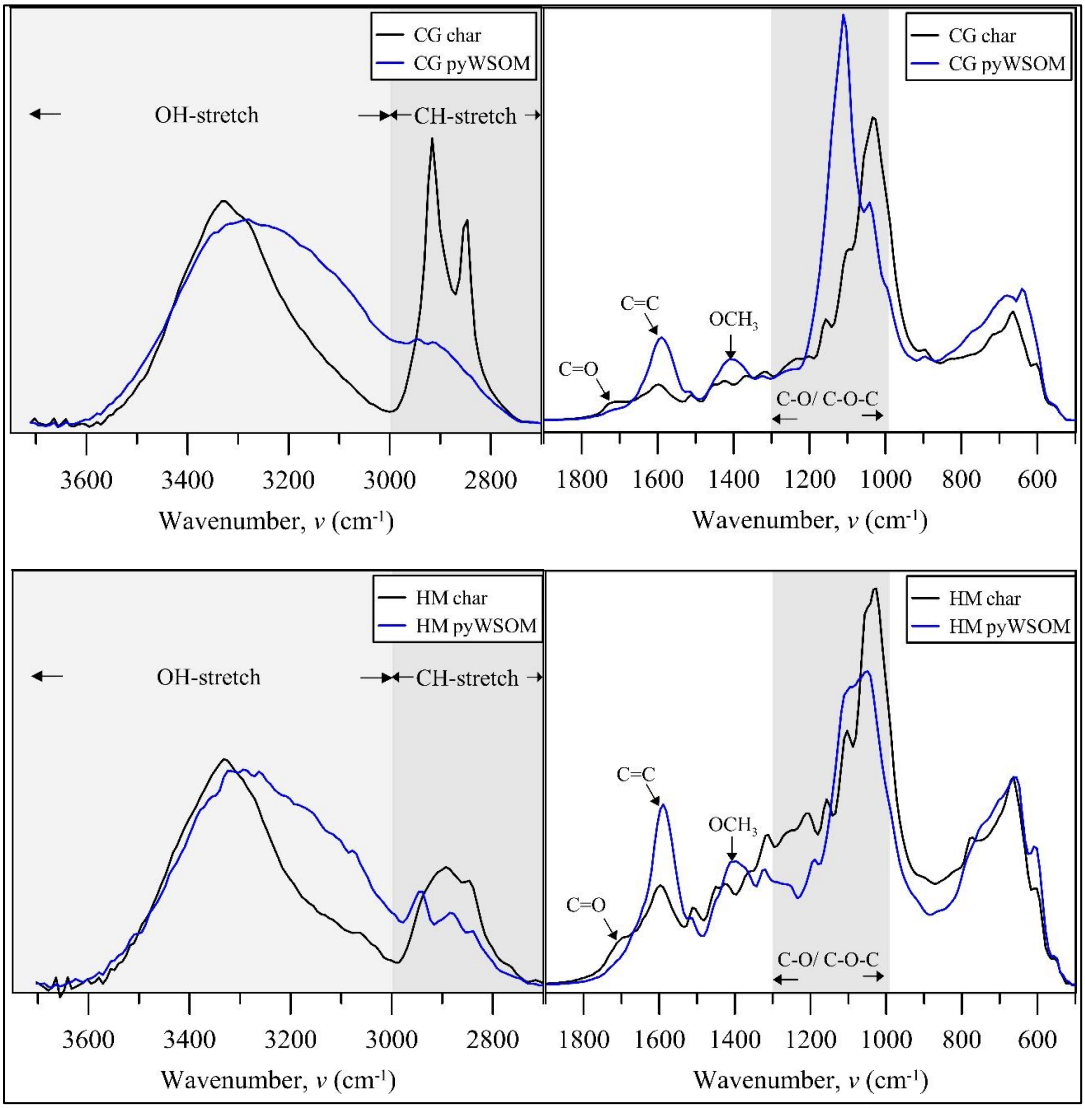

Figure 12. ATR-FTIR spectra in the fingerprint region (600-1800 cm^{-1}) and OH-CH stretch region (2700-3600 cm^{-1}) of unextracted chars, made from cordgrass (CG: top) and honey mesquite (HM: bottom) feedstocks, and their water-soluble fraction (Py-WSOM).

The low temperature degradation and depolymerization of cellulose components, most likely via a transglycosylation pathway (Harvey et al., 2012b), is supported by the reported peak yields of levoglucosan (anhydrosugar biomarker for transglycosylation; (Molton and Demmitt, 1977)) in the 250-300ºC combustion range (Figure 1). A similar peak for free lignin monomers occurs in the same temperature range, concomitant with a sharp decrease in the yield of polymeric lignin by-products (Figure 1), confirming the start of lignocellulose depolymerization and the release of monomeric soluble components. This is consistent with the significant cleavage of aryl-alkyl ether (C-O-C) linkages and dehydration recorded in pyrolized lignin models at a temperature as low as 220ºC (Haw and Schultz, 1985).

The amount of Py-WSOC extracted from the chars is summarized in Table 3 (16 and 21.5 $mg \cdot gdwt^{-1}$ for HM CG, respectively) which was 4-10 fold higher than recently reported values for water-extractable OC (Luo et al., 2011, Abiven et al., 2011). One plausible reason for this difference could be that a higher proportion of soluble constituents was present in our low temperature chars, as opposed to lower values observed in chars produced at temperatures >350ºC (<4 $mg \cdot gdwt^{-1}$ and <13 $mg \cdot gdwt^{-1}$ in HM and CG chars, respectively; data not shown). Alternatively, the high concentrations observed in the present study with respect to the few available data in the literature may also be due to the better extraction efficiency of the ASE system, which helps swell the particles and fully exchange solutes to the solvent ((Louchouarn et al., 2009); see also discussion below on monomer yields). A direct comparison of soluble component yields under laboratory extraction procedures (using ASE or simple suspension shaking) vs.

field conditions is complicated by the fact that the former methods provide "instantaneous" yields, whereas the latter may integrate long-term releases as the char particles are exposed to moisture. In addition, as the char particles age, their functionality increase (Cheng and Lehmann, 2009), and may release soluble components over extended periods. The ASE extraction thus probably provides an upper limit of the soluble components for unaltered char particles.

Table 3. Concentrations of organic carbon (OC) in chars and pyrogenic water-soluble organic matter (Py-WSOM), as well as the biomarkers in Py-WSOM from cordgrass (CG) and honey mesquite (HM) chars (temp: 250ºC).

Organic Matter Component	**HM**	**CG**
OC_{char}[a] ($mg \cdot g^{-1}$)	523	493
$OC_{py\text{-}WSOM}$ ($mg \cdot g^{-1}$)	16.0±0.4	21.5±0.5
Levoglucosan (free[b]) ($ug \cdot g^{-1}$)	313±12	1008±69
Lignin phenols (free[b]) ($mg \cdot g^{-1}$)	2.05±0.08	0.82±0.05
Lignin oxidation products (CuO[c]) ($mg \cdot g^{-1}$)	4.22±0.43	2.06±0.20

[a]. Kuo et al. (2008a,b)
[b]. Freely dissolved monomers in Py-WSOM
[c]. Lignin oxidation products (LOP) in Py-WSOM quantified using the CuO oxidation method.

The yields of levoglucosan and lignin monomers using MilliQ water as a solvent (Table 3) are comparable to those previously generated using a solution of MeOH:Cl_2CH_2 (Figure 1). The sum of free lignin monomers in Py-WSOM extracted

from the grass and wood chars was 40 ± 7% and 43 ± 10% of the total LOPs for CG and HM chars, respectively (Table 3). Such a high proportion of free monomers is consistent with the significant depolymerization reported in low temperature chars (Harvey et al., 2012b). We believe that it is this depolymerization which contributes to the release of small polar molecules to solution upon water extraction. Differences in the yields of lignin phenols and levoglucosan in Py-WSOM were directly proportional to the lignin vs. cellulose/hemicellulose content of the grass and wood feedstocks (Kuo et al., 2008b, Kuo et al., 2008a) indicating that plant tissue type will potentially influence the composition of Py-WSOM released to solution in soils.

3.3.2 Biodegradation of Py-WSOM

Control samples from the incubation experiments showed no significant decrease in pyrogenic dissolved organic carbon (Py-DOC) or combustion biomarkers over the course of the study (Figures 13 and 14), indicating that abiotic loss was negligible. In contrast, the concentrations of Py-DOC, polymeric and free lignin phenols, as well as levoglucosan in the treatments decreased exponentially over the course of the study (Figures 13 and 14). With the exception of Py-DOC (no lag time), biodegradation was initiated by microorganisms in the river water within 3 days (for phenols) and 6 days (for levoglucosan) from the start of the experiment. Less than 1% of the original concentration of free phenols and levoglucosan remained at the end of the study (37 days). Over the same period the loss of Py-DOC and polymeric lignin was 55% and 85-90%, respectively (Figure 14).

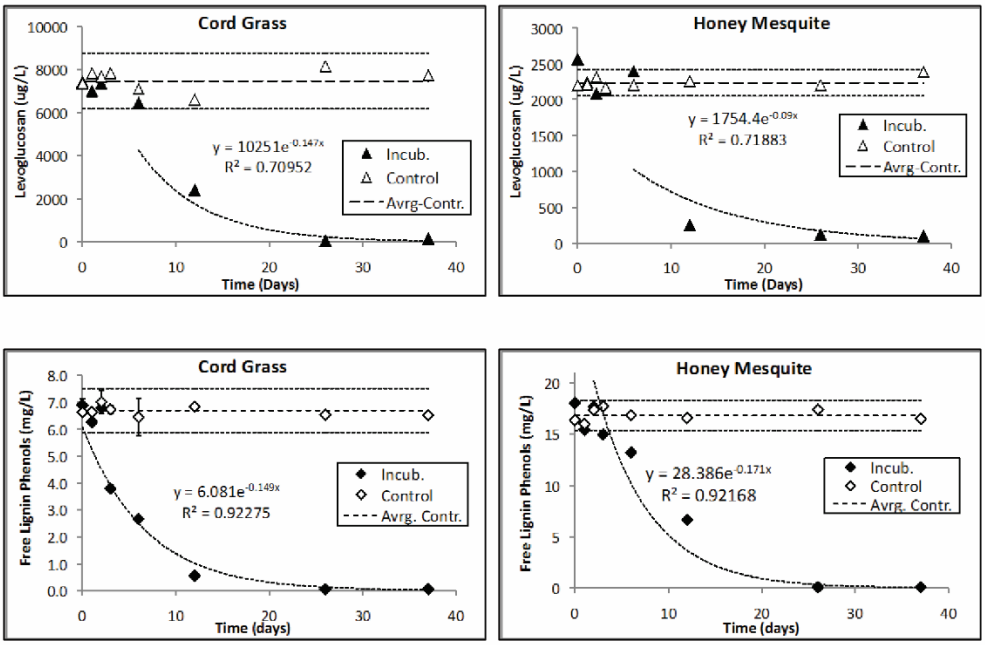

Figure 13. Concentrations of water-soluble biomarkers extracted from chars (temp: 250ºC) made from cordgrass (CG: left) and honey mesquite (HM: right) feedstocks. Top panel: levoglucosan. Bottom panel: free lignin phenols. The expanded uncertainty around the control average (U) is calculated as U = km, where m is one standard deviation of the analyte mean, and the coverage factor, k, is determined from the student's t-distribution corresponding to the associated degrees of freedom and 95% confidence level for each analyte.

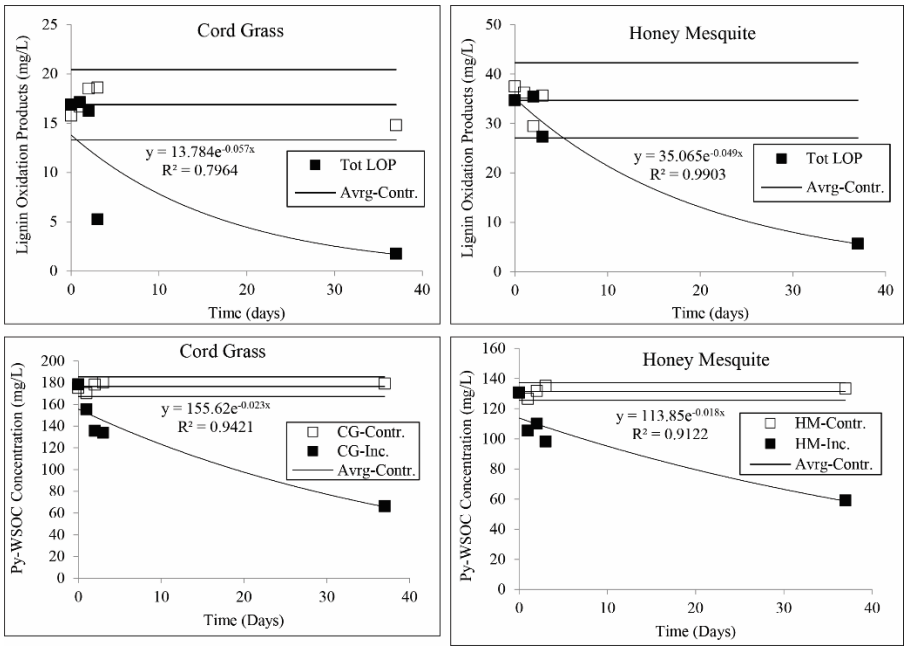

Figure 14. CuO lignin oxidation products (LOP: Top panels) and dissolved organic carbon (DOC: Bottom panels) concentrations in water extracts from chars (temp: 250ºC) made from cordgrass (CG: left) and honey mesquite (HM: right) feedstocks.

Degradation rate (k) and half-life ($t_{1/2}$) of the different Py-WSOM constituents was calculated using the following first-order kinetic model equation 1:

$$(1)\ Ct = C_0^{e-kt}$$

Where C_t is the remaining concentration at time t, C_0 the initial concentration at the end of lag time (still within the 95% confidence interval around the control), and k the degradation constant. It is important to note that these calculations are not equivalent to mineralization rates but rather represent the rate of degradation relative to the initial concentration, which is the sum of all losses to biological processes ranging from slight modifications of molecules, effectively taking them out of the analytical window applied, to complete mineralization. Overall, the degradation rate and half-life of free phenols and levoglucosan are relatively similar (0.09-0.17 d^{-1} to 4.1-7.7 d^{-1}, respectively;

Table 4), showing rapid biodegradation of these soluble biomarkers of biomass combustion in aquatic systems.

Table 4. Reaction rates (*k*) and half-lives ($t_{1/2}$) of freely dissolved lignin-derived phenols and levoglucosan, as well as dissolved organic carbon in solutions extracted from chars (temp: 250ºC) made from cordgrass (CG) and honey mesquite (HM) feedstocks.

	***k* (day^{-1})**		**$t_{1/2}$ (days)**	
Molecular Component	**HM**	**CG**	**HM**	**CG**
Σ8 free lignin phenols	-0.17	-0.15	4.1	4.7
Vanillyls (free)	-0.14	-0.14	5.0	5.1
Syringyls (free)	-0.20	-0.17	3.5	4.0
Levoglucosan (free)	-0.09	-0.15	7.7	4.7
Organic carbon	-0.02	-0.02	30.1	38.5
Σ8 – LOP	-0.05	-0.05	13.9	12.8

The similar degradation rates between anhydrosugar and aromatic lignin phenols seems surprising at first, particularly in the light of the longer lag time for the start of sugar vs. phenol degradation. Although levoglucosan assimilation by yeasts and fungi is a one step process through a specific levoglucosan kinase (Yasui et al., 1991, Xie et al., 2006), its degradation by aerobic bacteria is not as simple and consists of at least three steps whereby levoglucosan is ultimately reduced to glucose prior to its consumption (Yasui et al., 1991, Nakahara et al., 1994). The longer time lag time for the start of the anhydrosugar degradation may thus be related to the need for the appearance, in the bacterial consortium, of microorganisms with the appropriate dehydrogenating enzyme that catalyzes the initial step in the levoglucosan metabolism (Nakahara et al., 1994, Yasui et al., 1991). On the other hand, microorganisms capable of degrading lignin are relatively ubiquitous in the environment. Although fungi are the predominant

microorganisms responsible for lignin degradation (Kirk and Farrell, 1987), diverse sets of bacteria have also been shown to efficiently and completely degrade lignin monomers in solution under both aerobic and anaerobic conditions (Crawford and Crawford, 1980, Kawakami, 1980, Higuchi, 1985, Colberg and Young, 1985, Young and Frazer, 1987). In fact, the observed short half-life for lignin phenols is consistent with an earlier study of degradation of lignin monomers and dimers, showing a half-life ranging from 1-3 days for vanillyls and syringyls in culture media containing nutrient enrichment (Kawakami, 1980).

The enzymatic pathway for lignin phenol mineralization usually proceeds through several steps during which carboxylic and hydroxyl functional groups are added, followed by aromatic ring cleavage between two added proximal –OH groups (Kawakami, 1980, Chen and H-M, 1985). During the early stages of fragmentation of the polymeric lignin structure and the degradation of monomers and oligomers, the proportion of acid moieties (e.g. vanillic acid, as well as syringic acid in the case of hard wood and grass lignin) thus increase and become predominant intermediate products prior to hydroxylation and ring cleavage (Kawakami, 1980, Crawford and Crawford, 1980, Higuchi, 1985, Chen and H-M, 1985). This intermediate pathway to lignin degradation is clearly evident in the quantitative transformation, during the first 3-6 days incubation, of aldehydes (vanillin and syringaldehyde) to their respective acid forms (vanillic and syringic acids, respectively; Figure 15), and the significantly shorter half-life of aldehydes (1.8 ± 0.9 days) than that of acids (5.4 ± 1.8 days; t-test, $p<0.05$). The subsequent disappearance of acidic lignin phenols from solution does not necessarily

mean that they have been fully mineralized, but only that the compounds have "exited" the analytical window due to degradation-induced structural alteration (e.g. demethoxylation). Prior to gaseous end products, other short lived intermediate products may be released to solution, including quinones, polyhydroxylated aromatics, and carboxylated aliphatics (Crawford and Crawford, 1980, Chen and H-M, 1985, Higuchi, 1985).

Similarly, an increase in acid moieties of both vanillyl and syringyl phenols was also observed in the CuO-derived LOPs in Py-WSOM during the course of incubation (Figure 15), suggesting that the conversion of aldehydes to carboxylic acids is not limited to free monomers but also occurs in dissolved polymeric structures. This observation is slightly at odds with prior studies of dissolved LOP biodegradation in aquatic systems (Opsahl and Benner, 1998, Hernes and Benner, 2003), which show no significant change in acid to aldehyde ratio (Ad/Al) during short to long term incubations in the dark. The half-life of LOPs obtained here (13 days) are also shorter than those reported in these two previous studies (ca. 24-100 days; (Opsahl and Benner, 1998, Hernes and Benner, 2003)), but comparable with degradation loss of LOPs (64-96%) from fresh plant leachates over 21 days of incubation (Pellerin et al., 2010). The thermal fragmentation and depolymerization of plant OM in low temperature chars probably leads to a high proportion of soluble oligomers and easily accessible monomers. Leachates from both fresh low temperature chars and fresh plant OM thus may contain lignin that exists in a form that is more labile than that found in highly processed riverine DOM.

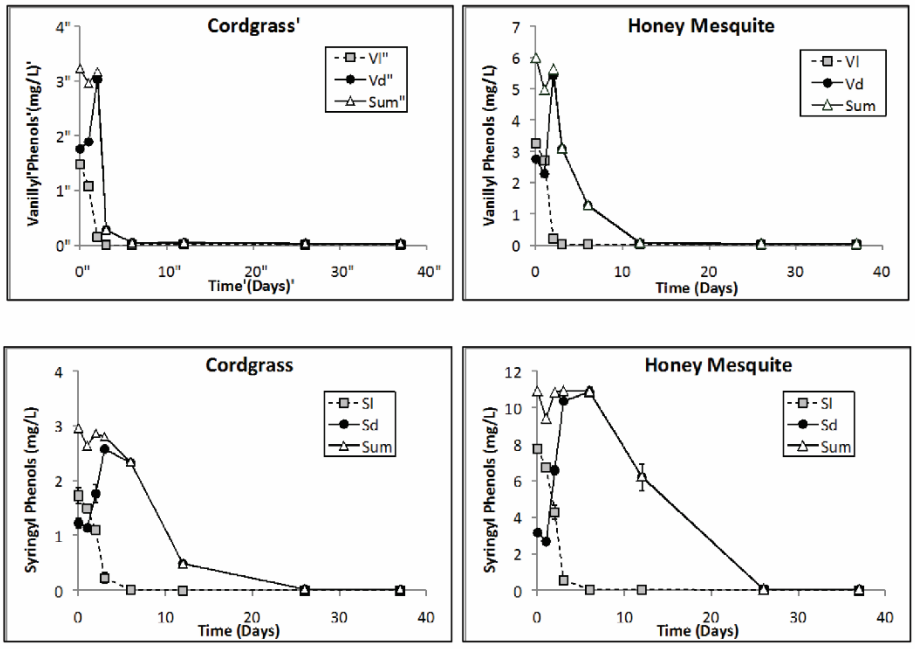

Figure 15. Concentrations of free lignin aldehyde and acid phenols in incubated solutions extracted from chars (temp: 250ºC) made from cordgrass (CG: left) and honey mesquite (HM: right) feedstocks. Top panel: vanillyl phenols. Bottom panel: syringyl phenols.

Finally, although the individual free phenol groups (e.g. syringyls vs. vanillyls) show overall similar degradations rate and half-life (Table 4), syringyls are characterized by a longer lag time than vanillyls (6 vs. 2 days, respectively). This has the effect of substantially raising the S/V ratio (a taxonomic indicator of vascular plant tissue; (Hedges and Ertel, 1982, Goñi and Hedges, 1992)) during the first days of incubation (Figure 16). Such an increase is also observed in the CuO-derived LOPs (Figure 14), indicating that vanillyl phenols in both monomer and polymer forms are transformed more rapidly than syringyl phenols. This contradicts earlier suggestions that syringyl moieties are inherently more labile than vanillyls (Hedges et al., 1988, Goñi et al., 1993)

due to their double methoxyl groups, which tend to be preferentially used by fungi and bacteria as energy source during the initial steps of lignin degradation (Crawford and Crawford, 1980, Chen and H-M, 1985, Young and Frazer, 1987). However, except for the reported higher lability of syringyls vs vanillyls during photochemical breakdown of dissolved lignin (Opsahl and Benner, 1998, Hernes and Benner, 2003), no clear and unambiguous trend emerges for the behavior of the two phenol groups (and thus S/V ratios) during aqueous microbial decay. This is confirmed by two prior dark incubations of river dissolved lignin for 28 days and 1.7 years (Opsahl and Benner, 1998, Hernes and Benner, 2003), which reported no significant change in S/V ratio under biological degradation. The massive changes in the S/V ratio in the present study (Figure 16) clearly indicate that more work is needed on the kinetics of dissolved lignin degradation, particularly when such lignin components are derived from thermal alteration of vascular plant OM and thus may have a very different molecular weight and functional group composition than dissolved lignin constituents derived from soil OM degradation.

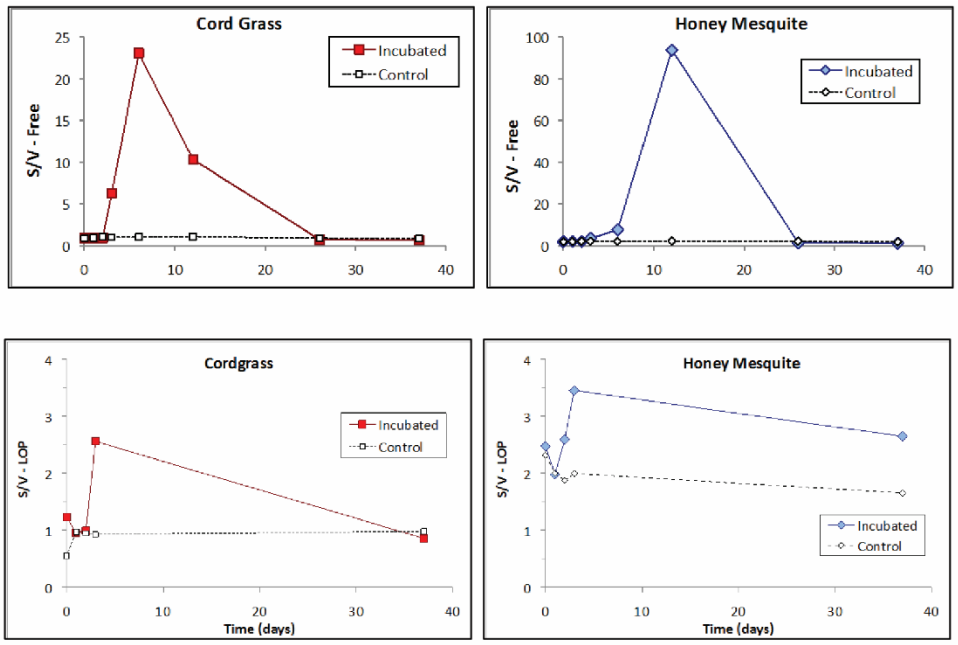

Figure 16. Dissolved syringyl to vanilly phenol ratios in incubated solutions extracted from chars (temp: 250ºC) made from cordgrass (CG: left) and honey mesquite (HM: right) feedstocks. Top panel: free phenols. Bottom panel: CuO-derived LOP.

3.3.3 Environmental significances of Py-WSOM

Due to improvements in analytical techniques, a few studies have recently switched the usual focus on the characterization of solid-phase PyC in environmental media, to the transfer of dissolved PyC from industrial/urban and fire-impacted watersheds to streams and eventually the coastal ocean (Hockaday et al., 2006, Hockaday et al., 2007, Mannino and Harvey, 2000, Ziolkowski and Druffel, 2010, Dittmar et al., 2012). However, all these studies have constrained the PyC quantification to only the most condensed carbon forms (e.g. polycyclic aromatic carbons) and biologically refractory fractions of the PyC continuum. To our knowledge, this is the first study that characterizes the soluble fraction from biomass burning that falls into the

low temperature PyC spectrum and which is comprised of a higher proportion of oxygen-rich, non-aromatic functional groups. Recent studies have shown that low temperature chars have a higher reactivity than the more condensed species prevalent in high temperature PyC, such as soot (Kuo et al., 2008a, Alexis et al., 2010, Zimmerman, 2010, Hilscher and Knicker, 2011, Luo et al., 2011, Harvey et al., 2012a, Singh et al., 2012). Luo et al. (2011) in particular demonstrated that low temperature chars not only generate a high proportion of soluble pyrogenic OC, but that this carbon fraction may support co-metabolic degradation of the solid-phase chars in soils. Similarly, Hilscher and Knicker (2011) showed that up to 3.2% of the PyC from a 350ºC char was transported as leachate in a soil column after 20 months incubation. Moreover, these authors showed that low temperature chars comprise OM constituents (O-alkyl C and alkyl C) that are more readily available to microorganisms and probably contributing to the PyC fraction that has an extremely short half-life (1-19 days). As shown in the present study, Py-WSOM comprise a large fraction of low molecular weight organics due to significant polymer fragmentation during low temperature combustion. Because of their high solubility in water, these organics may bypass soil sorption and thus be important contributors to exported DOM in fire-impacted watersheds (Hockaday et al., 2007).

The impact of low temperature char-derived Py-WSOM is particularly important in the light of recent findings by Alexis et al. (2007, 2010) on the flux of carbon to soil litter following a prescribed burning study in a scrub oak ecosystem in Florida. In such a system, for example, the post-fire carbon stocks in the litter (390 g-C$\cdot$m^{-2}), was

comprised of 20% charred and 80% “unburned” OM (Alexis et al., 2007). Assuming 10-30% of this unburned material could actually be classified as low temperature “brown carbon” and, using the 3-4% Py-DOC/POC ratio observed in the 250ºC chars here, then post-fire litter could yield 1-4 g-DOC·m^{-2}. Hilscher and Knicker (2011) further suggest that recalcitrance may not be the rate-limiting factor in soil PyC turnover times and that a continuous process of leaching and consumption of PyC should not be underestimated. Moreover, because a water-soluble fraction as little as 0.7% of the total charcoal OC has been shown to facilitate the degradation of 350ºC char during 87 days incubation (Luo et al., 2011), chars formed under lower temperature may have an even more significant impact on the production of co-substrates to soil pore water and streams.

Potential priming effects induced by terrigenous DOM in inland and coastal waters were recently discussed by Bianchi (2011) and recognized as an important process that needs to be incorporated into global carbon models in the context of climate change. Our study demonstrates that wildfires/biomass combustion may be an additional and important source of labile terrestrial OM to aquatic systems. Because simple organic aromatic monomers (e.g. benzoic acid) have been shown to induce a measureable priming effect during the degradation of fulvic acids in natural waters (de Haan, 1977), Py-WSOM released from low temperature chars might be important priming substrate and have a significant impact on the cycling of terrigenous DOM in streams and coastal systems. Moreover, their characteristic half-life (4-7 days for monomer, 2 weeks for oligomers, and a month for DOC; Table 2) suggest that they will be present in natural

waters within time-scales relevant to rapid mixing and transport in rivers and estuaries (weeks to months).

Considering the potential for a significantly increased frequency and intensity of wildfires in boreal forests, which represent one of the Earth's larger biomes (714 Pg), (Kasischke and French, 1995, Soja et al., 2007, Chapin et al., 2008, Running, 2006), one could thus anticipate a similar increase in the transfer of labile Py-WSOM to boreal aquatic systems. Arctic rivers transport vast amounts of terrigenous DOM to the Arctic Ocean (Amon et al., 2012). However, no information exists on the magnitude of the Py-WSOM fluxes in these rivers and how these could affect the cycling of non-fire-derived terrigenous DOM. An exploration of the presence and cycling of biomarkers for biomass combustion in rivers from fire-impacted watersheds may thus be critical for a better understanding of the role of wildfires on the transfer of both labile and refractory combustion OM to aquatic systems and the coastal ocean.

IV. EFFECTS OF *AVICENNIA GERMINANS* REPLACEMENT ON ORGANIC CARBON ACCUMULATION AND SEQUESTRATION WITHIN TEXAS COASTAL WETLANDS

4.1 Introduction

Coastal wetlands (e.g., estuarine emergent wetlands and mangrove forests) are unique in their ability to store large quantities of carbon as blue carbon (Blu-C) due to their high rates of soil accumulation and high biomass production in aboveground biomass, belowground biomass, and soil organic carbon (Adame et al., 2013, Mcleod et al., 2011). Coastal wetlands that are dominated by salt marsh or mangrove stands can directly mitigate the release of atmospheric CO_2 by sequestering carbon on decadal to millennial time scales (Mcleod et al., 2011, Duarte et al., 2005, Lo Iacono et al., 2008), making them an important sink of carbon along coastal margins (Kennedy et al., 2010, Sanders et al., 2010).

Salt marsh and *Avicennia germinans* (black mangrove) dominated wetlands comprise 278 km^2 of the Texas Gulf Coast (Armitage et al., 2015), which is 1.2% of the total conterminous United States tidal marsh and mangrove coverage (23,000 km^2) (Ward et al., 2016, Bridgham et al., 2006), and 0.05-0.17% of the entire globe's salt marsh and mangrove ecosystems (159,760-552,361 km^2) (Mcleod et al., 2011, Chmura et al., 2003, Duarte et al., 2005, Bird et al., 2004, Sanders et al., 2010, Giri et al., 2011). The Texas Gulf Coast is currently in a transitional period for temperate ecotonal wetlands, which is highlighted by the pioneer mangrove species *Avicennia germinans* becoming increasingly common in areas historically dominated by herbaceous and shrub

salt marsh vegetation (Bianchi et al., 2013, Comeaux et al., 2012, Osland et al., 2013). The increase in relative abundance for the Gulf of Mexico's A. *germinans* have been limited by periodic freezing events. However, as the last major freeze event occurred in 1983 (Giri et al., 2011, Saintilan et al., 2014), the entire Gulf of Mexico's 10,000 km^2 of salt marsh ecosystems have potentially become susceptible to A. *germinans* expansion (Saintilan and Rogers, 2015, Osland et al., 2013, Bianchi et al., 2013).

In mixed ecotones, salt marsh plants can actively facilitate *A. germinan*s propagule establishment in wetlands (Guo et al., 2013). The biotic interactions of salt marsh plants and expanding A. *germinans* populations are influenced by local plant assemblages, such as *Spartina alterniflora*, which can aid in the retention of mangrove propagules (Guo et al., 2013). Localized ecological shifts can be exacerbated by changes in regional weather patterns where reduced freeze episodes does not inhibit woody plant expansion (Perry and Mendelssohn, 2009).

Within the last 27 years, the aerial extent of salt marshes along the Texas Gulf Coast has significantly decreased (Armitage et al., 2015), while A. *germinans* areal coverage increased by 74% along the Texas Gulf Coast. However, the expansion of A. *germinans* accounted for only 6% (≈ -5 km^2) of the total salt marsh loss (-78 km^2) in this time period (Armitage et al., 2015), while sea level rise (SLR) and conversion into tidal flats accounted for the majority of salt marsh loss (≈ -73 km^2). This makes SLR and conversion into tidal flats the main process for salt marsh habitat loss along the Texas Gulf Coast over the past 27 years (Armitage et al., 2015).

Global SLR has increased by 0.15 $cm \cdot yr^{-1}$ over the past century and is projected to reach 60 cm in total by 2100 (Nicholls and Cazenave, 2010). Regionally, the Texas Gulf Coast's SLR ranges from 0.19 ± 0.09 $cm \cdot yr^{-1}$ at the Port Mansfield tidal gauge station to 0.64 ± 0.03 $cm \cdot yr^{-1}$ at Galveston Bay, which is influenced by localized subsidence ((Armitage et al., 2015) and references therein). Although woody encroachment into historically dominated salt marsh areas may not be occurring as rapidly in the Texas Gulf Coast as in other ecosystems (Saintilan and Rogers, 2015, Giri et al., 2011, Peterson, 2013), the loss of salt marshes due to SLR and mangrove-salt marsh biotic interactions could open up areas for mangrove propagule entrainment within wetlands.

Plant biomass from salt marsh plants and A. *germinans* contains lignin, cellulose and hemicellulose (Marchand et al., 2005). Lignin is the second most abundant naturally occurring polymer after cellulose, and is a complex and important structural component of vascular plants (Sarkanen and Ludwig, 1971). The lignin molecule, which is aromatic in structure, is considered recalcitrant in anoxic soils (Hedges and Mann, 1979, Hedges and Prahl, 1993) and can act as a sink for organic carbon (OC) in wetlands. In-situ storage of OC as plant biomass in wetlands is controlled by the coastal environment, which has highly reducing anoxic mineral soils with a relatively thin, oxidized sediment layer (0-15 cm) (Patrick Jr and DeLaune, 1977, Reddy and DeLaune, 2008).

The alkaline cupric oxidation (CuO) is used to analyze the lignin macropolymer within pure terrestrial vegetation, soils, and sediments (Ertel and Hedges, 1985, Prahl et al., 1994, Louchouarn et al., 1999, Goñi and Montgomery, 2000, Kuo et al., 2008a,

Hedges and Mann, 1979). The CuO method hydrolyzes the lignin macropolymer into three classes of methoxylated phenols: vanillyl (V), syringyl (S), and cinnamyl (C) (Hedges and Mann, 1979). The lignin oxidation products (LOPs) are made up of acid, aldehyde, and ketone classes in which V and S contain acids, aldehydes, and ketones while C contains only acids. (Kuo et al., 2008a). These ratios, along with the percent organic carbon attributed to lignin ($\%_{OC\text{-}L}$), are used in this study to understand the quality of organic carbon stored within salt marshes and A. *germinans* wetlands along the Texas Gulf Coast.

Here, we used five locations along the Texas Gulf Coast (two A. *germinans* dominated wetlands, two salt marsh dominated wetlands and one mixed A. *germinans*-salt marsh ecotone): to (1) understand the quality of OC accumulated within salt marsh and A. *germinans* wetlands located in transitional ecotones. (2) Examine how annual and long term OC accumulation changes with regional A. *germinans* wetland replacement and (3) examine the value of regional carbon accumulation along the Texas Gulf Coast.

4.2 Materials and methods

4.2.1 Site description

The Texas Gulf Coast is categorized as a micro-tidal environment with a tidal range of approximately 30 cm and wave heights of less than 1 m (however, it should be noted that during storm events, storm surges can reach up to 5.2 m) (Rego and Li, 2010). Over the course of two sampling campaigns (Summer 2012 & 2013), five back barrier estuarine wetland sites were sampled: two salt marsh dominated wetlands, two A. *germinans* dominated wetlands and one sites with mixed salt marsh-A. *germinans*

vegetation (Figure 17). The mixed salt marsh-A. *germinans* site was located on the east end of Galveston Island (29°19’58.44” N, 94°45’07.08” W), while the two salt marsh dominated wetlands were located on the west end of Galveston Island (29°09’03.26” N, 95°02’12.51” W) and Copano Bay (28°04’40.54” N, 97°13’20.52” W). The two A. *germinans* dominated wetlands were located at Port O’Connor (28°25’28.52” N, 96°24’57.17” W) and Mustang Island (27°44’16.36”N, 97°08’23.25” W).

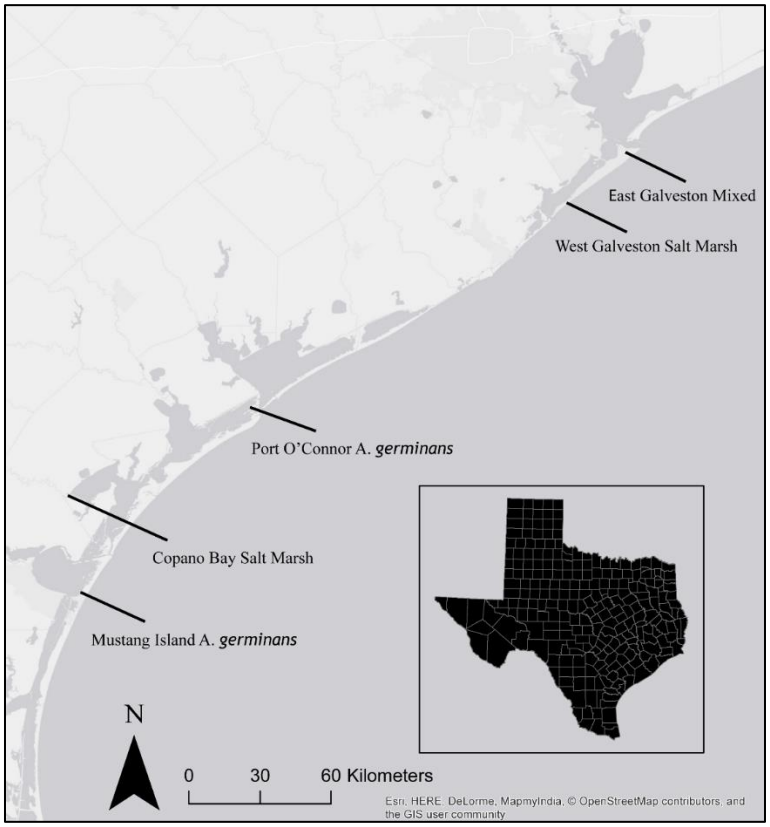

Figure 17. Sample locations for salt marsh and A. *germinans* wetlands located along the Texas Gulf Coast. The two salt marsh dominated wetlands sampled in this study are West Galveston Island & Copano Bay while the two A. *germinans* dominated wetlands are Port O’ Connor & Mustang Island. The East Galveston Island site contains a mixture of salt marsh and A. *germinans* ecotones. Base map is adopted from ESRI 2011. ArcGIS Desktop: Release 10. Redlands, CA: Environmental Systems Research Institute.

4.2.2 Experimental design and field sampling

In this study, we used a random sampling method to record aboveground biomass for salt marsh dominated sites. Three transects (50 m in length) were established perpendicular to the shoreline, and plots were sampled at ten random points along each transect. All marsh vegetation in each of the ten 1-m^2 sampling plots was clear-cut to the soil boundary. The collected biomass was washed with DI water, dried at 60°C and weighed in the laboratory at Texas A&M University at Galveston to determine biomass (kg/m^2).

Individual tree height and crown width was measured along three 50 meter x 1 meter transects, at each A. *germinans* dominated site. Aboveground A. *germinans* biomass was directly measured on three trees at both Port O'Connor and Mustang Island. Three A. *germinans* trees (approximate height < 0.5 m, 0.5-1 m, and > 1 m) were excavated from Mustang Island. The relationship for aboveground dry biomass and tree height ($R^2 = 0.74$) was used to extrapolate aboveground biomass based on A. *germinans* tree height at both A. *germinans* dominated sites (Figure 18).

Aboveground biomass for the West Galveston Island wetland location was dominated by *Spartina alterniflora* at the low and mid marsh elevations, and by *Batis maritima* at the high marsh. The dominant salt marsh grass at the Copano Bay site was B. *maritima* at the mid and high marsh elevations, and was mixed B. *maritima* and S. *alterniflora* at the low marsh. The only mangrove found within our sampling sites is A. *germinans*.

To quantify soil carbon and lignin content three soil cores were collected at each of the five wetland sites (East Galveston Island, West Galveston Island, Port O' Connor, Copano Bay and Mustang Island) along a 50 m transect perpendicular to the shoreline. The soil cores were extracted perpendicular to water line and denoted with the relative elevation reference (i.e., core 3 = low elevation, core 2 = middle elevation, and core 1 = high elevation) at each wetland site. The salt marsh wetland site elevation was determined by dominating vegetation type (i.e., S. *alterniflora* = low marsh, B. *maritima* = mid marsh and high marsh) (Tiner, 1999). Each soil core was ≈ 46 cm in core depth, and sectioned in the field. The first 10 cm was partitioned into 1 cm increments, and the rest into 2 cm increments. Pre-sectioned soil cores were placed into pre-combusted vials, weighed and freeze dried for 48 hours, after which the samples were homogenized and subsampled for further analysis.

4.2.3 Radiochronological dating, stable carbon isotopic and molecular analysis

Lead 210 and Cs 137 activity were determined in sediment samples using a high-purity Germanium (HPGe) well detector. Estimated linear sedimentation rates were applied to the excavated soil cores when the natural log of the unsupported activity to depth had a linear correlation greater than 0.50 ($R^2 > 0.50$) (Table 5 and Figure 19). Linear sedimentation rates were measured on the middle elevation soil cores for East Galveston, West Galveston Island, Copano Bay and Port O'Connor. When linear sedimentation rates were not available for individual soil cores, literature values for similar locations were applied in order to calculate dry accumulation for wetland soil

cores (Table 5) (Comeaux et al., 2012). Literature values were applied to Mustang Island and East Galveston Island (Comeaux et al., 2012).

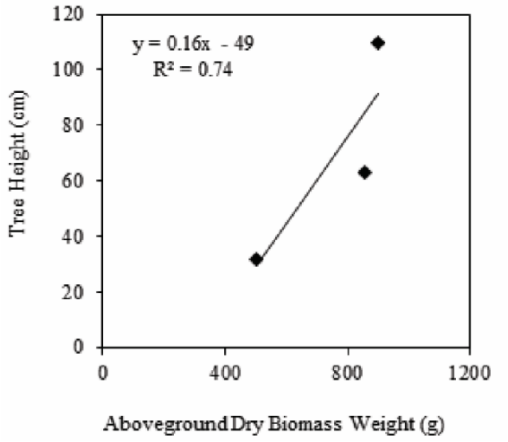

Figure 18. Relationship for A. *germinans* tree height and aboveground dry biomass. Tree height and aboveground biomass relationship extrapolated from three trees (approximate height < 0.5 m, 0.5-1 m, and > 1 m).

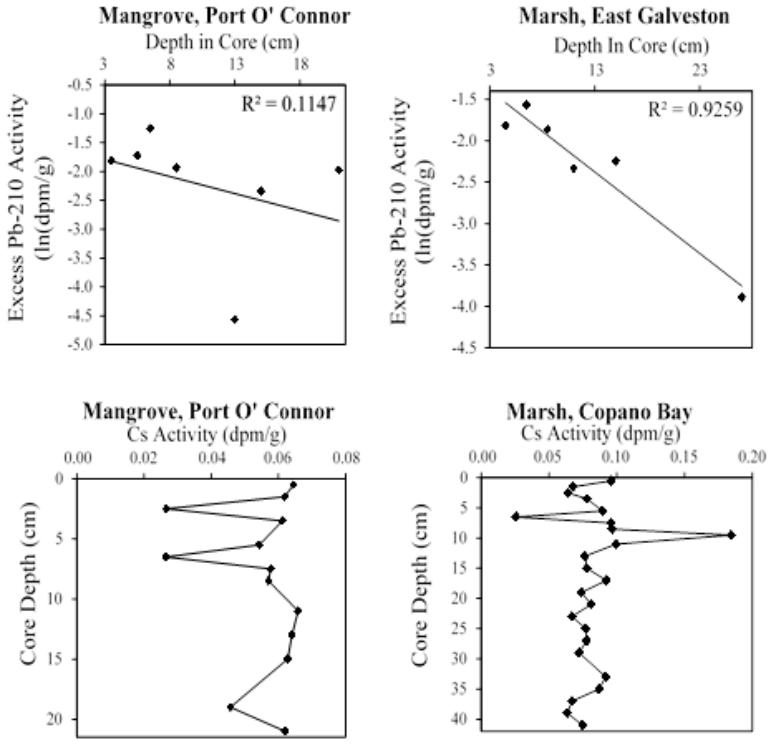

Figure 19. Down core excess ^{210}Pb linear regression curves and down core ^{137}Cs activity were used to estimate linear sedimentation rates for salt marsh wetlands with low bioturbation. Linear regression of ^{210}Pb for A. *germinans* dominated wetlands, Port O' Connor and Mustang Island, were rejected due to low R^2. Published values for ^{210}Pb linear sedimentation rates from Comeaux et al., 2012 were used for both A. *germinans* study sites.

Table 5. Estimated radiochemical sedimentation rate averages for A. *germinans* and salt marsh study sites located along the Texas Gulf Coast. Linear sedimentation rates are represented as cm yr^{-1} for soil cores retrieved for this study and compared to soil cores collected in a previous study looking at similar sites wetlands (Comeaux et al., 2012).

Study Site	^{210}Pb (cm·yr^{-1}) This Study	^{137}Cs (1963) (cm·yr^{-1}) This Study	^{210}Pb (cm·yr^{-1}) Comeaux et al 2012	^{137}Cs (1963) (cm·yr^{-1}) Comeaux et al 2012
East Galveston Island Marsh-A. *germinans* Ecotone	0.32 ± 0.08	0.40 ± 0.06	0.31 ± 0.14	0.45 ± 0.10
West Galveston Island Salt Marsh	0.35 ± 0.05	--	--	0.22 ± 0.06
Copano Bay Salt Marsh	0.29 ± 0.05	0.21 ± 0.06	0.26 ± 0.04	0.18 ± 0.06
Port O' Connor A. *germinans*	--	0.43 ± 0.07	--	--
Mustang Island A. *germinans*	--	--	0.54 ± 0.15	0.74 ± 0.21

Total organic carbon was measured directly from pre-acidified wetland soil sub-samples. Briefly, sub-samples were pre-weighed into conical centrifugal tubes in which 1-2 ml of 1 N hydrochloric acid was added and mixed. The mixture was placed into a centrifuge and spun down to separate the sediments from the solution. After removing the supernatant, samples were dried for 18-24 hours at 60°C. The samples were then weighed and measured on a Costech Elemental Analyzer (ECS 4010 CHNSO) for %OC. Sub samples of the acidified sediments were analyzed on a Thermo-Electron Dual-Inlet Gas-Source Stable Isotope Mass Spectrometer for the determination of the carbon stable isotope signatures ($\delta^{13}C$) at Baylor University's Stable Isotope Laboratory.

Lignin oxidation products (LOPs) were analyzed using the method developed by Hedges & Ertel (1982) using, modifications (Kuo et al., 2008b, Louchouarn et al., 2010). Briefly, ground homogenized samples containing 2-5 mg^{-1} of OC were combined with

CuO (≈ 330 mg) and, $Fe(NH_4)_2(SO_4)_2 \cdot 6H_2O$ (≈ 100 mg) in stainless steel reaction vessels. All reaction vessels were filled with ≈ 3 ml of 2 N Argon-sparged NaOH solution and, placed in a customized purging block and closed under the absence of O_2. The stainless steel reaction vessels were heated at 155ºC for 3 h in a customized Hewlett-Packard 5890 gas chromatography system fitted with a rotating carousel. After cooling, d7-trans-cinnamic acid was added to each reaction vessel as a surrogate standard. The aqueous solution was acidified with 6 N HCL (to a pH ≤ 1) and extracted in ethyl acetate. Ethyl acetate extracts were chemically dried with sodium sulfate; then dried to completion in a LabConco™ solvent concentrator and re-suspended in pyridine. Aliquots of pyridine solutions were derivatized using N, O-bis (trimethylsilyl) trifluoroacetamide (BSTFA) containing 1% trimethylchlorosilane (9:1 BSTFA:TMS Supelco, PA, USA) at 75°C for 15 minutes.

Separation and quantification of trimethylsilyl (TMS) derivatives of LOP's were performed using a Varian triple quadrupole 480-300 GC/MS system fitted with a fused silica column (J&W DB-5MS, 30 m x 0.25 mm i.d., 0.25 μm film thickness; Agilent Technologies). Each sample was injected, under split less mode (Louchouarn et al., 2010). The mass spectrometer was operated in the electron ionization mode (EI = 70 eV) using full scan (FS). Compound identification was performed using retention times and by comparing full mass spectra with those of commercially available standards. We used the literature accepted total sum of 8 methoxylated lignin-derived phenols (sigma-8 or Σ8; vanillin, acetovanillone, vanillic acid, syringealdehyde, acetosyringone, syringic acid, p-coumaric acid and ferulic acid) to quantify annual and 100 year lignin

accumulation (Louchouarn et al., 2000). The percentage of organic carbon attributed to lignin (%OC-L) was estimated using literature values for the molar concentration of individual lignin phenols within the lignin polymer (Benner et al., 1990).

The quantification of carbon and lignin accumulation in these wetland soils is based upon the estimated sedimentation rate for each study site (Table 5). The mass accumulation (OC-M_a) was calculated using equation 2, where the %OC and solid interval accumulation (S_a), is the total solids multiplied by a given core interval. Lignin mass accumulation (L-M_a) was calculated using equation 3, where the sum of lignin oxidation products (sig-8) is multiplied by S_a. Annual OC and Lignin flux (OC_{flux} and L_{flux}) was calculated from equations 4 and 5, where OC_{flux} and L_{flux} is the product of the mass accumulation and the local sedimentation rate (LSR).

$$(2)\ OC\text{-}M_a\ (g\text{-}OC\cdot m^{-2}) = (\%OC\cdot S_a)\cdot 100$$

$$(3)\ L\text{-}M_a\ (g\text{-}L\cdot m^{-2}) = (sig\text{-}8\cdot S_a)\cdot 10$$

$$(4)\ OC_{flux}\ (g\text{-}OC\cdot m^{-2}\cdot yr^{-1}) = (OC\text{-}Ma\cdot LSR)\cdot 10$$

$$(5)\ L_{flux}\ (g\text{-}L\cdot m^{-2}\cdot yr^{-1}) = (L\text{-}Ma\cdot LSR)*10$$

4.3 Results

4.3.1 Molecular signature of wetland vegetation and soil organic carbon

The molecular signatures, i.e. stable carbon isotope ($\delta^{13}C$) and percent organic carbon attributed to lignin ($\%_{OC\text{-}L}$) of above ground S. *alterniflora*, B. *maritima*, and A. *germinans* vegetation are represented in Table 6. The $\delta^{13}C$ signatures for the above ground salt marsh vegetation S. *alterniflora* and B. *maritima* are $^{-}13.6$ ‰ and $^{-}27.8$ ‰, respectively. The $\%_{OC\text{-}L}$ for above ground S. *alterniflora* and B. *maritima* are 16.4 $\%_{OC\text{-}L}$ and 19.2 $\%_{OC\text{-}L}$. The $\delta^{13}C$ signatures for A. *germinans* leaf, branch, and root are $^{-}26.1$ ‰, $^{-}27.5$ ‰, and $^{-}23.2$ ‰, respectively. The $\%_{OC\text{-}L}$ for A. *germinans* leaf, branch, and root are 5.7 $\%_{OC\text{-}L}$, 12.7 $\%_{OC\text{-}L}$, and 14.1 $\%_{OC\text{-}L}$, respectively.

The down core $\delta^{13}C$ signatures for the A. *germinans* dominated sites, Port O' Connor and Mustang Island, have lower $\delta^{13}C$ signatures at the surface of the core (0-1 cm), while there is a down core OC enrichment of 1.0-5.8 ‰ for all three soil cores (Figure 20). Assuming the soil organic carbon contains deposition from A. *germinans* leaf, branch and root. The OC enrichment of 1.0-5.8 ‰ potentially changes the soil deposited A. *germinans* leaf, branch and root $\delta^{13}C$ signatures to $^{-}25.1$-$^{-}20.3$ ‰, $^{-}26.5$-$^{-}21.7$ ‰, and $^{-}22.2$-$^{-}17.4$ ‰, respectively. The A. *germinans* dominated wetlands at Port O' Connor and Mustang Island store 11.4-30.8 ± 4.4-15.8 $\%_{OC\text{-}L}$ in the top 0-22 cm and 7.4-12.7 ± 1.7-8.7 $\%_{OC\text{-}L}$ down core (22-46 cm) (Figure 20).

Table 6. Vegetation source signatures; %OC attributed to lignin (%OC-Lignin) and stable carbon isotope ($\delta^{13}C$) for A. *germinans* and salt marsh vegetation.

Vegetation Type	%OC-L	$\delta^{13}C$
A. *germinans* Leaf	5.7	-26.1
A. *germinans* Branch	12.7	-27.5
A. *germinans* Root	14.1	-23.2
S. *alterniflora*	16.4	-13.6
B. *maritima*	19.2	-27.8

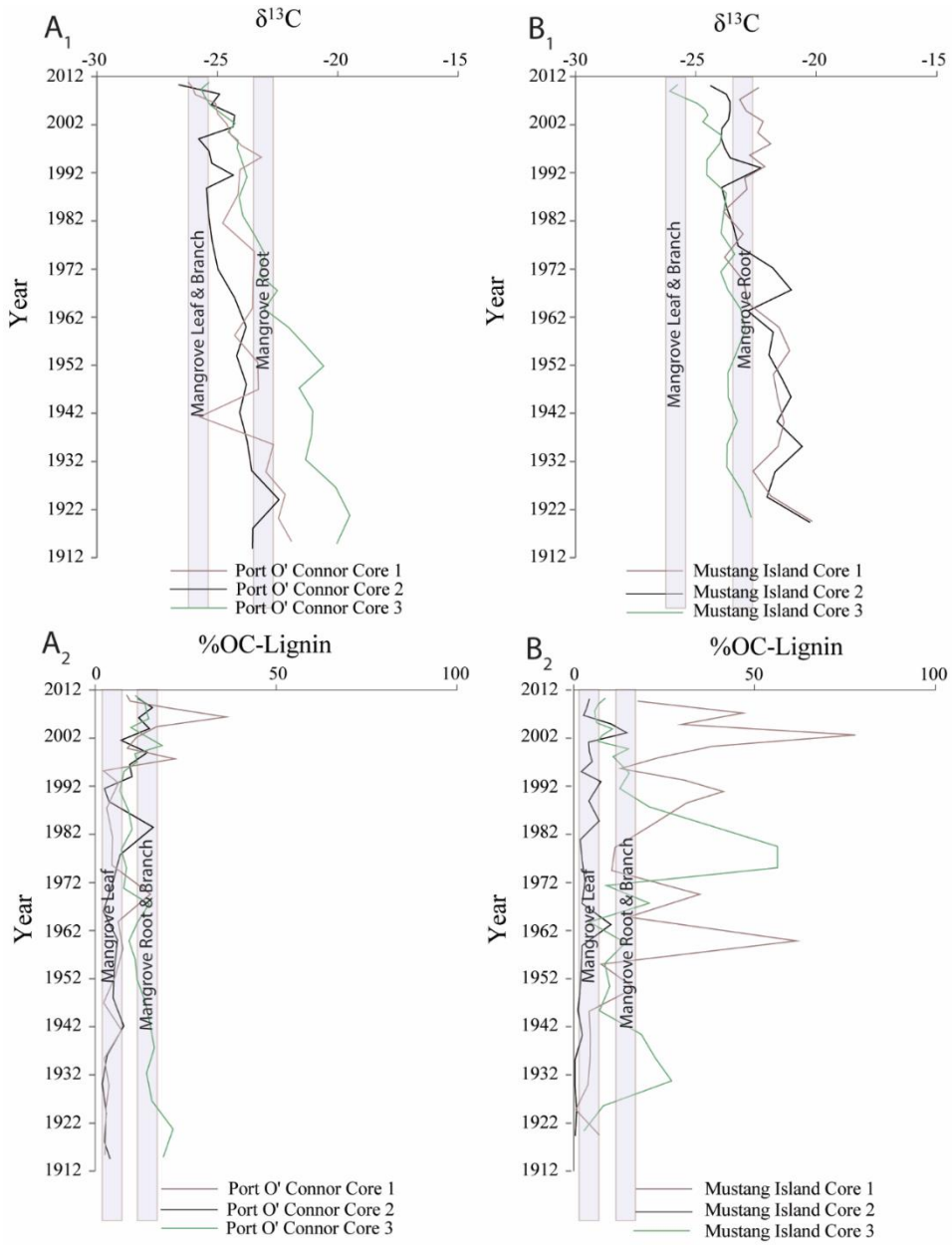

Figure 20. Soil and vegetation stable carbon isotope signatures ($\delta^{13}C$) and %OC attributed to lignin ($\%_{OC\text{-}L}$) for A. *germinans* wetlands Port O' Connor (A_1 & A_2) and Mustang Island (B_1 & B_2). Three soil cores are represented for each site (core 1, core 2 and core 3.

The dominant salt marsh species for all three Copano Bay soil cores is B. *maritima* (-27.8 ‰). Relative to the surface soil (0-1 cm), the three Copano Bay soil cores have down core $\delta^{13}C$ signatures enriched by 2.2-6.8 ‰ (Figure 21). In comparison, the salt marsh dominated site, West Galveston Island, is represented by two different above ground plant assemblages, with B. *maritima* dominating at core 1 (relative high elevation) and S. *alterniflora* dominating at cores 2 and 3 (relative mid and low elevations, respectively). The West Galveston Island core 1, which is located furthest from the water and at the highest relative elevation is enriched by 7.1‰ down core (Figure 21). In comparison, the down core $\delta^{13}C$ signatures for core 2 are closer to the above ground S. *alterniflora* vegetation signature (-13.6 ‰). Lastly, the down core signature for core 3 is slightly depleted relative to the surface soil signature (-0.3-$^{-}$1.2 ‰) (Figure 21).

The salt marsh dominated wetlands West Galveston Island and Copano Bay store 10.1-22.0 ± 8.3-9.7 $\%_{OC\text{-}L}$ in the top 0-22 cm and 3.6-4.0 ± 1.8-1.4 $\%_{OC\text{-}L}$ down core (22-46 cm) (Figure 21). Down core (22-46 cm), both Copano Bay and West Galveston Island wetlands store 3.6-4.0 ± 1.8-1.4 $\%_{OC\text{-}L}$. All six salt marsh dominated wetland soil cores illustrate an accumulation of $\%_{OC\text{-}L}$ higher than the vegetation source within the top 0-22 cm (Figure 21). This is most likely due to preferential storage of lignocellulose and the presence of salt marsh root matter within the soil profile.

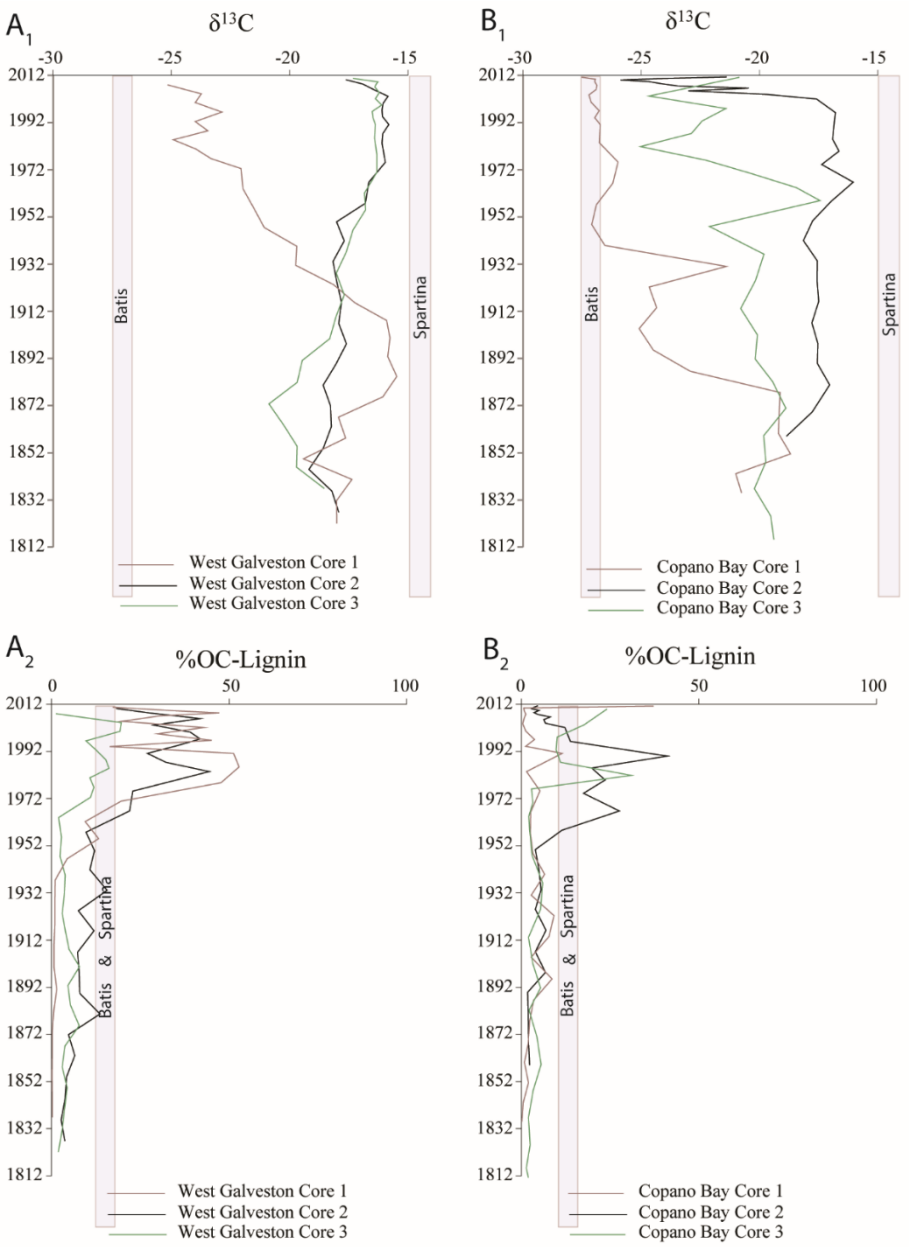

Figure 21. Soil and vegetation stable carbon isotope signatures ($\delta^{13}C$) and %OC attributed to lignin ($\%_{OC\text{-}L}$) for salt marsh wetlands West Galveston Island (A_1 & A_2) and Copano Bay (B_1 & B_2). Three soil cores are represented for each site (core 1, core 2 and core 3).

4.3.2 Organic carbon accumulation

The mean above ground dry biomass for salt marsh and A. *germinans* sites are 198 ± 45 and 333 ± 119 g·m^{-2}, respectively (Table 7). The mean above ground OC for salt marsh and A. *germinans* are 81 ± 18 and 142 ± 52 g-OC·m^{-2}, respectively (Table 7).

Table 7. Biomass organic carbon (OC) for A. *germinans* and salt marsh dominated ecosystems located along the Texas Gulf Coast. Above ground biomass is represented as "above biomass" and "above OC" for A. *germinans* stands.

Wetland Type	Above Biomass (g·m^{-2})	Above OC (g-OC·m^{-2})
A. *germinans*	772 ± 70	329 ± 30
Salt Marsh	198 ± 45	81 ± 18

The local variability for A. *germinans* OC accumulation are represented in Table 8. The highest local variability for A. *germinans* 100 year OC accumulation is Port O' Connor core 1 and core 2, (4,508 ± 119 and 1,668 ± 55 g-OC·m^{-2}, respectively). The lowest local variability for A. *germinans* 100 year OC accumulation is Mustang Island core 1 and core 2, (1,095 ± 49 and 1,758 ± 37 g-OC·m^{-2}, respectively). The highest local variability for A. *germinans* annual OC accumulation is Mustang Island core 1 and core 3, (10 ± 1 and 41 ± 12 g-OC·m^{-2}·yr^{-1}, respectively). The lowest local variability for A. *germinans* 100 year OC accumulation is Mustang Island core 1 and core 2, (10 ± 1 and 15 ± 2 g-OC·m^{-2}·yr^{-1}, respectively).

The local variability for salt marsh OC accumulation are represented in Table 9. The highest local variability for salt marsh 100 year OC accumulation is Copano Bay

core 1 and core 2, (1,400 ± 222 and 4,088 ± 181 g-OC·m^{-2}, respectively). The lowest local variability for salt marsh 100 year OC accumulation is West Galveston Island core 1 and core 3, (2,397 ± 424 and 2,340 ± 723 g-OC·m^{-2}, respectively). The highest local variability for salt marsh annual OC accumulation is Copano Bay core 1 and core 2, (13 ± 2 and 39 ± 3 g-OC·m^{-2}·yr^{-1}, respectively). The lowest local variability for salt marsh annual OC accumulation is West Galveston Island core 2 and core 3, (22 ± 1 and 23 ± 4 g-OC·m^{-2}·yr^{-1}, respectively).

The highest A. *germinans* 100 year OC accumulation is Port O'Connor site (3,326 ± 134 g-OC·m^{-2}) (Table 10). In comparison, Mustang Islands total 100 year OC accumulation is 2,249 ± 97 g-OC·m^{-2}. The highest A. *germinans* annual OC accumulation is Port O'Connor (32 ± 5 g-OC·m^{-2}·yr^{-1}). In comparison, Mustang Islands annual OC accumulation is 27 ± 5 g-OC·m^{-2}·yr^{-1} (Table 9).

The highest salt marsh 100 year OC accumulation is Copano Bay (2,856 ± 195 g-OC·m^{-2}) (Table 10). In comparison the lowest 100 year OC accumulation is West Galveston Island (2,338 ± 416 g-OC·m^{-2}). The highest annual salt marsh OC accumulation is Copano Bay (27 ± 2 g-OC·m^{-2}·yr^{-1}). In comparison the lowest annual salt marsh OC accumulation is West Galveston Island (23 ± 3 g-OC·m^{-2}·yr^{-1}) (Table 10).

The 100 year OC accumulation for salt marsh and A. *germinans* dominated wetlands are similar, 2,597 ± 306 and 2,788 ± 116 g-OC·m^{-2}, respectively (Table 11). The annual OC accumulation for salt marsh and A. *germinans* sites are also similar, 25 ± 3 and 30 ± 5 g-OC·m^{-2}·yr^{-1}, respectively (Table 11).

When the entire Texas Gulf Coast is accounted for, the mean carbon inventory (i.e. sum of the above ground biomass-OC and 100 year soil-OC accumulation) are similar for both salt marsh and A. *germinans* dominated wetlands, 2,678 ± 324 and 2,985 ± 182 g-OC·m^{-2}, respectively.

4.3.3 Lignin accumulation

The local variability for A. *germinans* lignin accumulation is represented in Table 8. The highest local variability for A. *germinans* 100 year lignin accumulation is Mustang Island core 1 and core 3, (159 ± 5 and 462 ± 18 g-L·m^{-2}, respectively). The lowest local variability for A. *germinans* 100 year lignin accumulation is Port O' Connor core 2 and core 3, (116 ± 10 and 257 ± 9 g-L·m^{-2}, respectively). The highest local variability for A. *germinans* annual OC accumulation is Mustang Island core 1 and core 3, (1.5 ± 0.1 and 4.7 ± 0.2 g-L·m^{-2}·yr^{-1}, respectively). The lowest local variability for A. *germinans* 100 year lignin accumulation is Port O' Connor core 2 and core 3, (1.2 ± 0.1 and 2.4 ± 0.1 g-L·m^{-2}·yr^{-1}, respectively).

The local variability for salt marsh lignin accumulation are represented in Table 9. The highest local variability for salt marsh 100 year lignin accumulation is West Galveston Island core 1 and core 2, (137 ± 15 and 520 ± 8 g-L·m^{-2}, respectively). The lowest local variability for salt marsh 100 year lignin accumulation is Copano Bay core 1 and core 3, (125 ± 4 and 314 ± 3 g-L·m^{-2}, respectively). The highest local variability for salt marsh annual lignin accumulation is Copano Bay core 1 and core 2, (1.2 ± 0.1 and 3.0 ± 0.2 g-L·m^{-2}·yr^{-1}, respectively). The lowest local variability for salt marsh

annual lignin accumulation is Copano Bay core 1 and core 3, (1.2 ± 0.1 and 0.9 ± 0.1 g-L·m^{-2}·yr^{-1}, respectively).

The highest A. *germinans* 100 year lignin accumulation is Mustang Island (350 ± 14 g-L·m^{-2}) (Table 10). In comparison, total 100 year lignin accumulation at Port O'Connor was 269 ± 13 g-L·m^{-2}. The highest A. *germinans* annual lignin accumulation is Mustang Island (3.4 ± 0.2 g-L·m^{-2}·yr^{-1}). In comparison, Port O' Connors annual lignin accumulation is 2.7 ± 0.2 g-OC·m^{-2}·yr^{-1} (Table 10).

The highest salt marsh 100 year lignin accumulation is West Galveston Island (324 ± 3 g-L·m^{-2}) (Table 10). In comparison the lowest 100 year lignin accumulation is Copano Bay (178 ± 7 g-L·m^{-2}). The highest annual salt marsh OC accumulation is West Galveston Island (3.2 ± 0.1 g-L·m^{-2}·yr^{-1}). In comparison the lowest annual salt marsh OC accumulation is Copano Bay (1.7 ± 0.1 g-L·m^{-2}·yr^{-1}) (Table 10).

The 100 year lignin accumulation for salt marsh wetlands is lower than A. *germinans* dominated wetlands, 251 ± 5 vs. 309 ± 15 g-L·m^{-2}, respectively (Table 11). Also, annual lignin accumulation for salt marsh wetlands is lower than A. *germinans*, 2.5 ± 0.1 vs. 3.1 ± 0.2 g-L·m^{-2}·yr^{-1}, respectively (Table 11).

Table 8. Organic carbon (OC) & lignin (L) 100 year accumulation and OC & L annual accumulation flux for two A. *germinans* dominated and one mixed (A. *germinans* and salt marsh) wetland sites located along the Texas Gulf Coast. Relative zones correspond to soil cores extracted perpendicular to the estuarine water land boundary.

Location	Soil Core (Relative Zone)	Wetland Type	100 year OC Accumulation ($g\text{-}OC \cdot m^{-2}$)	100 year Lignin Accumulation ($g\text{-}L \cdot m^{-2}$)	OC Annual Accumulation ($g\text{-}OC \cdot m^{-2} \cdot yr^{-1}$)	Lignin Annual Accumulation ($g\text{-}L \cdot m^{-2} \cdot yr^{-1}$)
East Galveston Island	--	Mixed	1,529 ± 105	342 ± 53	15 ± 1	3.3 ± 0.6
Mustang Island	1 (High)	A. *germinans*	1,095 ± 49	159 ± 5	10 ± 1	1.5 ± 0.1
Mustang Island	2 (Middle)	A. *germinans*	1,758 ± 37	428 ± 4	15 ± 2	4.1 ± 0.4
Mustang Island	3 (Low)	A. *germinans*	3,893 ± 205	462 ± 18	41 ± 12	4.7 ± 0.2
Port O' Connor	1 (High)	A. *germinans*	4,508 ± 119	434 ± 11	47 ± 7	4.5 ± 0.5
Port O' Connor	2 (Middle)	A. *germinans*	1,668 ± 55	116 ± 10	16 ± 1	1.2 ± 0.1
Port O' Connor	3 (Low)	A. *germinans*	3,326 ± 227	257 ± 9	32 ± 6	2.4 ± 0.1

Table 9. Organic carbon (OC) & lignin (L) 100 year accumulation and OC & L annual accumulation for two salt marsh dominated and one mixed (salt marsh and A. *germinans*) wetland sites located along the Texas Gulf Coast. Relative zones correspond to soil cores extracted perpendicular to the water land boundary.

Location	Soil Core (Relative Zone)	Wetland Type	100 year OC Accumulation ($g\text{-}OC \cdot m^{-2}$)	100 year Lignin Accumulation ($g\text{-}L \cdot m^{-2}$)	OC Annual Accumulation ($g\text{-}OC \cdot m^{-2} \cdot yr^{-1}$)	Lignin Annual Accumulation ($g\text{-}L \cdot m^{-2} \cdot yr^{-1}$)
East Galveston Island	--	Mixed	3,663 ± 303	348 ± 34	36 ± 4	3.4 ± 0.4
Copano Bay	1 (High)	Salt Marsh	1,400 ± 222	125 ± 4	13 ± 2	1.2 ± 0.1
Copano Bay	2 (Middle)	Salt Marsh	4,088 ± 181	310 ± 8	39 ± 3	3.0 ± 0.2
Copano Bay	3 (Low)	Salt Marsh	3,098 ± 181	98 ± 8	29 ± 1	0.9 ± 0.1
West Galveston Island	1 (High)	Salt Marsh	2,397 ± 424	137 ± 15	24 ± 5	1.4 ± 0.2
West Galveston Island	2 (Middle)	Salt Marsh	2,277 ± 101	520 ± 8	22 ± 1	5.0 ± 0.1
West Galveston Island	3 (Low)	Salt Marsh	2,340 ± 723	314 ± 3	23 ± 4	3.1 ± 0.1

Table 10. Organic carbon (OC) & lignin (L) 100 year accumulation and annual accumulation for three salt marsh and three A. *germinans* sites located along the Texas Gulf Coast.

Location	Wetland Type	100 year OC Accumulation ($g\text{-}OC \cdot m^{-2}$)	100 year Lignin Accumulation ($g\text{-}L \cdot m^{-2}$)	OC Annual Accumulation ($g\text{-}OC \cdot m^{-2} \cdot yr^{-1}$)	Lignin Annual Accumulation ($g\text{-}L \cdot m^{-2} \cdot yr^{-1}$)
Mustang Island	A. *germinans*	2,249 ± 97	350 ± 14	27 ± 5	3.4 ± 0.2
Port O' Connor	A. *germinans*	3,326 ± 134	269 ± 15	32 ± 5	2.7 ± 0.2
Copano Bay	Salt Marsh	2,856 ± 195	178 ± 7	27 ± 2	1.7 ± 0.1
West Island Galveston	Salt Marsh	2,338 ± 416	324 ± 3	23 ± 3	3.2 ± 0.1

Table 11. Average organic carbon (OC) and lignin (L) 100 year accumulation and OC & L annual accumulation for salt marsh and A. *germinans* sites (excluding East Galveston Island mixed) located along the Texas Gulf Coast.

Wetland Type	100 year OC Accumulation ($g\text{-}OC \cdot m^{-2}$)	100 year Lignin Accumulation ($g\text{-}L \cdot m^{-2}$)	OC Annual Accumulation ($g\text{-}OC \cdot m^{-2} \cdot yr^{-1}$)	Lignin Annual Accumulation ($g\text{-}L \cdot m^{-2} \cdot yr^{-1}$)
A. *germinans*	2,788 ± 116	309 ± 15	30 ± 5	3.1 ± 0.2
Salt Marsh	2,597 ± 306	251 ± 5	25 ± 3	2.5 ± 0.1

4.4 Discussion

4.4.1 Molecular signature of accumulated wetland OC

Locally, salt marsh and A. *germinans* dominated wetlands, accumulate lignocellulose differently. Also, the litter accumulated within these wetlands potentially degrade at different rates. Regionally, there are similarities in salt marsh and A. *germinans* mean carbon inventory which illustrate a baseline for OC storage along the Texas Gulf Coast. The greater quantity of lignin storage within A. *germinans* wetlands

points to a more recalcitrant form of OC accumulated within A. *germinans* wetland soils

The West Galveston Island salt marsh is dominated by S. *alterniflora* at the low and mid elevations and B. *maritima* at high elevations; while the Copano Bay salt marsh is dominated by S. *alterniflora* at low elevations and B. *maritima* at mid and high marsh elevations. Port O' Connor and Mustang Island contain one species of mangrove; A. *germinans*, a pioneer species that expanded its northern boundary through propagule dispersion and reduced freezing events (Cavanaugh et al., 2014); these sites are therefore classified as salt marsh and A. *germinans* study locations.

The dominant low elevation salt marsh plant found within regularly flooded tidal salt marshes along the Texas Gulf of Mexico is the C4 plant S. *alterniflora* ($\delta^{13}C \approx$ -13.6‰) (Benner et al., 1987, Tiner, 1999). Although regularly flooded low elevation salt marshes along the Texas Gulf Coast are dominated by S. *alterniflora*, irregularly flooded mid elevation salt marshes host multiple plant assemblages including C3 plant B. *maritima* ($\delta^{13}C \approx$ -27.8‰) (Lonard et al., 2014, Guo et al., 2013, Haines, 1977, Winemiller et al., 2007, Ember et al., 1987). Stable carbon isotopic signatures for A. germinans leaf, stem and surface sediment have been reported as -28.5 ± 0.1‰, -26.7 ± 0.2‰ & -25.5 ± 0.1‰, respectively (Vane et al., 2013).

The signature of organic matter ($\delta^{13}C$ & $\%_{OC\text{-}L}$) accumulated within wetland soils is directly influenced by the parent plant material and the breakdown of this parent plant material within soils. These results illustrate that along the Texas Gulf Coast, salt marsh dominated wetlands are made up of both C4 and C3 plants, which have varying $\delta^{13}C$ signatures. In contrast, Texas Gulf Coast wetlands dominated by A. *germinans* are

comprised predominantly of plants with C3 $\delta^{13}C$ signatures. The C3 A. *germinans* dominated wetland soil OC, however, show an enrichment of 1.0-5.8‰ down core. While $\delta^{13}C$ signatures in the top of the soil cores are representative of the $\delta^{13}C$ signature of the parent plant material, the heavier $\delta^{13}C$ signatures in deeper (and older) soil horizons point to a mixture of C3 and C4 plants. The upward slow decrease in $\delta^{13}C$ signatures was progressive until the early to mid-1980's when the last severe freezes affected the coast of Texas. These trends suggest a historical record of transition from mixed vegetation to a more uniform ecotone dominated by mangrove and reflective of more amenable climatic conditions for this marsh species.

The aboveground parent plant material has a large impact on the $\%_{OC\text{-}L}$ accumulated down core. The parent plant material for salt marsh C4-C3 plants, S. *alterniflora* and B. *maritima,* have similar OC-L proportion (16.4 and 19.2 $\%_{OC\text{-}L}$, respectively). As OC is accumulated within all of the salt marsh dominated study sites (Copano Bay and West Galveston Island), the proportion is consistent with that of fresh plant materials (10.1-22.0 ± 8.3-9.7 $\%_{OC\text{-}L}$). In contrast, within the top 0-22 cm, there is a decrease in $\%_{OC\text{-}L}$ below 22 cm, 3.6-4.0 ± 1.4-1.8 $\%_{OC\text{-}L}$, at both Copano Bay and West Galveston Island. Both salt marsh dominant sites have soil $\%_{OC\text{-}L}$ signatures that suggest that litter components do not undergo preferential degradation within the upper 22 cm of wetland soil. In comparison, A. *germinans* soils show lower above ground biomass $\%_{OC\text{-}L}$ (leaf = 5.7, branch = 12.7 and root = 14.1 $\%_{OC\text{-}L}$). In spite of the lower $\%_{OC\text{-}L}$ in A. *germinans* plant organic matter, the down core OC-L proportions suggest a preferential accumulation of lignin within the soil (Figure 20). For example, within the first 0-22 cm

both Port O' Connor and Mustang Island wetland soils store 11.4-30.8 ± 4.4-15.8 $\%_{OC\text{-}L}$ while down core these systems store 7.4-12.7 ± 1.7-8.7 $\%_{OC\text{-}L}$, respectively.

Recent work on West Galveston Island and Port O'Connor core 2 (mid elevation) suggest that the biochemical composition of litter material controls the composition of OC stored within wetland soils. For example, the lignocellulosic composition (lignin and neutral sugars associated with cellulose) of S. *alterniflora* have a different sensitivity to decomposition than the lignocellulosic components of A. *germinans* (Stern. A., et al 2017 (In Preparation)). Figure $22_{A\ \&\ B}$ illustrates the stable carbon signature of uncharacterized OC, bulk OC and neutral sugars + lignin OC within the West Galveston Island and Port O' Connor core 2. The higher $\delta^{13}C$ signature for West Galveston Island core 2, uncharacterized OC, points to the preferential storage of lignin in the top 25 cm (≈ 70 years) (Figure 22_A). This is likely driven by the microbial degradation of cellulose which is associated with S. *alterniflora* biomass. In comparison, the Port O' Connor uncharacterized $\delta^{13}C$ signature is similar to the bulk $\delta^{13}C$ signature and neutral sugar + lignin $\delta^{13}C$ signature, which indicates that A. *germinans* OC preservation is not controlled by biomass type and/or shifts in above ground biomass have not affected soil OC accumulation (Figure 22_B). This illustrates that locally, salt marsh and A. *germinans* dominated wetlands, accumulate lignocellulose differently and that the litter accumulated within these wetlands potentially degrade at different rates.

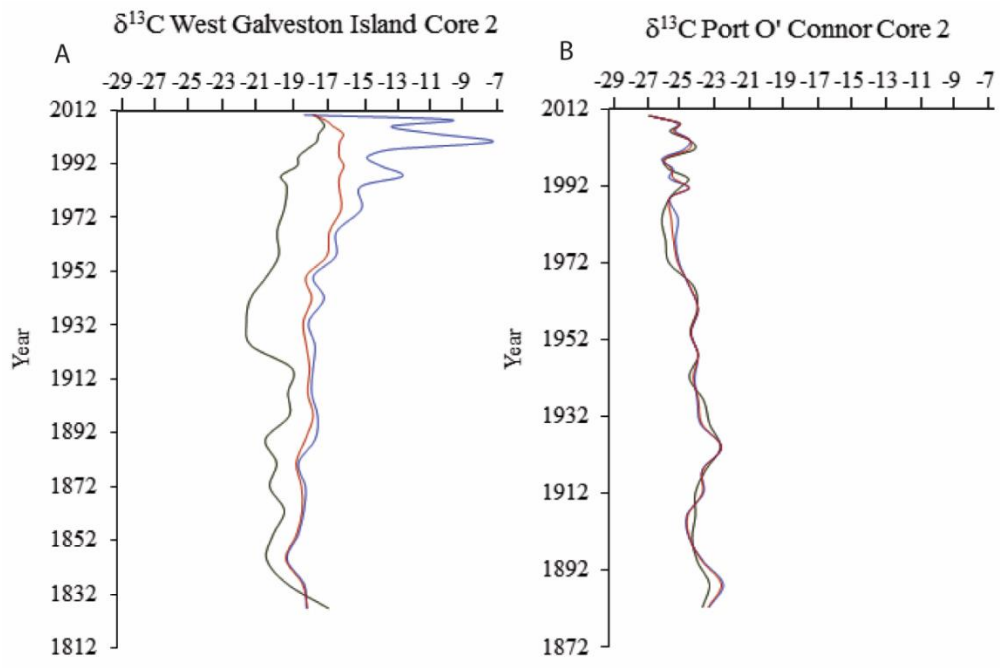

Figure 22. Stable carbon isotope modeling for the uncharacterized proportion of soil OC associated with bulk soil carbon, neutral sugars and lignin. Wetland soil core 2 (mid elevation) was extracted from both, salt marsh dominated West Galveston Island and A. *germinans* dominated Port O' Connor (A and B, respectively). Uncharacterized soil $\delta^{13}C$, neutral sugar + lignin $\delta^{13}C$ and bulk $\delta^{13}C$ are represented by blue, black and red lines, respectively. Quantification of neutral sugars from Stern et al., 2017 (in preparation).

4.4.2 Regional and global wetland OC accumulation

Over the past 20 years, the Texas Gulf Coast region has experienced a loss of 78 km^2 of salt marsh and an increase in A. *germinans* area of 14 km^2 (Armitage et al., 2015). Armitage et al. (2015) attributed the overall loss of salt marsh ecosystems to local sea level rise, which outpaces salt marsh soil accumulation. The expansion of A. *germinans*, however, is attributed to the absence of severe freezing episodes during the study period (Armitage et al., 2015, Osland et al., 2013). When integrating the total gains and losses of Texas Coastal wetland coverage over the past 20 years, we can

estimate the impact of regional wetland coverage changes on OC accumulation. For example, the total loss of salt marsh habitat accounts for -4.5 Gg of above ground OC loss, while the total expansion of A. *germinans* habitat accounts for an increase in1.9 Gg of above ground OC. This data suggests that A. *germinans* replacement from 1990-2010 has led to a net replacement of 44% of above ground stocks of OC. Concurrently, a net loss of long term (100 year) soil OC accumulation (-117 Gg-OC) is observed over the 20 year study period.

Although global salt marsh and mangrove land cover is only 1.3% of terrestrial forest types, mangrove and salt marsh ecosystems sequester similar loads of carbon as terrestrial systems, 121.6 and 180.8 Tg-OC·yr^{-1}, respectively (Mcleod et al., 2011). Globally, the OC burial for salt marsh and tropical mangroves is approximately 0.5-87.0 ± 0.05-0.9 and 31.1-34.4 ± 5.4-5.9 Tg-OC·yr^{-1}, respectively (Mcleod et al., 2011, Chmura et al., 2003, Duarte et al., 2005, Spalding, 2010). In comparison, the Texas Gulf Coast wetlands, which make up less than 0.1% of the estimated global salt marsh and A. *germinans* land cover (278 km^2), annually accumulate 7.1 ± 0.6 Gg-OC·yr^{-1}, which is ≈ 0.02% of the global OC burial (Table 12). This number is significantly less than a previous estimate of Texas coastal wetland OC accumulation by Bianchi et al. (2013) and includes refined high-resolution spatial classification of wetland cover in these systems from Armitage et al. (2015). However, if we assume that all salt marsh wetlands located along the Gulf of Mexico become dominated by A. *germinans*, and the estimated wetland aerial extent estimate is the 2.5 million acres used in Bianchi et al (Duke and Kruczynski, 1992), we may then calculate a lower range estimate (0.27 ± 0.05 Tg-OC yr-

1) for potential annual OC accumulation (versus 1.29 ± 0.32 Tg-OC·yr^{-1}) (Bianchi et al., 2013). The difference in these estimates, therefore, highlight the heterogeneity of carbon burial in these systems and the impacts that local carbon accumulation "hot spots" have on regional estimates and the importance of high resolution spatial categorization. These parameters are important to consider when determining regional and global carbon budgets and models.

Table 12. Carbon sequestration averages for global and regional (Texas Gulf Coast) wetlands. Global averages estimated from listed sources and Mcleod et al 2011.

Wetland Type	Area (km^2)	Carbon burial Rate (g-OC·m^{-2} yr^{-1})	Carbon Burial (Gg-OC·yr^{-1})	Sources
Global Salt Marsh	22,000 - 400,000	218 ± 24	4,800 – 87,200 ± 500 – 9,600	Mcleod et.(2011); Chmura et al. (2003); Duarte et al. (2005a)
Global Mangrove	137,760 – 152,361	226 ± 39	31,100 – 34,400 ± 5,400 – 5,900	Chmura et al. (2003); Bird et al. (2004); Lovelock et al. (2010); Sanders et al. (2010); Giri et al. (2010); Spalding et al. (2010)
Texas A. *germinans*	38*	30 ± 5	1.0 ± 0.1	This study
Texas Salt Marsh	240*	25 ± 3	6.0 ± 0.5	This study
* Area calculated for A. *germinans* and salt marsh ecotones located along the Texas Gulf Coast (A.R. Armitage 2015)				

4.4.3 Carbon equivalent value of CO_2 accumulated along the Texas Gulf Coast

The values of marine wetlands are measured as direct and indirect services to local, regional and global communities, which include pollution containment, food production, storm protection, carbon sequestration, tourism and cultural significance (Zarate-Barrera and Maldonado, 2015). Although sometimes difficult, and certainly with

assumptions, these values can be estimated in a hypothetical market in an effort to place a monetary value on these coastal and estuarine wetland services (Murray et al., 2011). For example, the indirect service of coastal wetland carbon sequestration was analyzed within a hypothetical market, in which the Kyoto Protocol issued economical values for the importance of carbon sequestration in respect to Green House Gas (GHG) mitigation (Zarate-Barrera and Maldonado, 2015).

The GHG mitigation application of low and high market values per metric ton of CO_2 ($t\text{-}CO_2^{-1}$) can range from the $\$4.20\text{-}\$35.00 \cdot 10^6\text{-}CO_2^{-1}$, depending on the exchange market (i.e., Chicago Climate Exchange vs. 2008 Kyoto Protocol compliance driven market, respectively) (Jenkins et al., 2010, Zarate-Barrera and Maldonado, 2015). The CO_2 equivalent of carbon (CO_2e) is estimated by dividing the molecular weight of CO_2 ($44.01\ g \cdot mol^{-1}$) by the molecular weight of carbon ($12.01\ g \cdot mol^{-1}$) (Kauffman et al., 2013). The estimated CO_2e loads calculated for the salt marsh and A. *germinans* wetlands contained within the Texas Gulf Coast are represented in Table 13. Using refined aerial wetland coverage for the Texas Gulf Coast (Armitage et al., 2015), and assuming that marine wetlands directly sequester CO_2 as soil OC, the estimated monetary value for the Texas Gulf Coastal wetland soil OC stocks range from 11.2 ± 1.2 to 93.7 ± 9.9 million USD, depending on the respective GHG market. Using the annual wetland OC accumulation presented in this study; we estimate that the annual monetary value of GHG mitigation for the Texas Gulf wetlands range from; 109,439 ± 9,248 to 911,995 ± 77,070 USD per year, depending on the respective GHG market.

Table 13. The Texas Gulf Coast wetland carbon dioxide load for both salt marsh and A. *germinans* wetland types. Estimates of CO_2 equivalent (CO_2e) are determined using aboveground and soil carbon inventories for both wetland types. Total areal expanse for the Texas Gulf Coast wetland coverage was adopted from Armitage et al., 2015.

Wetland Type	Area (km^2)	Above Biomass Load ($Gg \cdot CO_2e$)	Soil Load ($Gg \cdot CO_2e$)	Total Load ($Gg \cdot CO_2e$)
A. *germinans*	38	46 ± 4	400 ± 18	446 ± 22
Salt Marsh	240	71 ± 16	2,290 ± 270	2,361 ± 286
The CO_2 equivalent (CO_2e) is estimated by multiplying carbon by the molecular ratio of 3.67 (Kauffman et al 2014).				

Carbon sequestration within coastal wetlands is an important long term sink and may help mitigate GHG emissions. The overall quantity and quality of the organic carbon sequestered within these margins are controlled by sedimentation rates and turnover by microbial activity. Due to the long term carbon sequestration strength of these systems, it is important to understand the ecosystem level shifts that have the potential to alter the type of OC accumulation within coastal wetlands. The Texas Gulf Coast region, along with other Gulf Coastal regions, are experiencing an increase in A. *germinans* expansion into historically salt marsh dominant wetlands. Although previous studies suggest that the shift from salt marsh to A. *germinans* dominated wetlands drastically alter OC accumulation rates (Bianchi et al., 2013), we have identified that increased A. *germinans* OC accumulation rates are a local phenomenon, and when integrated across multiple wetland sites, these wetlands accumulate similar rates of OC. Therefore, it is important to understand spatial heterogeneity of carbon storage before assessing its value in a monetary market. For example, with mitigation work, identifying

carbon storage hot-spots can help maximize the carbon storage during urban development and decrease the impacts of ecosystem shifts on carbon storage through management practices.

4.4.4 Potential threats to OC accumulation along coastal environments

Threats to coastal ecosystems ability to accumulate organic carbon in sediments include the loss of global vegetated ecosystems (Mcleod et al., 2011), rising sea levels (Kirwan and Megonigal, 2013) and increased coastal development (Waycott et al., 2009, Pendleton et al., 2012). The term "Coastal Squeeze" was first cited as a conservation tool in the observation of seaward loss of saltmarshes in the United Kingdom due to natural losses along rocky shorelines (Doody, 2004). Recently, this term has been adopted to explain the pressures on coastal wetlands in the presence of increased sea level rise and extensive land use change (Taylor et al., 2016, Spencer et al., 2016, Karstens et al., 2016).

The increase in extensive land use change as the addition of impervious surfaces (concrete and asphalt) along coastal boundaries can put pressures on vegetation and organic carbon cycling (i.e., modification of storage, sources and movement pathways) through intensified construction, waste water run-off, and freshwater diversion (Torio and Chmura, 2013, Schlacher et al., 2006). In order to understand the potential impacts of increased extensive land use change in terms of the addition of impervious surfaces and projected sea level along the upper portion of the Texas Gulf Coast, we analyzed high and medium intensity land use development (80% and 50-80% of surfaces covered by impervious surfaces, respectively) for the Houston Texas metropolitan area and the

projected 100 year sea level rise (Figure 23). The potential impact on carbon accumulation and storage, due to extensive land use change and sea level rise, is highest along the coast. The "Coastal Squeeze" scenario threatens the northern migration of marine wetlands due to coastal development and could have a great effect on future carbon sequestration potential along heavily populated areas.

This study illustrates regional similarities in the annual OC accumulation and 100 year OC accumulation for salt marsh and A. *germinans* dominated wetlands. Due to the larger areal extent of salt marsh wetlands, the Texas Gulf Coast salt marsh community contains a larger carbon load in comparison to Texas A. *germinans* stands. The effects of local ecosystem change (i.e., A. *germinans* expansion) had a lesser effect on annual and long term OC accumulation along the Texas Gulf Coast when compared to habitat loss due to sea level rise and coastal squeeze. The similarity in salt marsh and A. *germinans* mean carbon inventory illustrates the baseline for OC storage along the Texas Gulf Coast, while the greater quantity of lignin storage within A. *germinans* wetlands points to a more recalcitrant form of OC accumulated within A. *germinans* wetland soils. It is important to keep in mind that habitat loss is at least as important as vegetation type in order to maintain carbon sequestration potential within Texas Coastal wetlands; in respect to a changing climate.

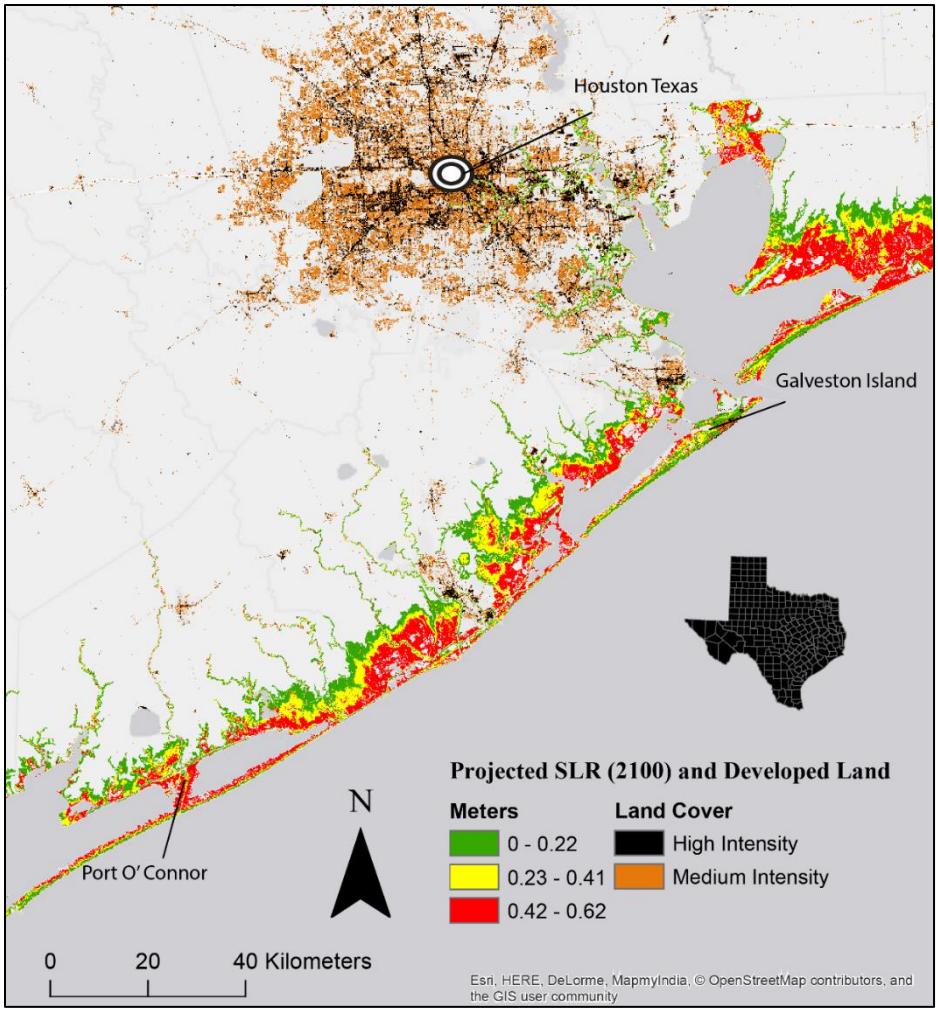

Figure 23. Projected 100 year sea level rise and 2010 Developed Land along the south east Texas Gulf Coast. Base map is adopted from ESRI 2011. ArcGIS desktop: release 10. Redlands, CA: Environmental Systems Research Institute. The data was collected from NOAA's coastal change and analysis program (C-CAP), ESRI NOAA Sea Level Rise digital coast.

V. GENERAL CONCLUSIONS

This research focuses on the solubilization, degradation, and sequestration of terrestrial organic carbon in light of thermal alteration and vegetation replacement. The results and observations illustrate the effects of low temperature thermal alterations on the solubilization and degradation of terrestrial organic carbon, along with a regional quantification of wetland carbon accumulation among shifting ecosystems.

During low to mid temperature pyrolysis (200-650°C) of terrestrial organic carbon, there is a fraction of Py-WSOC associated with increased surface functionality. This water soluble fraction is likely associated with components of the plant cell wall indicating that carbohydrate and lignin free phenol rich functional groups (-OH and C-O) are associated with the release of low to mid temperature Py-WSOC.

Incubation experiments on low temperature pyrogenic water soluble organic matter (Py-WSOM) indicates that Py-WSOC has a half-life of 30-40 days. In comparison, the turnover rate for combustion biomarkers (levoglucosan and free lignin phenols) was shorter, with levoglucosan and free lignin phenols having a half-life around 3-4 days and polymeric lignin components 13-14 days. The latter observations contradict earlier studies on the biodegradation of dissolved lignin and point to the need for re-assessment of lignin degradation kinetics in well-mixed riverine systems, particularly when such lignin components are derived from thermally altered plant material that may exist in a form more labile than that in highly processed riverine dissolved organic matter (DOM).

Coastal wetland organic carbon (OC) accumulation along the Texas Gulf Coast, both annual and long term (100 year), are similar for salt marsh and A. *germinans* dominated wetlands. Although OC accumulation, both annual and long term, are similar between salt marsh and A. *germinans* dominated wetlands, when integrated across the entire Texas Gulf Coast, salt marsh dominated wetlands contain a larger total load of OC for the Texas Gulf Coast due to their larger areal extent; however this may change as salt marshes are lost along the Texas Gulf Coast. The similarity in salt marsh and A. *germinans* mean carbon inventory illustrates the baseline for OC storage along the Texas Gulf Coast, while the greater quantity of lignin storage within A. *germinans* wetlands points to a more recalcitrant form of OC accumulated within A. *germinans* wetland soils. It is important to keep in mind that habitat loss is at least as important as vegetation type in order to maintain carbon sequestration potential within Texas Coastal wetlands; in respect to a changing climate.

This work highlights the importance of understanding the composition of materials exported from terrestrial to aquatic systems, as well as changes in ecosystems play on carbon stocks and storage. Therefore, understanding transformation and transportation of terrestrial carbon is imperative to determine its overall fate in the environment.

REFERENCES

Abiven, S., Hengartner, P., Schneider, M.P., Singh, N. and Schmidt, M.W., 2011. Pyrogenic carbon soluble fraction is larger and more aromatic in aged charcoal than in fresh charcoal. *Soil Biology & Biochemistry*, 43(7), pp.1615-1617.

Accardi-Dey, A., 2003. Black carbon in marine sediments: quantification and implications for the sorption of polycyclic aromatic hydrocarbons. (*Doctoral Dissertation*, Massachusetts Institute of Technology).

Adame, M.F., Kauffman, J.B., Medina, I., Gamboa, J.N., Torres, O., Caamal, J.P., Reza, M. and Herrera-Silveira, J.A., 2013. Carbon stocks of tropical coastal wetlands within the karstic landscape of the Mexican Caribbean. *PLoS One*, *8*(2), p.e56569.

Alexis, M.A., Rasse, D.P., Rumpel, C., Bardoux, G., Péchot, N., Schmalzer, P., Drake, B. and Mariotti, A., 2007. Fire impact on C and N losses and charcoal production in a scrub oak ecosystem. *Biogeochemistry*, *82*(2), pp.201-216.

Alexis, M.A., Rumpel, C., Knicker, H., Leifeld, J., Rasse, D., Péchot, N., Bardoux, G. and Mariotti, A., 2010. Thermal alteration of organic matter during a shrubland fire: A field study. *Organic Geochemistry*, *41*(7), pp.690-697.

Amon, R.M.W., Rinehart, A.J., Duan, S., Louchouarn, P., Prokushkin, A., Guggenberger, G., Bauch, D., Stedmon, C., Raymond, P.A., Holmes, R.M. and McClelland, J.W., 2012. Dissolved organic matter sources in large Arctic rivers. *Geochimica et Cosmochimica Acta*, *94*, pp.217-237.

Amon, R.M.W. and Benner, R., 1996. Photochemical and microbial consumption of dissolved organic carbon and dissolved oxygen in the Amazon River system. *Geochimica et Cosmochimica Acta*, *60*(10), pp.1783-1792.

Armitage, A.R., Highfield, W.E., Brody, S.D. and Louchouarn, P., 2015. The contribution of mangrove expansion to salt marsh loss on the Texas Gulf Coast. *PloS One*, *10*(5), p.e0125404.

Ascough, P.L., Bird, M.I., Francis, S.M., Thornton, B., Midwood, A.J., Scott, A.C. and Apperley, D., 2011. Variability in oxidative degradation of charcoal: Influence of production conditions and environmental exposure. *Geochimica et Cosmochimica Acta*, *75*(9), pp.2361-2378.

Baldock, J.A. and Smernik, R.J., 2002. Chemical composition and bioavailability of thermally altered *Pinus resinosa* (Red pine) wood. *Organic Geochemistry*, *33*(9), pp.1093-1109.

Battin, T.J., Luyssaert, S., Kaplan, L.A., Aufdenkampe, A.K., Richter, A. and Tranvik, L.J., 2009. The boundless carbon cycle. *Nature Geoscience*, *2*(9), pp.598-600.

Benner, R., Fogel, M.L., Sprague, E.K. and Hodson, R.E., 1987. Depletion of 13 C in lignin and its implications for stable carbon isotope studies. *Nature*, *329*(6141), pp.708-710.

Benner, R., Weliky, K. and Hedges, J.I., 1990. Early diagenesis of mangrove leaves in a tropical estuary: Molecular-level analyses of neutral sugars and lignin-derived phenols. *Geochimica et Cosmochimica Acta*, *54*(7), pp.1991-2001.

Bianchi, T.S., Allison, M.A., Zhao, J., Li, X., Comeaux, R.S., Feagin, R.A. and Kulawardhana, R.W., 2013. Historical reconstruction of mangrove expansion in the Gulf of Mexico: Linking climate change with carbon sequestration in coastal wetlands. *Estuarine, Coastal and Shelf Science*, *119*, pp.7-16.

Bilba, K. and Ouensanga, A., 1996. Fourier transform infrared spectroscopic study of thermal degradation of sugar cane bagasse. *Journal of Analytical and Applied Pyrolysis*, *38*(1-2), pp.61-73.

Bird, M., Chua, S., Fifield, L.K., Teh, T.S. and Lai, J., 2004. Evolution of the Sungei Buloh–Kranji mangrove coast, Singapore. *Applied Geography*, *24*(3), pp.181-198.

Bowman, D.M., Balch, J.K., Artaxo, P., Bond, W.J., Carlson, J.M., Cochrane, M.A., D'Antonio, C.M., DeFries, R.S., Doyle, J.C., Harrison, S.P. and Johnston, F.H., 2009. Fire in the Earth system. *Science*, *324*(5926), pp.481-484.

Bridgham, S.D., Megonigal, J.P., Keller, J.K., Bliss, N.B. and Trettin, C., 2006. The carbon balance of North American wetlands. *Wetlands*, *26*(4), pp.889-916.

Cavanaugh, K.C., Kellner, J.R., Forde, A.J., Gruner, D.S., Parker, J.D., Rodriguez, W. and Feller, I.C., 2014. Poleward expansion of mangroves is a threshold response to decreased frequency of extreme cold events. *Proceedings of the National Academy of Sciences*, *111*(2), pp.723-727.

Chapin III, F.S., Trainor, S.F., Huntington, O., Lovecraft, A.L., Zavaleta, E., Natcher, D.C., McGuire, A.D., Nelson, J.L., Ray, L., Calef, M. and Fresco, N., 2008. Increasing wildfire in Alaska's boreal forest: pathways to potential solutions of a wicked problem. *BioScience*, *58*(6), pp.531-540.

Chen, C.L. and Chang, H.M., 1985. *Chemistry of Lignin Biodegradation*. Academic Press Inc. Orlando, Florida.

Cheng, C.H. and Lehmann, J., 2009. Ageing of black carbon along a temperature gradient. *Chemosphere*, *75*(8), pp.1021-1027.

Chmura, G.L., Anisfeld, S.C., Cahoon, D.R. and Lynch, J.C., 2003. Global carbon sequestration in tidal, saline wetland soils. *Global Biogeochemical Cycles*, *17*(4).

Colberg, P.J. and Young, L.Y., 1985. Anaerobic degradation of soluble fractions of [14C-lignin] lignocellulose. *Applied and Environmental Microbiology*, *49*(2), pp.345-349.

Comeaux, R.S., Allison, M.A. and Bianchi, T.S., 2012. Mangrove expansion in the Gulf of Mexico with climate change: Implications for wetland health and resistance to rising sea levels. *Estuarine, Coastal and Shelf Science*, *96*, pp.81-95.

Crawford, D.L. and Crawford, R.L., 1980. Microbial degradation of lignin. *Enzyme and Microbial Technology*, *2*(1), pp.11-22.

De Haan, H., 1977. Effect of benzoate on microbial decomposition of fulvic acids in Tjeukemeer (The Netherlands). *Limnology and Oceanography*, *22*(1), pp.38-44.

DeLaune, R.D., Patrick, W.H. and Van Breemen, N., 1990. Processes governing marsh formation in a rapidly subsiding coastal environment. *Catena*, *17*(3), pp.277-288.

Dennis, A., Fraser, M., Anderson, S. and Allen, D., 2002. Air pollutant emissions associated with forest, grassland, and agricultural burning in Texas. *Atmospheric Environment*, *36*(23), pp.3779-3792.

Ding, Y., 2013. Environmental dynamics of dissolved black carbon in aquatic ecosystems.(*Doctoral Dissertation*, Florida International University).

Dittmar, T., 2008. The molecular level determination of black carbon in marine dissolved organic matter. *Organic Geochemistry*, *39*(4), pp.396-407.

Dittmar, T., De Rezende, C.E., Manecki, M., Niggemann, J., Ovalle, A.R.C., Stubbins, A. and Bernardes, M.C., 2012. Continuous flux of dissolved black carbon from a vanished tropical forest biome. *Nature Geoscience*, *5*(9), pp.618-622.

Doody, J.P., 2004. 'Coastal squeeze'–an historical perspective. *Journal of Coastal Conservation*, *10*(1), pp.129-138.

Doyle, T.W., Krauss, K.W., Conner, W.H. and From, A.S., 2010. Predicting the retreat and migration of tidal forests along the northern Gulf of Mexico under sea-level rise. *Forest Ecology and Management*, *259*(4), pp.770-777.

Duarte, C.M., Middelburg, J.J. and Caraco, N., 2005. Major role of marine vegetation on the oceanic carbon cycle. *Biogeosciences*, *2*(1), pp.1-8.

Duke, T.W. and Kruczynski, W.L., 1992. Status and trends of emergent and submerged vegetated habitats, Gulf of Mexico, USA EPA 800-R-92-003. *Gulf of Mexico Program, US Environmental Protection Agency, Stennis Space Center, Mississippi*.

Elias, V.O., Simoneit, B.R., Cordeiro, R.C. and Turcq, B., 2001. Evaluating levoglucosan as an indicator of biomass burning in Carajas, Amazonia: A comparison to the charcoal record. *Geochimica et Cosmochimica Acta*, *65*(2), pp.267-272.

Ember, L.M., Williams, D.F. and Morris, J.T., 1987. Processes that influence carbon isotope variations in salt marsh sediments. *Marine Ecology Progress Series*, *36*, pp.33-42.

Ertel, J.R. and Hedges, J.I., 1985. Sources of sedimentary humic substances: Vascular plant debris. *Geochimica et Cosmochimica Acta*, *49*(10), pp.2097-2107.

Evans, R.J., Milne, T.A. and Soltys, M.N., 1986. Direct mass-spectrometric studies of the pyrolysis of carbonaceous fuels: III. Primary pyrolysis of lignin. *Journal of Analytical and Applied Pyrolysis*, *9*(3), pp.207-236.

Feng, X., Hills, K.M., Simpson, A.J., Whalen, J.K. and Simpson, M.J., 2011. The role of biodegradation and photo-oxidation in the transformation of terrigenous organic matter. *Organic Geochemistry*, *42*(3), pp.262-274.

Feng, X., Simpson, A.J., Wilson, K.P., Williams, D.D. and Simpson, M.J., 2008. Increased cuticular carbon sequestration and lignin oxidation in response to soil warming. *Nature Geoscience*, *1*(12), pp.836-839.

Ghimire, B., Williams, C.A., Collatz, G.J. and Vanderhoof, M., 2012. Fire-induced carbon emissions and regrowth uptake in western US forests: Documenting variation across forest types, fire severity, and climate regions. *Journal of Geophysical Research: Biogeosciences*, *117*(G3).

Giri, C., Ochieng, E., Tieszen, L.L., Zhu, Z., Singh, A., Loveland, T., Masek, J. and Duke, N., 2011. Status and distribution of mangrove forests of the world using earth observation satellite data. *Global Ecology and Biogeography*, *20*(1), pp.154-159.

Goldberg, E. D. 1985. *Black Carbon in the Environment: Properties and Distribution.* John Wiley & Sons. New York, New York.

Goñi, M.A. and Hedges, J.I., 1990. Potential applications of cutin-derived CuO reaction products for discriminating vascular plant sources in natural environments. *Geochimica et Cosmochimica Acta*, *54*(11), pp.3073-3081.

Goñi, M.A. and Montgomery, S., 2000. Alkaline CuO oxidation with a microwave digestion system: Lignin analyses of geochemical samples. *Analytical Chemistry*, *72*(14), pp.3116-3121.

Goñi, M.A., Nelson, B., Blanchette, R.A. and Hedges, J.I., 1993. Fungal degradation of wood lignins: Geochemical perspectives from CuO-derived phenolic dimers and monomers. *Geochimica et Cosmochimica Acta*, *57*(16), pp.3985-4002.

Guo, H., Zhang, Y., Lan, Z. and Pennings, S.C., 2013. Biotic interactions mediate the expansion of black mangrove (*Avicennia germinans*) into salt marshes under climate change. *Global Change Biology*, *19*(9), pp.2765-2774.

Gustafsson, Ö., Kruså, M., Zencak, Z., Sheesley, R.J., Granat, L., Engström, E., Praveen, P.S., Rao, P.S.P., Leck, C. and Rodhe, H., 2009. Brown clouds over South Asia: Biomass or fossil fuel combustion?. *Science*, *323*(5913), pp.495-498.

Haines, E.B., 1977. The origins of detritus in Georgia salt marsh estuaries. *Oikos*, pp.254-260.

Harvey, O.R., Herbert, B.E., Kuo, L.J. and Louchouarn, P., 2012. Generalized two-dimensional perturbation correlation infrared spectroscopy reveals mechanisms for the development of surface charge and recalcitrance in plant-derived biochars. *Environmental Science & Technology*, *46*(19), pp.10641-10650.

Harvey, O.R., Kuo, L.J., Zimmerman, A.R., Louchouarn, P., Amonette, J.E. and Herbert, B.E., 2012. An index-based approach to assessing recalcitrance and soil carbon sequestration potential of engineered black carbons (biochars). *Environmental Science & Technology*, *46*(3), pp.1415-1421.

Haw, J.F. and Schultz, T.P., 1985. Carbon-13 CP/MAS NMR and FT-IR study of low-temperature lignin pyrolysis. *Holzforschung-International Journal of the Biology, Chemistry, Physics and Technology of Wood*, *39*(5), pp.289-296.

Hedges, J.I., Blanchette, R.A., Weliky, K. and Devol, A.H., 1988. Effects of fungal degradation on the CuO oxidation products of lignin: A controlled laboratory study. *Geochimica et Cosmochimica Acta*, *52*(11), pp.2717-2726.

Hedges, J.I., Eglinton, G., Hatcher, P.G., Kirchman, D.L., Arnosti, C., Derenne, S., Evershed, R.P., Kögel-Knabner, I., De Leeuw, J.W., Littke, R. and Michaelis, W., 2000. The molecularly-uncharacterized component of nonliving organic matter in natural environments. *Organic geochemistry*, *31*(10), pp.945-958.

Hedges, J.I. & Ertel, J.R., 1982. Characterization of lignin by gas capillary chromatography of cupric oxide oxidation products. *Analytical Chemistry*, 54(2), pp.174-178.

Hedges, J.I., Keil, R.G. and Benner, R., 1997. What happens to terrestrial organic matter in the ocean?. *Organic geochemistry*, *27*(5), pp.195-212.

Hedges, J.I. and Mann, D.C., 1979. The characterization of plant tissues by their lignin oxidation products. *Geochimica et Cosmochimica Acta*, *43*(11), pp.1803-1807.

Hedges, J.I. and Oades, J.M., 1997. Comparative organic geochemistries of soils and marine sediments. *Organic Geochemistry*, *27*(7), pp.319-361.

Hedges, J.I. and Prahl, F.G., 1993. *Early Diagenesis: Consequences for Applications of Molecular Biomarkers. In Organic Geochemistry*. Springer Publishing Company. New York, New York.

Hernes, P.J. and Benner, R., 2003. Photochemical and microbial degradation of dissolved lignin phenols: Implications for the fate of terrigenous dissolved organic matter in marine environments. *Journal of Geophysical Research: Oceans*, *108*(C9).

Higuchi, T. 1985. *Biosynthesis of Lignin. In: Biosynthesis and Biodegradation of Wood Components*. Academic Press Inc, Orlando, Florida.

Hilscher, A. and Knicker, H., 2011. Degradation of grass-derived pyrogenic organic material, transport of the residues within a soil column and distribution in soil organic matter fractions during a 28 month microcosm experiment. *Organic Geochemistry*, *42*(1), pp.42-54.

Hockaday, W.C., Grannas, A.M., Kim, S. and Hatcher, P.G., 2006. Direct molecular evidence for the degradation and mobility of black carbon in soils from ultrahigh-resolution mass spectral analysis of dissolved organic matter from a fire-impacted forest soil. *Organic Geochemistry*, *37*(4), pp.501-510.

Hockaday, W.C., Grannas, A.M., Kim, S. and Hatcher, P.G., 2007. The transformation and mobility of charcoal in a fire-impacted watershed. *Geochimica et Cosmochimica Acta*, *71*(14), pp.3432-3445.

Horn, S.J., Vaaje-Kolstad, G., Westereng, B. and Eijsink, V., 2012. Novel enzymes for the degradation of cellulose. *Biotechnology for Biofuels*, *5*(1), p.45.

Hunsinger, G.B., Mitra, S., Warrick, J.A. and Alexander, C.R., 2008. Oceanic loading of wildfire-derived organic compounds from a small mountainous river. *Journal of Geophysical Research: Biogeosciences*, *113*(G2).

Jaffé, R., Ding, Y., Niggemann, J., Vähätalo, A.V., Stubbins, A., Spencer, R.G., Campbell, J. and Dittmar, T., 2013. Global charcoal mobilization from soils via dissolution and riverine transport to the oceans. *Science*, *340*(6130), pp.345-347.

Jenkins, W.A., Murray, B.C., Kramer, R.A. and Faulkner, S.P., 2010. Valuing ecosystem services from wetlands restoration in the Mississippi Alluvial Valley. *Ecological Economics*, *69*(5), pp.1051-1061.

Karstens, S., Jurasinski, G., Glatzel, S. and Buczko, U., 2016. Dynamics of surface elevation and microtopography in different zones of a coastal Phragmites wetland. *Ecological Engineering*, *94*, pp.152-163.

Kasischke, E.S. and French, N.H., 1995. Locating and estimating the areal extent of wildfires in Alaskan boreal forests using multiple-season AVHRR NDVI composite data. *Remote Sensing of Environment*, *51*(2), pp.263-275.

Kauffman, J.B., Heider, C., Norfolk, J. and Payton, F., 2014. Carbon stocks of intact mangroves and carbon emissions arising from their conversion in the Dominican Republic. *Ecological Applications*, *24*(3), pp.518-527.

Kawakami, H. 1980. *Degradation of Lignin-Related Aromatics and Lignins by Several Pseudomonads.* CRC Press Inc. Boca Raton, Florida.

Kawamura, K., Izawa, Y., Mochida, M. and Shiraiwa, T., 2012. Ice core records of biomass burning tracers (levoglucosan and dehydroabietic, vanillic and p-hydroxybenzoic acids) and total organic carbon for past 300years in the Kamchatka Peninsula, Northeast Asia. *Geochimica et Cosmochimica Acta*, *99*, pp.317-329.

Keiluweit, M., Nico, P.S., Johnson, M.G. and Kleber, M., 2010. Dynamic molecular structure of plant biomass-derived black carbon (biochar). *Environmental Science & Technology*, *44*(4), pp.1247-1253.

Kennedy, H., Beggins, J., Duarte, C.M., Fourqurean, J.W., Holmer, M., Marbà, N. and Middelburg, J.J., 2010. Seagrass sediments as a global carbon sink: Isotopic constraints. *Global Biogeochemical Cycles*, *24*(4).

Kirk, T.K. and Farrell, R.L., 1987. Enzymatic" combustion": The microbial degradation of lignin. *Annual Reviews in Microbiology*, *41*(1), pp.465-501.

Kirwan, M.L. and Megonigal, J.P., 2013. Tidal wetland stability in the face of human impacts and sea-level rise. *Nature*, *504*(7478), pp.53-60.

Knicker, H., Hilscher, A., González-Vila, F.J. and Almendros, G., 2008. A new conceptual model for the structural properties of char produced during vegetation fires. *Organic Geochemistry*, *39*(8), pp.935-939.

Kuder, T. and Kruge, M.A., 2001. Carbon dynamics in peat bogs: Insights from substrate macromolecular chemistry. *Global Biogeochemical Cycles*, *15*(3), pp.721-727.

Kuo, L.J., Herbert, B.E. and Louchouarn, P., 2008. Can levoglucosan be used to characterize and quantify char/charcoal black carbon in environmental media? *Organic Geochemistry*, *39*(10), pp.1466-1478.

Kuo, L.J., Louchouarn, P. and Herbert, B.E., 2008. Fate of CuO-derived lignin oxidation products during plant combustion: Application to the evaluation of char input to soil organic matter. *Organic Geochemistry*, *39*(11), pp.1522-1536.

Kuo, L.J., Louchouarn, P. and Herbert, B.E., 2011. Influence of combustion conditions on yields of solvent-extractable anhydrosugars and lignin phenols in chars: Implications for characterizations of biomass combustion residues. *Chemosphere*, *85*(5), pp.797-805.

Kuo, L.J., Louchouarn, P., Herbert, B.E., Brandenberger, J.M., Wade, T.L. and Crecelius, E., 2011. Combustion-derived substances in deep basins of Puget Sound: Historical inputs from fossil fuel and biomass combustion. *Environmental Pollution*, *159*(4), pp.983-990.

Lammers, K., Arbuckle-Keil, G. and Dighton, J., 2009. FT-IR study of the changes in carbohydrate chemistry of three New Jersey pine barrens leaf litters during simulated control burning. *Soil Biology and Biochemistry*, *41*(2), pp.340-347.

Lindell, M.J., Granéli, W. and Tranvik, L.J., 1995. Enhanced bacterial growth in response to photochemical transformation of dissolved organic matter. *Limnology and Oceanography*, *40*(1), pp.195-199.

Liu, Q., Zhong, Z., Wang, S. and Luo, Z., 2011. Interactions of biomass components during pyrolysis: A TG-FTIR study. *Journal of Analytical and Applied Pyrolysis*, *90*(2), pp.213-218.

Lo Iacono, C., Mateo, M.A., Gracia, E., Guasch, L., Carbonell, R., Serrano, L., Serrano, O. and Danobeitia, J., 2008. Very high-resolution seismo-acoustic imaging of seagrass meadows (Mediterranean Sea): Implications for carbon sink estimates. *Geophysical Research Letters*, *35*(18), pp.1-5.

Lonard, R.I., Judd, F.W. and Stalter, R., 2014. Biological flora of coastal dunes and wetlands: *Borrichia frutescens* (L.) DC. *Journal of Coastal Research*, *31*(3), pp.749-757.

Louchouarn, P., Amon, R.M., Duan, S., Pondell, C., Seward, S.M. and White, N., 2010. Analysis of lignin-derived phenols in standard reference materials and ocean dissolved organic matter by gas chromatography/tandem mass spectrometry. *Marine Chemistry*, *118*(1), pp.85-97.

Louchouarn, P., Chillrud, S.N., Houel, S., Yan, B., Chaky, D., Rumpel, C., Largeau, C., Bardoux, G., Walsh, D. and Bopp, R.F., 2007. Elemental and molecular evidence of soot-and char-derived black carbon inputs to New York City's atmosphere during the 20th century. *Environmental Science & Technology*, *41*(1), pp.82-87.

Louchouarn, P., Kuo, L.J., Wade, T.L. and Schantz, M., 2009. Determination of levoglucosan and its isomers in size fractions of aerosol standard reference materials. *Atmospheric Environment*, *43*(35), pp.5630-5636.

Louchouarn, P., Lucotte, M. and Farella, N., 1999. Historical and geographical variations of sources and transport of terrigenous organic matter within a large-scale coastal environment. *Organic Geochemistry*, *30*(7), pp.675-699.

Louchouarn, P., Opsahl, S. and Benner, R., 2000. Isolation and quantification of dissolved lignin from natural waters using solid-phase extraction and GC/MS. *Analytical Chemistry*, *72*(13), pp.2780-2787.

Luo, Y., Durenkamp, M., De Nobili, M., Lin, Q. and Brookes, P.C., 2011. Short term soil priming effects and the mineralisation of biochar following its incorporation to soils of different pH. *Soil Biology and Biochemistry*, *43*(11), pp.2304-2314.

Mannino, A. and Harvey, H.R., 2000. Terrigenous dissolved organic matter along an estuarine gradient and its flux to the coastal ocean. *Organic Geochemistry*, *31*(12), pp.1611-1625.

Marchand, C., Disnar, J.R., Lallier-Verges, E. and Lottier, N., 2005. Early diagenesis of carbohydrates and lignin in mangrove sediments subject to variable redox conditions (French Guiana). *Geochimica et Cosmochimica Acta*, *69*(1), pp.131-142.

Masiello, C.A., 2004. New directions in black carbon organic geochemistry. *Marine Chemistry*, *92*(1), pp.201-213.

Masiello, C.A. and Druffel, E.R.M., 1998. Black carbon in deep-sea sediments. *Science*, *280*(5371), pp.1911-1913.

Masiello, C.A. and Louchouarn, P., 2013. Fire in the ocean. *Science*, *340*(6130), pp.287-288.

McConnell, J.R., Edwards, R., Kok, G.L., Flanner, M.G., Zender, C.S., Saltzman, E.S., Banta, J.R., Pasteris, D.R., Carter, M.M. and Kahl, J.D., 2007. 20th-century industrial black carbon emissions altered arctic climate forcing. *Science*, *317*(5843), pp.1381-1384.

Mcleod, E., Chmura, G.L., Bouillon, S., Salm, R., Björk, M., Duarte, C.M., Lovelock, C.E., Schlesinger, W.H. and Silliman, B.R., 2011. A blueprint for blue carbon: Toward an improved understanding of the role of vegetated coastal habitats in sequestering CO_2. *Frontiers in Ecology and the Environment*, *9*(10), pp.552-560.

Mitra, S., Zimmerman, A.R., Hunsinger, G. and Woerner, W.R., 2013. *Black Carbon in Coastal and Large River Systems. In Biogeochemical Dynamics at Major River-Coastal Interfaces: Linkages with Global Change*. Cambridge University Press, Cambridge, Massachusetts.

Molton, P.M. and Demmitt, T.F., 1977. Reaction mechanisms in cellulose pyrolysis: A literature review. *Battelle Pacific Northwest Labs*. Richland, Washington. Report BNWL-2297.

Murray, B.C., Pendleton, L., Jenkins, W.A. and Sifleet, S., 2011. Green payments for blue carbon: Economic incentives for protecting threatened coastal habitats. *Duke University Nicholas Institute for Environmental Policy Solutions*. Durham, North Carolina. Report NI-1104.

Myers-Pigg, A.N., Louchouarn, P. and Teisserenc, R., 2017. Flux of Dissolved and Particulate Low-Temperature Pyrogenic Carbon from Two High-Latitude Rivers Across the Spring Freshet Hydrograph. *Frontiers in Marine Science*, *38*(4), pp.1-11.

Myers-Pigg, A.N., Louchouarn, P., Amon, R.M., Prokushkin, A., Pierce, K. and Rubtsov, A., 2015. Labile pyrogenic dissolved organic carbon in major Siberian Arctic rivers: Implications for wildfire-stream metabolic linkages. *Geophysical Research Letters*, *42*(2), pp.377-385.

Nakahara, K., Kitamura, Y., Yamagishi, Y., Shoun, H. and Yasui, T., 1994. Levoglucosan dehydrogenase involved in the assimilation of levoglucosan in *Arthrobacter* sp. I-552. *Bioscience, Biotechnology, and Biochemistry*, *58*(12), pp.2193-2196.

Nguyen, T.H., Brown, R.A. and Ball, W.P., 2004. An evaluation of thermal resistance as a measure of black carbon content in diesel soot, wood char, and sediment. *Organic Geochemistry*, *35*(3), pp.217-234.

Nicholls, R.J. and Cazenave, A., 2010. Sea-level rise and its impact on coastal zones. *Science*, *328*(5985), pp.1517-1520.

Norwood, M.J., Louchouarn, P., Kuo, L.J. and Harvey, O.R., 2013. Characterization and biodegradation of water-soluble biomarkers and organic carbon extracted from low temperature chars. *Organic Geochemistry*, *56*, pp.111-119.

Opsahl, S. and Benner, R., 1995. Early diagenesis of vascular plant tissues: Lignin and cutin decomposition and biogeochemical implications. *Geochimica et Cosmochimica Acta*, *59*(23), pp.4889-4904.

Opsahl, S. and Benner, R., 1998. Photochemical reactivity of dissolved lignin in river and ocean waters. *Limnology and Oceanography*, *43*(6), pp.1297-1304.

Osland, M.J., Enwright, N., Day, R.H. and Doyle, T.W., 2013. Winter climate change and coastal wetland foundation species: salt marshes vs. mangrove forests in the southeastern United States. *Global Change Biology*, *19*(5), pp.1482-1494.

Pastorova, I., Botto, R.E., Arisz, P.W. and Boon, J.J., 1994. Cellulose char structure: A combined analytical Py-GC-MS, FTIR, and NMR study. *Carbohydrate Research*, *262*(1), pp.27-47.

Patrick Jr, W.H. and DeLaune, R.D., 1977. Chemical and biological redox systems affecting nutrient availability in the coastal wetlands. *Geoscience and Man*, *18*(13), p.137.

Pauly, M. and Keegstra, K., 2008. Cell-wall carbohydrates and their modification as a resource for biofuels. *The Plant Journal*, *54*(4), pp.559-568.

Pellerin, B.A., Hernes, P.J., Saraceno, J., Spencer, R.G. and Bergamaschi, B.A., 2010. Microbial degradation of plant leachate alters lignin phenols and trihalomethane precursors. *Journal of Environmental Quality*, *39*(3), pp.946-954.

Pendleton, L., Donato, D.C., Murray, B.C., Crooks, S., Jenkins, W.A., Sifleet, S., Craft, C., Fourqurean, J.W., Kauffman, J.B., Marbà, N. and Megonigal, P., 2012. Estimating global "blue carbon" emissions from conversion and degradation of vegetated coastal ecosystems. *PloS One*, *7*(9), p.e43542.

Perry, C.L. and Mendelssohn, I.A., 2009. Ecosystem effects of expanding populations of *Avicennia germinans* in a Louisiana salt marsh. *Wetlands*, *29*(1), pp.396-406.

Peterson, J.M., 2013. Ecological interactions influencing *Avicennia germinans* propagule dispersal and seedling establishment at mangrove-saltmarsh boundaries. (*Doctoral Dissertation*, University of South Florida).

Prahl, F.G., Ertel, J.R., Goni, M.A., Sparrow, M.A. and Eversmeyer, B., 1994. Terrestrial organic carbon contributions to sediments on the Washington margin. *Geochimica et Cosmochimica Acta*, *58*(14), pp.3035-3048.

Preston, C.M. and Schmidt, M.W., 2006. Black (pyrogenic) carbon in boreal forests: A synthesis of current knowledge and uncertainties. *Biogeosciences Discussions*, *3*(1), pp.211-271.

Reddy, K.R. and DeLaune, R.D., 2008. *Biogeochemistry of Wetlands: Science and Applications*. CRC Press Inc. Boca Raton, Florida.

Regnier, P., Friedlingstein, P., Ciais, P., Mackenzie, F.T., Gruber, N., Janssens, I.A., Laruelle, G.G., Lauerwald, R., Luyssaert, S., Andersson, A.J. and Arndt, S., 2013. Anthropogenic perturbation of the carbon fluxes from land to ocean. *Nature Geoscience*, *6*(8), pp.597-607.

Rego, J.L. and Li, C., 2010. Storm surge propagation in Galveston Bay during hurricane Ike. *Journal of Marine Systems*, *82*(4), pp.265-279.

Rosenstock, B., Zwisler, W. and Simon, M., 2005. Bacterial consumption of humic and non-humic low and high molecular weight DOM and the effect of solar irradiation on the turnover of labile DOM in the Southern Ocean. *Microbial Ecology*, *50*(1), pp.90-101.

Rumpel, C., Alexis, M., Chabbi, A., Chaplot, V., Rasse, D.P., Valentin, C. and Mariotti, A., 2006. Black carbon contribution to soil organic matter composition in tropical sloping land under slash and burn agriculture. *Geoderma*, *130*(1), pp.35-46.

Running, S.W., 2006. Is global warming causing more wildfires? *Science*, *313*(5789), pp.927-928.

Running, S.W., 2008. Ecosystem disturbance, carbon, and climate. *Science*, *321*(5889), pp.652-653.

Saintilan, N. and Rogers, K., 2015. Woody plant encroachment of grasslands: A comparison of terrestrial and wetland settings. *New Phytologist*, *205*(3), pp.1062-1070.

Saintilan, N., Wilson, N.C., Rogers, K., Rajkaran, A. and Krauss, K.W., 2014. Mangrove expansion and salt marsh decline at mangrove poleward limits. *Global Change Biology*, *20*(1), pp.147-157.

Sánchez-García, L., de Andrés, J.R., Gélinas, Y., Schmidt, M.W. and Louchouarn, P., 2013. Different pools of black carbon in sediments from the Gulf of Cádiz (SW

Spain): Method comparison and spatial distribution. *Marine Chemistry*, *151*, pp.13-22.

Sanders, C.J., Smoak, J.M., Naidu, A.S., Sanders, L.M. and Patchineelam, S.R., 2010. Organic carbon burial in a mangrove forest, margin and intertidal mud flat. *Estuarine, Coastal & Shelf Science*, *90*(3), pp.168-172.

Santín, C., Doerr, S.H., Kane, E.S., Masiello, C.A., Ohlson, M., Rosa, J.M., Preston, C.M. and Dittmar, T., 2016. Towards a global assessment of pyrogenic carbon from vegetation fires. *Global Change Biology*, *22*(1), pp.76-91.

Sarkanen, K.V. and Ludwig, C.H., 1971. *Liguins. Occurrence, Formation, Structure, and Reactions.* Wiley-Interscience. New York, New York.

Savitzky, A. and Golay, M.J., 1964. Smoothing and differentiation of data by simplified least squares procedures. *Analytical Chemistry*, *36*(8), pp.1627-1639.

Schlacher, T.A., Schoeman, D.S., Lastra, M., Jones, A., Dugan, J., Scapini, F. and McLachlan, A., 2006. Neglected ecosystems bear the brunt of change. *Ethology Ecology & Evolution, 18(*4), pp.349-351.

Schmidt, M.W. and Noack, A.G., 2000. Black carbon in soils and sediments: Analysis, distribution, implications, and current challenges. *Global Biogeochemical Cycles*, *14*(3), pp.777-793.

Schneider, M.P., Pyle, L.A., Clark, K.L., Hockaday, W.C., Masiello, C.A. and Schmidt, M.W., 2013. Toward a "molecular thermometer" to estimate the charring temperature of wildland charcoals derived from different biomass sources. *Environmental Science & Technology*, *47*(20), pp.11490-11495.

Singh, J.S. and Gupta, S.R., 1977. Plant decomposition and soil respiration in terrestrial ecosystems. *The Botanical Review*, *43*(4), pp.449-528.

Singh, N., Abiven, S., Torn, M.S. and Schmidt, M.W.I., 2012. Fire-derived organic carbon in soil turns over on a centennial scale. *Biogeosciences*, *9*(8), pp.2847-2857.

Soja, A.J., Tchebakova, N.M., French, N.H., Flannigan, M.D., Shugart, H.H., Stocks, B.J., Sukhinin, A.I., Parfenova, E.I., Chapin, F.S. and Stackhouse, P.W., 2007. Climate-induced boreal forest change: Predictions versus current observations. *Global and Planetary Change*, *56*(3), pp.274-296.

Spalding, M. 2010. *World Atlas of Mangroves.* Routledge. Abingdon, United Kingdom.

Spencer, T., Schuerch, M., Nicholls, R.J., Hinkel, J., Lincke, D., Vafeidis, A.T., Reef, R., McFadden, L. and Brown, S., 2016. Global coastal wetland change under sea-level rise and related stresses: The DIVA Wetland Change Model. *Global and Planetary Change*, *139*, pp.15-30.

Taylor, B., Paterson, D. and Hanley, N., 2016, April. Assessing the carbon benefit of saltmarsh restoration. *EGU General Assembly Conference Abstracts*, 18, pp. 16,398.

Teal, J.M., 1962. Energy flow in the salt marsh ecosystem of Georgia. *Ecology*, *43*(4), pp.614-624.

Tiner, R.W., 1999. *Wetland Indicators: A Guide to Wetland Identification, Delineation, Classification, and Mapping.* CRC Press Inc. Boca Raton, Florida.

Torio, D.D. and Chmura, G.L., 2013. Assessing coastal squeeze of tidal wetlands. *Journal of Coastal Research*, *29*(5), pp.1049-1061.

Vane, C.H., Kim, A.W., Moss-Hayes, V., Snape, C.E., Diaz, M.C., Khan, N.S., Engelhart, S.E. and Horton, B.P., 2013. Degradation of mangrove tissues by arboreal termites (*Nasutitermes acajutlae*) and their role in the mangrove C cycle (Puerto Rico): Chemical characterization and organic matter provenance using bulk δ13C, C/N, alkaline CuO oxidation-GC/MS, and solid-state 13C NMR. *Geochemistry, Geophysics, Geosystems*, *14*(8), pp.3176-3191.

Ward, N.D., Bianchi, T.S., Medeiros, P.M., Seidel, M., Richey, J.E., Keil, R.G. and Sawakuchi, H.O., 2017. Where carbon goes when water flows: Carbon cycling across the aquatic continuum. *Frontiers in Marine Science, 4: Article No. 7*, *4*(PNNL-SA-122717).

Ward, R.D., Friess, D.A., Day, R.H. and MacKenzie, R.A., 2016. Impacts of climate change on mangrove ecosystems: A region by region overview. *Ecosystem Health and Sustainability*, *2*(4).

Waycott, M., Duarte, C.M., Carruthers, T.J., Orth, R.J., Dennison, W.C., Olyarnik, S., Calladine, A., Fourqurean, J.W., Heck, K.L., Hughes, A.R. and Kendrick, G.A., 2009. Accelerating loss of seagrasses across the globe threatens coastal ecosystems. *Proceedings of the National Academy of Sciences*, *106*(30), pp.12377-12381.

Wiedemeier, D.B., Abiven, S., Hockaday, W.C., Keiluweit, M., Kleber, M., Masiello, C.A., McBeath, A.V., Nico, P.S., Pyle, L.A., Schneider, M.P. and Smernik, R.J., 2015. Aromaticity and degree of aromatic condensation of char. *Organic Geochemistry*, *78*, pp.135-143.

Winemiller, K.O., Akin, S. and Zeug, S.C., 2007. Production sources and food web structure of a temperate tidal estuary: Integration of dietary and stable isotope data. *Marine Ecology Progress Series*, *343*, pp.63-76.

Xie, H., Zhuang, X., Bai, Z., Qi, H. and Zhang, H., 2006. Isolation of levoglucosan-assimilating microorganisms from soil and an investigation of their levoglucosan kinases. *World Journal of Microbiology and Biotechnology*, *22*(9), pp.887-892.

Yang, H., Yan, R., Chen, H., Zheng, C., Lee, D.H. and Liang, D.T., 2006. In-depth investigation of biomass pyrolysis based on three major components: hemicellulose, cellulose and lignin. *Energy & Fuels*, *20*(1), pp.388-393.

Yang, H., Yan, R., Chen, H., Lee, D.H. and Zheng, C., 2007. Characteristics of hemicellulose, cellulose and lignin pyrolysis. *Fuel*, *86*(12), pp.1781-1788.

Young, L.Y. and Frazer, A.C., 1987. The fate of lignin and lignin-derived compounds in anaerobic environments. *Geomicrobiology Journal*, *5*(3-4), pp.261-293.

Zarate-Barrera, T.G. and Maldonado, J.H., 2015. Valuing blue carbon: Carbon sequestration benefits provided by the marine protected areas in Colombia. *PloS One*, *10*(5), p.e0126627.

Zimmerman, A.R., 2010. Abiotic and microbial oxidation of laboratory-produced black carbon (biochar). *Environmental Science & Technology*, *44*(4), pp.1295-1301.

Zimmerman, A.R., Gao, B. and Ahn, M.Y., 2011. Positive and negative carbon mineralization priming effects among a variety of biochar-amended soils. *Soil Biology and Biochemistry*, *43*(6), pp.1169-1179.

Ziolkowski, L.A., Chamberlin, A.R., Greaves, J. and Druffel, E.R., 2011. Quantification of black carbon in marine systems using the benzene polycarboxylic acid method: A mechanistic and yield study. *Limnology and Oceanography: Methods*, *9*.

Ziolkowski, L.A. and Druffel, E.R., 2010. Aged black carbon identified in marine dissolved organic carbon. *Geophysical Research Letters*, *37*(16).